Self-Study Manual on Optical Radiation Measurements: Part III—Applications, Chapter 1

Fred E. Nicodemus, Editor

Chapter 1. Measurement of Solar Terrestrial Spectral Irradiance in the Ozone Cut-Off Region, Henry J. Kostkowski, Robert D. Saunders, John F. Ward, Charles H. Popenoe, and A.E.S. Green

Preparation and publication of this Technical Note has been supported by funding from agencies listed on pp. vi & vii of the Preface.

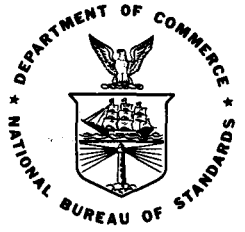

U.S. DEPARTMENT OF COMMERCE, Malcolm Baldrige, Secretary

NATIONAL BUREAU OF STANDARDS, Ernest Ambler, Director

Issued December 1982

PREFACE

Preparation of the NBS Self-Study Manual on Optical Radiation Measurements is an important part of our effort to meet the needs of the National Measurement System with respect to the measurement of optical electromagnetic radiation. Significant needs exist for measurements with uncertainties of about one percent, but the uncertainties actually achieved are often 5 to 10 percent, or even more. These relatively poor accuracies, as compared to those in many other types of physical measurements, result to a great extent from the multidimensional character of optical radiation; radiant energy is distributed and may vary with position, direction, wavelength, polarization, and time. Measurement results are also affected by various instrumental and environmental parameters. In addition, many of those who make measurements of optical radiation have little or no training or experience in this field and are limited in the amount of time they can devote to acquiring the needed information, understanding, and proficiency with measurement techniques. Moreover, there are few schools that offer courses in radiometry, and there are almost no adequate texts or references dealing with this entire subject.

The idea of producing a Self-Study Manual at NBS to try to fill some of this void was developed by one of us (HJK) in the latter part of 1973. Detailed planning got under way in the summer of 1974 when a full-time editor (FEN) was appointed. The first nine chapters were published in a series of four NBS Technical Notes (910- series) up to June 1979. However, subsequent progress was slowed by administrative uncertainties and problems that affected the availability of authors (causing several changes in scheduling) and that finally ended all direct NBS funding for the project on September 30, 1979. Welcome transfers of funds from a number of other federal agencies were obtained to carry the project to September 30, 1980, with the hope that it could then be restored to the NBS budget. When that failed to materialize, outside funding was again obtained to September 30, 1981 (through FY 81).

Meanwhile, the program director (HJK) retired at the end of May 1981, and the editor (FEN) on September 29, 1981. However, remaining FY 81 funds were used for a grant to Catholic University of America (CUA), with whom NBS negotiated a cooperative agreement under which CUA hired the full-time editor (FEN) who continues, as before, at NBS (same address and telephone), working closely with the new project head (JBS) there. CUA will also engage the services of three other former NBS employees: Dr. Kostkowski as part-time consultant throughout the project and as author of two more chapters, and Dr. Venable and Mr. Richmond as authors of one chapter each, as outlined in more detail below.

This Technical Note 910-5, with the first chapter of Part III--Applications, is a departure from Part I--Concepts, and the only one now scheduled. Its objectives and significance are explained in the abstract and in the opening section, and are further amplified below in a brief discussion of the reasons for our preoccupation with Part I--Concepts.

Our aim for the entire Manual has been to provide a comprehensive tutorial treatment that is complete enough for self instruction. That is what is meant in the title by "self-study"; the Manual does not contain explicitly programmed learning steps as that term often connotes. In addition, through detailed, yet concise, chapter summaries, the Manual is designed to serve also as a convenient reference source. Those already familiar with a topic should turn immediately to the summary at the end of the appropriate chapter. They can determine from that summary what, if any, of the body of the chapter they want to read for more details.

The material in the Manual is presented at the level of a college graduate in science or engineering, but even for those with facility in college mathematics and a first course in physics, it's not at all easy reading in spite of our best efforts at clarity and simplicity. This is an unavoidable result of the primary aim ("to make one-percent measurements commonplace") coupled with the fact that it must serve the needs of so many different fields, including astronomy and astrophysics, mechanical heat-transfer engineering, illumination engineering, photometry, meteorology, photo-biology and photo-chemistry, optical pyrometry, remote sensing, military infrared applications, etc.

Apparently it is very difficult for those who have not been directly involved to realize the full implications of that situation. Each of us tends to think of radiometry and radiometric measurements in terms of our immediate experiences and requirements. What each of us would like to have is a set of simple, carefully designed procedures, with appropriate cautions concerning likely sources of error, for making our own particular measurements. However, the next reader wants the same thing, but for entirely different measurements. The desired radiometric quantities to be measured are different, the instrumentation is different, the ambient conditions are different -- the possible ways in which significant differences may exist, in terms of the radiation parameters (position, direction, spectrum, time or frequency of modulation or fluctuation, and polarization) as well as instrumental and environmental parameters, are so numerous that any attempt to cover them all with a "cookbook" treatment of specific measurement procedures would be impossibly unwieldy and could never be completed within any conceivable budget limitations short of utopia. The only way in which we can hope to effectively assist every reader who needs to make one-percent measurements is to provide you, the reader, with material which, with sufficient effort on your part, will help you to develop sufficient understanding and grasp of basic principles to solve your own particular measurement problems. That's why we have concentrated on the basic material of Part I--Concepts and why it is not easy reading. The problems of radiometry in general just aren't simple ones, even when limited to classical radiometry in the domain of geometrical optics (ray optics). Although we have kept within that limitation so far, we recognize the increasingly urgent need for similar treatment of the problems of coherent radiation and we are happy to announce that the next chapter to be published, in a few months we hope, will be Part I, Chapter 10, "Introduction to Coherence in Radiometry" by John B. Shumaker.

The basic approach and focal point of the treatment in this Manual is the measurement equation, first introduced in detail but limited to the radiation parameters of position, direction, and spectrum, in Chapter 5. We believe that every measurement problem should be addressed with such an equation, relating the quantity desired to the data obtained, through a detailed characterization of the instruments used and the radiation field observed, in terms of all of the relevant parameters. These parameters always include the radiation parameters (listed above), as well as environmental and instrumental parameters peculiar to each measurement configuration. The objective of the Manual is to develop the basic concepts required so that the reader will be able to use this measurement-equation approach. It is our belief that this is the only way that uncertainties in the measurement of optical radiation can generally be limited to one, or at most a few, percent.

The original, overall plan for the Manual organized it into three Parts:

Part I--Concepts:

Step-by-step buildup of the *measurement equation* in terms of the radiation parameters, the properties and characteristics of sources, optical paths, and receivers, and the environmental and instrumental parameters. Useful quantities are defined and discussed, and their relevance to various applications in many different fields (photometry, heat-transfer engineering, astronomy, photo-biology, etc.) is indicated. However, discussions of actual devices and measurement situations in this part are mainly for purposes of illustrating concepts and basic principles.

Part II--Instrumentation:

Descriptions, properties, and other pertinent data concerning typical instruments, devices, and components involved in common measurement situations. Included is material dealing with sources, detectors, filters, atmospheric paths, choppers (and other types of optical modulators), prisms, gratings, polarizers, radiometers, photometers, spectroradiometers, spectrophotometers, etc.

Part III--Applications:

Measurement techniques for achieving a desired level of, or improving, the accuracy of a measurement. Included will be a very wide variety of examples of environmental and instrumental parameters with discussions of their effects and how to deal with them. The examples will also be drawn from the widest possible applications in illumination engineering, radiative heat transfer, military infrared devices, remote sensing, meteorology, astronomy and astrophysics, photo-chemistry, photo-biology, etc.

That was our rather ambitious plan when we started out; limitations of support and available resources, particularly available authors, have determined how much, or how little, we could accomplish. So far, as indicated above, we have concentrated on Part I--Concepts. The Part I chapters already, or soon to be, published are:

1. Introduction, by F. E. Nicodemus, H. J. Kostkowski, and A. T. Hattenburg

2. Distribution of Optical Radiation with Respect to Position and Direction--Radiance, by F. E. Nicodemus and H. J. Kostkowski

3. Spectral Distribution of Optical Radiation, by F. E. Nicodemus and H. J. Kostkowski

4. More on the Distribution of Optical Radiation with Respect to Position and Direction, by Fred E. Nicodemus

5. An Introduction to the Measurement Equation, by Henry J. Kostkowski and Fred E. Nicodemus

6. Distribution of Optical Radiation with Respect to Polarization, by John B. Shumaker

7. The Relative Spectral Responsivity and Slit-Scattering Function of a Spectroradiometer, by Henry J. Kostkowski

8. Deconvolution, by John B. Shumaker

9. Physically Defining Measurement-Beam Geometry by Using Opaque Barriers, by Fred E. Nicodemus

10. Introduction to Coherence in Radiometry, by John B. Shumaker.

Chapters 1, 2, and 3 were in TN 910-1; 4 and 5 in TN 910-2; 6 in TN 910-3; and 7, 8, and 9 in TN 910-4. In addition, the final draft for chapter 10 (Part I) is now being revised and should be ready for publication in TN 910-6 within one or two months following the publication of this Technical Note 910-5.

Contingent on the availability of outside funding support, we hope that, during the next two to three years, we can continue the current arrangements with Catholic University of America as described above and complete the following additional chapters of Part I--Concepts:

Distribution of Optical Radiation with Respect to Time, by Fred E. Nicodemus

Linearity Considerations and Calibrations, by John B. Shumaker

Spectrophotometry, by William H. Venable, Jr.

Blackbody Radiation and Temperature Scales, by Henry J. Kostkowski

Physical Photometry, by A. T. Hattenburg

Thermal Radiation Properties of Matter, by Joseph C. Richmond

Spectroradiometry of Spectral Lines, by Henry J. Kostkowski.

As stated above, the measurement-equation approach is central to the entire Manual and the material presented in each chapter needs to be related to the approach introduced in Chapter 5. Depending on how well this is accomplished in each chapter, there may be need at the end to have a final summary chapter for this purpose, tying up loose ends and putting the whole Part I into perspective. Also, examples of various categories of environmental and instrumental parameters and their significance could be usefully presented and discussed. But it's too soon to evaluate this need at present.

Incidentally, in preparing material for the Manual, we have had the pleasure of rediscovering the fact that the best way to learn anything is to try to teach it to someone else. The exercise of preparing tutorial material for such wide general application has required us to analyze our own measurement activities in a different way, broadening our understanding and resulting in improved methods and more accurate results. Note that all references to measurement accuracy or uncertainty in this preface are concerned not only with precision (relating to the repeatability of measurement results) but also with accuracy (relating to agreement with the "truth" which, while unknowable in the last analysis, is approximated by analyses and estimates based on the widest possible experience, including agreement with measurements of the same quantities by others, particularly when they have used different instrumentation and methods of measurement).

ACKNOWLEDGMENTS. The field measurements in Florida, reported in this chapter, were carried out with the valuable assistance of the Staff of the Interdisciplinary Center for Aeronomy and other Atmospheric Sciences (ICAAS), Physics Department, University of Florida, and in particular, Dr. David Doda.

We would like to thank Dr. William Fastie of Johns Hopkins University for the loan, for testing purposes, of an early version of the spectroradiometer used in this investigation, and for various helpful discussions about this instrument.

As indicated above, we have been entirely supported by funds from other federal agencies since September 30, 1979. This is one of the first publications since that date, so it is our first opportunity to publicly acknowledge that most welcome support.

The project to carry out the field measurements of solar UV reported here and to analyze the data and prepare the reports, including this chapter for the Manual, has been supported substantially by the Environmental Protection Agency, Office of Research and Development, Washington, D.C. (Dr. Herbert L. Wiser). During the period FY 80 to the present in FY 82, all of the other support of the Self-Study Manual Project has been from funds provided to the National Bureau of Standards by:

DoD, CCG (tri-service Calibration Coordination Group), Working Group for IR/Laser (Mr. Major L. Fecteau - Army; Mr. Robert Hinebaugh - Air Force; Dr. Felix Schweizer - Navy)

Naval Weapons Center, China Lake, California (Dr. Jon A. Wunderlich)

USAF, Air Staff, Pentagon, Washington, D.C. (Lt. Col. John E. Dunkle) through USAF, Space Division, Los Angeles, California (Maj. Robert Chadbourne)

Naval Air Systems Command, Washington, D.C. (Mr. E. T. Hooper and Mr. Robert C. Thyberg)

USAF, Avionics Laboratory, Wright-Patterson AFB, Ohio (Dr. Paul J. Huffman and Mr. William J. Cannon)

Defense Advanced Research Projects Agency (DARPA), Arlington, Virginia (Dr. Robert W. Fossum through Dr. John Meson)

U.S. Army, BMD Advanced Technology Center, Huntsville, Alabama (Dr. William O. Davies)

NASA Hq., Environmental Observation Program, Washington, D.C. (Dr. L. C. Greenwood and Dr. S. G. Tilford)

Solar Energy Research Institute (SERI), Golden, Colorado (Dr. Keith Masterson)

U.S. Army, Office of Missile Electronic Warfare, Electronic Warfare Laboratory, White Sands Missile Range, New Mexico (Mr. Thomas A. Atherton).

We are deeply indebted to a great many individuals for invaluable "feedback" that has encouraged us and has helped us to put these chapters together more effectively. We renew our strong invitation to all readers to submit comments, criticisms, and suggestions. In particular, we would welcome illustrative examples and problems from as widely different areas of application as possible.

We are especially grateful to Mrs. Betty Castle for the skillful and conscientious effort that produced the excellent typing and layout of still another difficult text.

Fred E. Nicodemus, Editor

John B. Shumaker, Project Head

Henry J. Kostkowski, Consultant

March 1982

Contents

List of Figures

List of Tables

SELF-STUDY MANUAL on OPTICAL RADIATION MEASUREMENTS

Part III. Applications

This is the first chapter in Part III (Applications) of this Manual. Material developed in earlier chapters is used to perform state-of-the-art measurements in Gainesville, Florida, of solar terrestrial spectral irradiance between 290 [nm] and 340 [nm].[1] The measurement equation is used to design the experiment and to address the effects of polarization, non-linearity, spectral scattering, distortion, slit-scattering function, spectral irradiance calibration, and wavelength calibration. Estimates are made of the uncertainties associated with all these factors. The total uncertainty is estimated to be about 10 percent. An appendix includes details for computing the solar terrestrial spectral irradiance between 280 and 310 [nm]. Suggestions are made for reducing the uncertainty by about one third and for further research in UV solar terrestrial measurements.

Key Words: atmospheric attenuation; atmospheric ozone; optical radiation measurements; radiometry; solar radiation; spectroradiometry; UV spectral measurements.

Chapter 1. Measurement of Solar Terrestrial Spectral Irradiance in the Ozone Cut-Off Region*

by Henry J. Kostkowski†, Robert D. Saunders, John F. Ward, Charles H. Popenoe, and A.E.S. Green**

In this CHAPTER. We use the material developed in all the previous chapters of this Self-Study Manual to illustrate how a very difficult radiometric problem is attacked and solved. The problem is the measurement of solar terrestrial spectral irradiance between about 290 [nm] and 340 [nm], the region where absorption by atmospheric ozone produces a sharp cut-off in the observed spectrum. In addition to its general tutorial value, the chapter has applications in research on the biological effects of UV and in atmospheric ozone determinations.

THE PROBLEM -- WHAT and WHY. The optical radiation measurement problem that this chapter addresses is the determination of the solar spectral irradiance at a point on the earth's surface at wavelengths less than about 340 [nm]. A typical plot of the spectral irradiance (averaged over a wavelength interval of 1 [nm]) in this region is shown in figure 1. The sharp spectral cut-off is caused by absorption in atmospheric ozone.

---

*Equipment, experimental measurements, and analyses associated with this chapter were extensively supported by the Environmental Protection Agency.

†Current address, Spectroradiometry Consulting, 3972 Wilcoxson Drive, Fairfax, Virginia 22031.

**Physics Department, University of Florida, Gainesville.

[1]Unit symbols are all enclosed in square brackets to emphasize dimensionality and encourage routine checks of unit-dimension consistency, as discussed in Chapter 1 of Part I, on p. 8 of NBS TN 910-1.

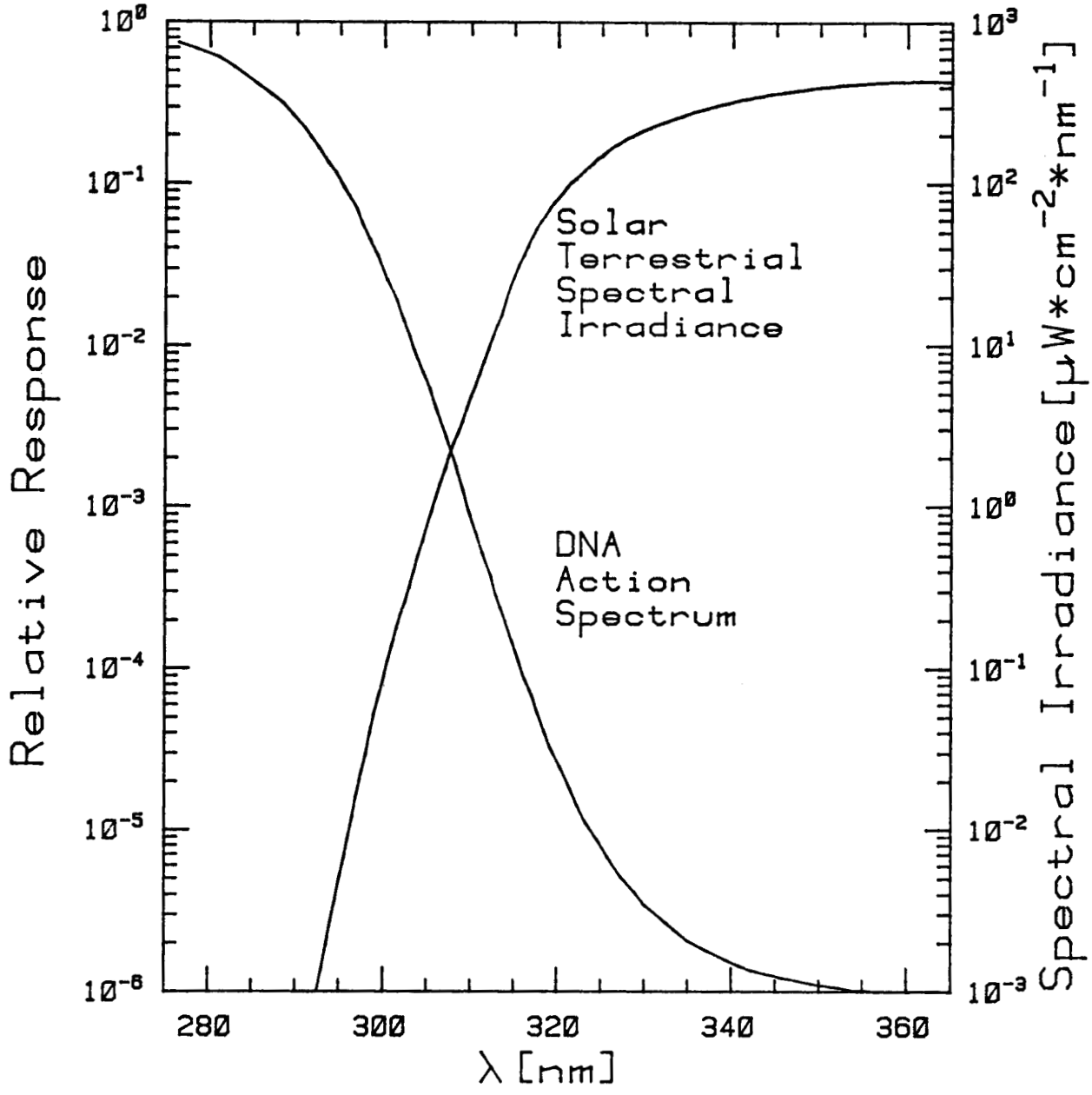

Figure 1. Typical solar terrestrial spectral irradiance, averaged over a wavelength interval of 1 [nm], and the action spectrum for DNA.

A major application for the measurement of solar terrestrial spectral irradiance in the "ozone cut-off region" occurs in the many investigations that are being conducted on the effect of this radiation on living things. Optical radiation in this region is generally damaging to animals and plants. The action spectrum (relative spectral effectiveness) for destroying DNA in cells is shown in figure 1. The damage produced by an additional increment of irradiance at 310 [nm] is a thousand times more than at 350 [nm]. Therefore accurate measurement of this solar terrestrial spectral irradiance is important in experiments investigating its biological effect. Unfortunately, accurate measurements of the spectral irradiance in this region are very difficult because of its rapid change with wavelength and the very large magnitude of that change.

Another application of solar terrestrial measurements in this region is in determining the amount of ozone in the atmosphere. This quantity is usually obtained from measurements at wavelengths between 305 [nm] and 340 [nm] using the Dobson method [1][1]. Because ozone has a much larger effect on the shorter wavelength radiation, it has been suggested [2,3] that measurement of the shape of the solar terrestrial spectrum in the "cut-off region" be used as a means for determining atmospheric ozone thicknesses. A major step in pursuing this suggestion is a demonstration that the greater difficulties inherent in these measurements do not outweigh the advantage of increased sensitivity for ozone determination.

Finally, the measurement of the solar terrestrial spectral irradiance in the ozone cut-off region is of interest to us in this Manual because it is a very difficult radiometric problem, and it provides an opportunity to illustrate the application of many of the concepts and techniques introduced in Part I.

MEASUREMENT CONFIGURATION. The first step that should be taken in most optical radiation measurement problems, as discussed in Chapter 5, Part I--Concepts (p. 87, 910-2)[2] [4], is the preparation of a diagram of the entire measurement configuration. This should show the size and location of the unknown source and the calibration standard relative to the measuring instrument, the location of any sources of unwanted or background radiation, the spectral distribution and approximate magnitude of the radiometric quantity of interest for all the sources (unknown, standard, and background), and details of the measuring instrument including size and position of the receiving aperture, acceptance solid angle and spectral responsivity function (Chapters 9 and 7, 910-4) [5,6].

Usually the complete measurement configuration will not be known when one begins planning a measurement but will evolve as these plans evolve. The first bits of information will often be obtained from talking with colleagues, from technical reports, or from

---

[1]Figures in brackets indicate literature references listed at the end of this chapter.

[2]References to specific material in various chapters of the Self-Study Manual will be given in this form -- (page number or chapter, NBS Technical Note number).

the archival literature. In some cases, preliminary measurements must be made in order to get the required information. The final detailed configuration is only available after the measurements have been completed. Even then, one can often use what was learned in the first measurement to change the configuration and make a second more accurate or more efficient measurement. We will indicate, in presenting our configuration, some of this evolution, but, in general, the configuration described will be the one actually used in the measurements we made in Gainesville, Florida, during June 1980.

Approximate spectral irradiance. The first thing we sought relative to the measurement configuration was an approximation to what we were trying to measure -- the spectral distribution and magnitude of the solar terrestrial spectral irradiance. This was obtained at a solar symposium that we had attended a few years ago and is shown in figure 1. A report by Bener [7] and a few preliminary measurements confirmed the general shape and magnitude shown in figure 1. The approximation was further refined by calculations[1] made using data from the literature on extraterrestrial sunlight in high spectral resolution and typical transmittances of atmospheric molecules, particles (aerosols) and ozone. Ultimately, a set of ozone and aerosol data obtained in our June measurements was factored in. The distribution shown in figure 2 was calculated for a spectral slit width of 1 [nm]. It represents an average of the computed spectral irradiance weighted by a triangular slit-scattering function (p. 15, 910-4) [6] with a (full) width at half-height of 1 [nm]. Using a much smaller spectral slit width (0.003 [nm]), the calculations of the average spectral irradiance have the appearance shown in figure 3. Figure 4 gives the results for spectral slit-widths of 0.18 and 0.34 [nm] with, in addition, two different assumed conditions of atmospheric attenuation. In this latter figure we have also included the spectral irradiance of a 1000 watt [W] tungsten halogen lamp standard at a distance of 50 [cm].

The important points to note relative to the solar spectral irradiance distribution are:

1. The spectral irradiance has a great deal of spectral structure (Fraunhofer lines) so that with the spectral resolution normally available in spectroradiometry the quantity determined will be an average weighted by the spectral responsivity function of the measuring instrument.
2. For a spectral slit width of 1 [nm] the averaging process has "washed out" most of the structure.

Geometry. The next aspect of the measurement configuration we examined was the geometry. The set-up available to us for making the solar measurements was in a roof-top laboratory. A solar tracker on the roof directed the solar beam through a hole in the roof down to the spectroradiometer, as shown in figure 5.

[1]Details of these calculations are presented in Appendix 1A.

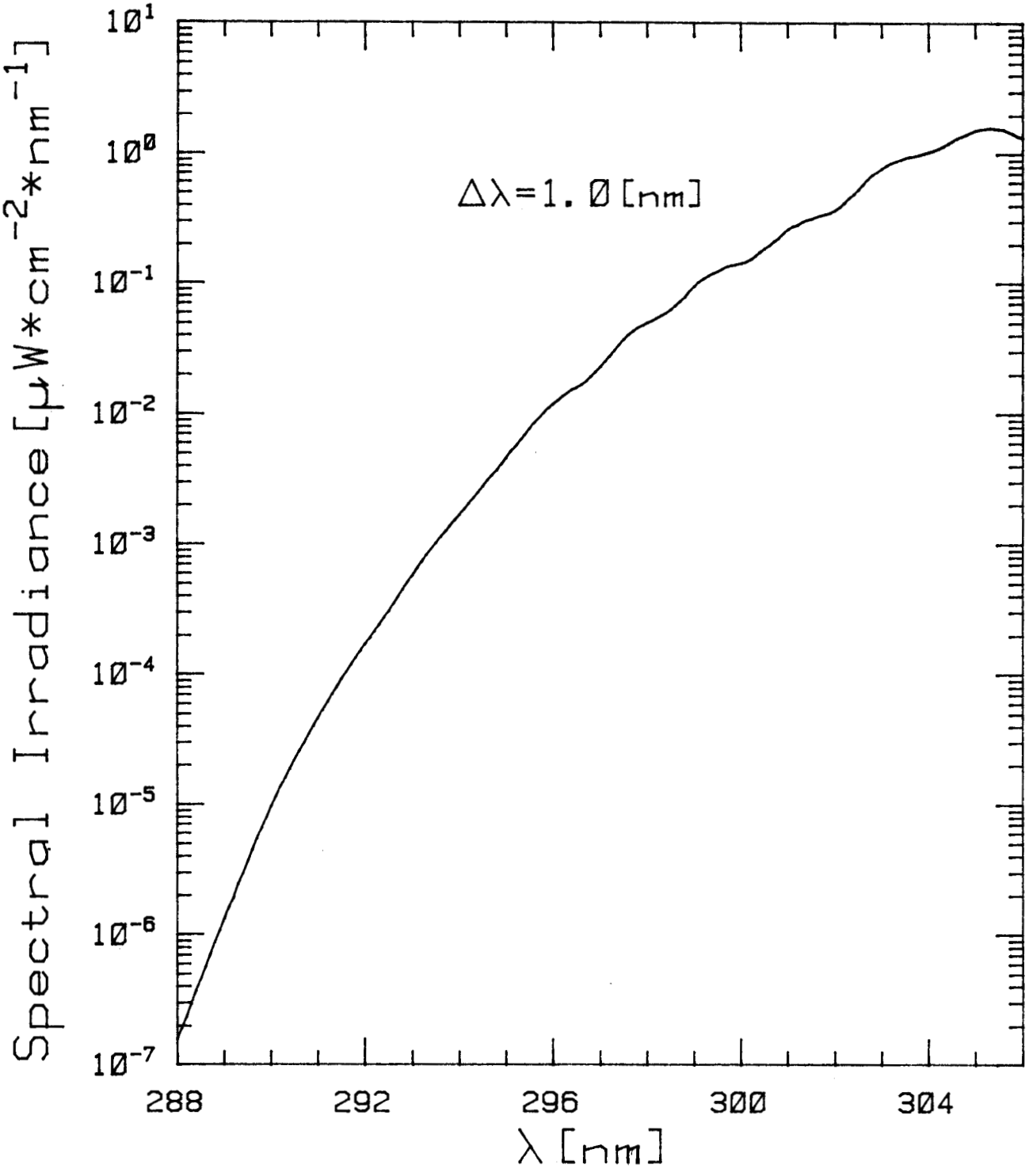

Figure 2. Calculated solar terrestrial spectral irradiance (triangular slit-scattering function with a 1 [nm] spectral slit width).

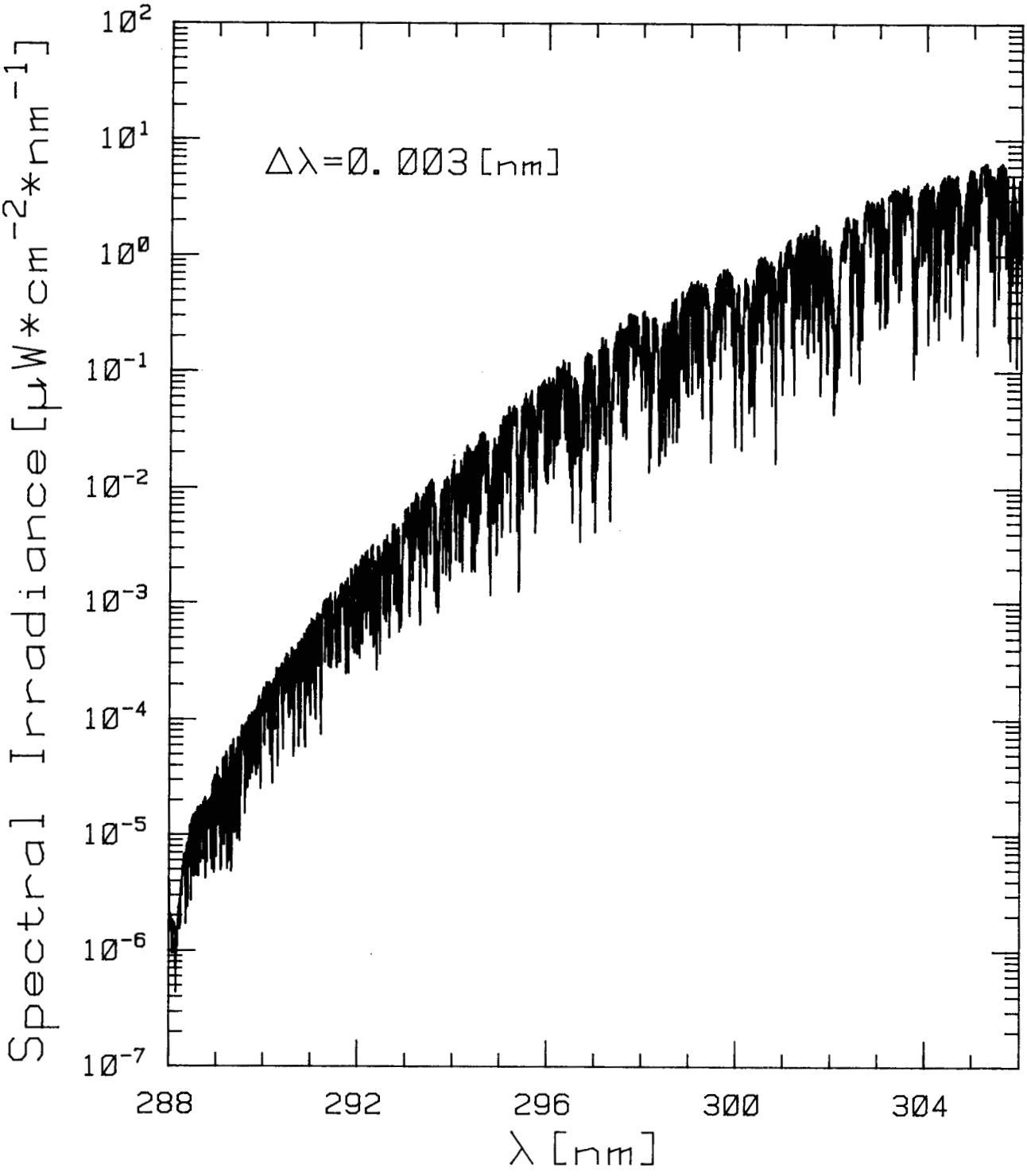

Figure 3. Calculated solar terrestrial spectral irradiance (0.003 [nm] spectral slit width).

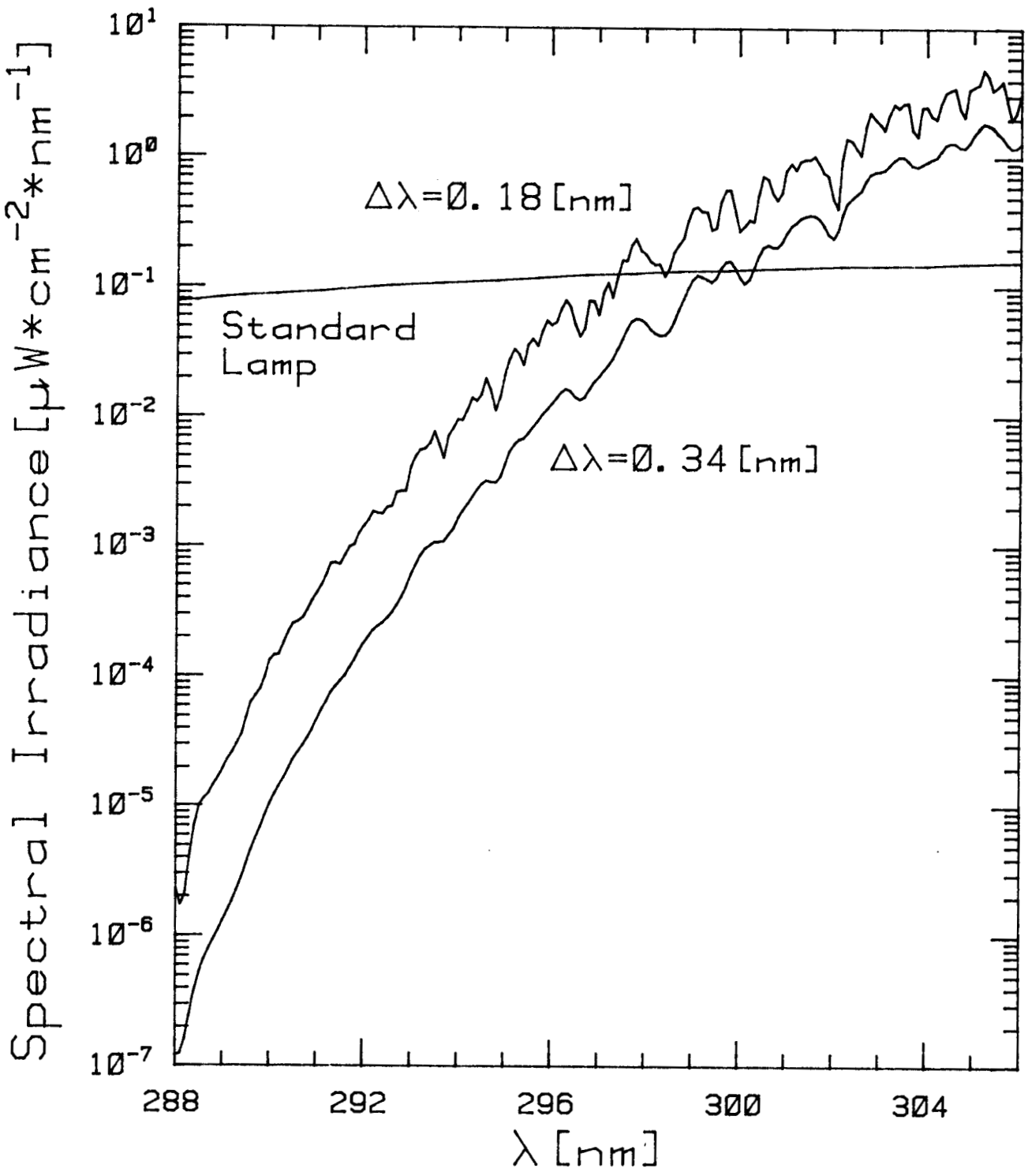

Figure 4. Calculated solar terrestrial spectral irradiance (0.18 and 0.34 [nm] spectral slit widths) and a 1000 [W] tungsten-halogen-standard-lamp spectrum at 50 [cm]. (Vertical separation of the solar curves is due to different assumed atmospheric attenuation conditions.)

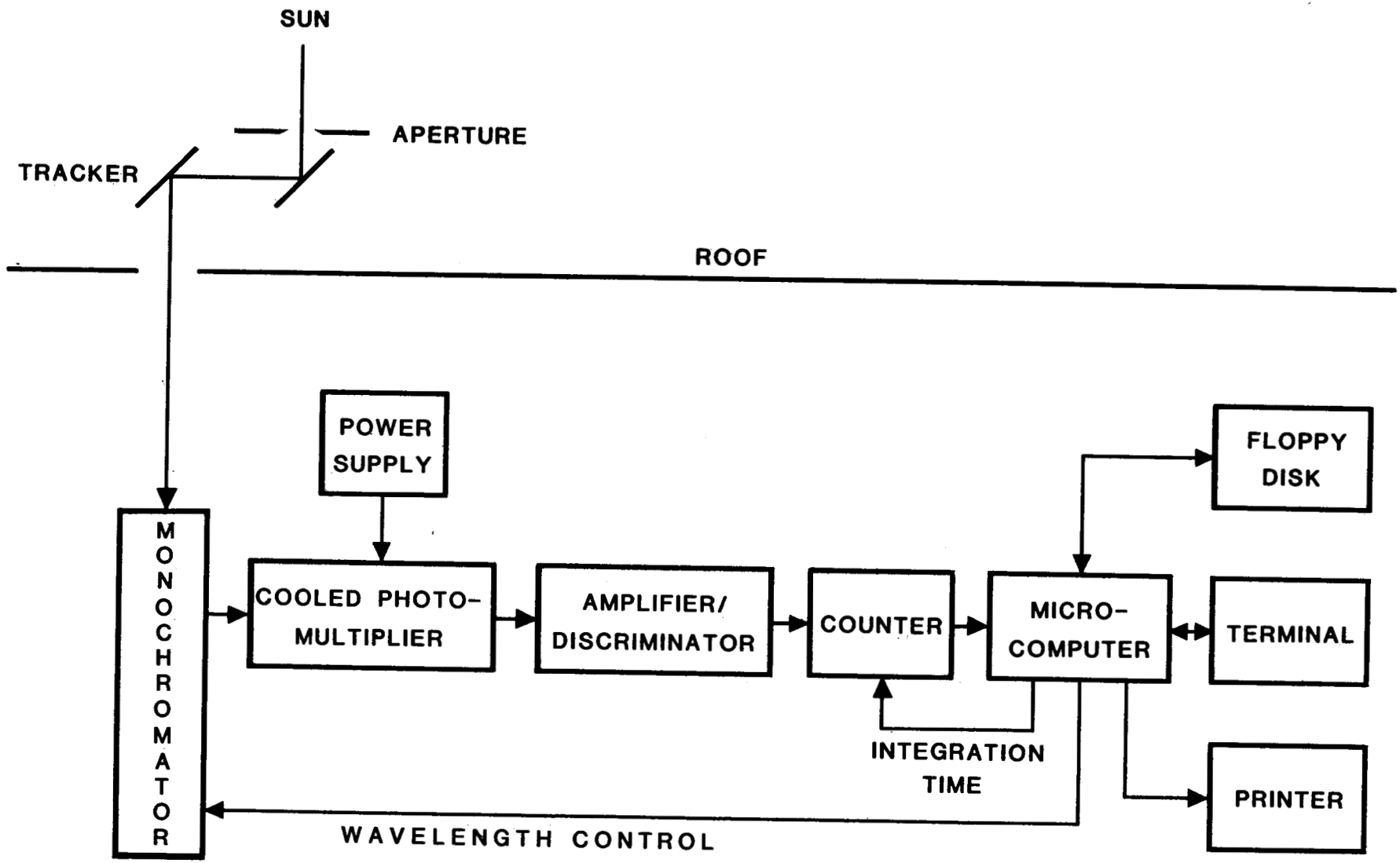

Figure 5. Set-up used for solar terrestrial spectroradiometry.

The tracker consists of two plane mirrors (see figure 15 as well as figure 5). The two mirrors can be rotated as a unit about a vertical axis through the center of the mirror closest to the monochromator, and the mirror farthest from the monochromator can be rotated about a horizontal axis through the centers of both mirrors. Both rotations are computer controlled [3]. The various parts of the spectroradiometer shown in the block diagram of figure 5 will be discussed later.

Since we were interested in determining the spectral irradiance of the direct sun rather than the global irradiance (sun plus sky), we had to limit our field of view so that we included negligible sky irradiance. In order to minimize the effect of any tracking errors, we chose a 3.25-inch [in] aperture resulting in a sufficiently large field of view (see figure 6) relative to tracking errors but one for which we thought the sky

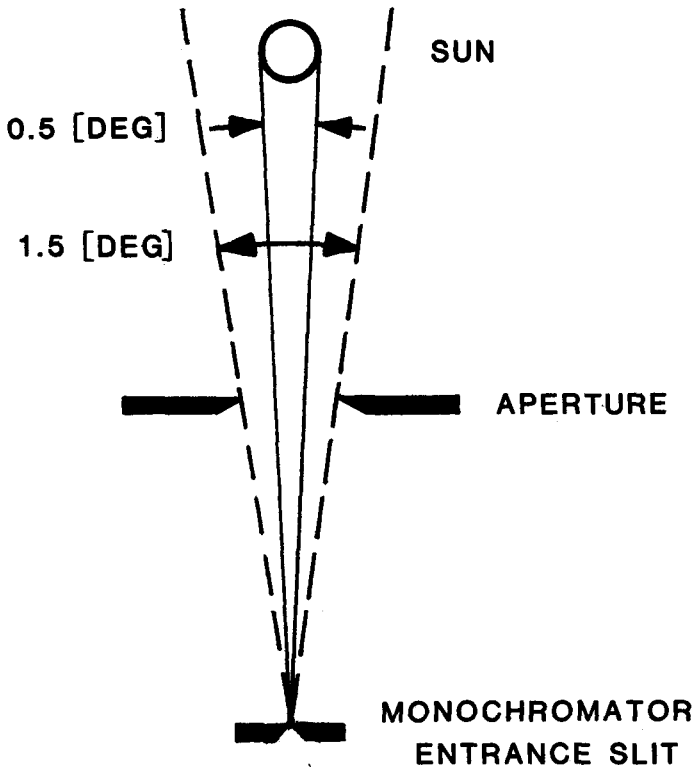

Figure 6. Measurement configuration (without a diffuser).

irradiance would be negligible, 1.5 [deg]. Measurements made by blocking out the sun with opaque discs of various diameters confirmed that the sky irradiance was negligible[1] with the 1.5 [deg] field -- about 0.5 percent that of the sun.

Measurement with and without a diffuser. Normally, spectral irradiance measurements are made with a diffuser (e.g. an averaging sphere) as the first optical element in the spectroradiometer (p. 71, 910-2) [4]. The purpose of this is to insure that the spectral flux responsivity is invariant with direction of the incident flux. In this case, the measurement equation (p. 65, 910-2) [4]

$$S(\lambda_o) = \int_{\Delta\lambda}\int_{A}\int_{\omega} R_\Phi \cdot L_\lambda \cdot \cos\theta \cdot d\omega \cdot dA \cdot d\lambda \tag{1.1}$$

may be reduced to

$$S(\lambda_o) = \int_{\Delta\lambda}\int_{A} R_\Phi \cdot E_\lambda \cdot dA \cdot d\lambda, \tag{1.2}$$

which is the equation required for a measurement of spectral irradiance E_λ. We used a 1/32 [in] thick piece of teflon as a transmitting diffuser, positioning it so that it approximately filled the field of view of the monochromator. The geometry of our measurement configuration (not to scale) using this diffuser is shown in figure 7.

There is one enormous disadvantage of the diffuser. It reduces the flux reaching the detector by a large factor. In our case this was about 1000. Therefore, below 305 [nm], where we were beginning to be energy limited, we rarely used a diffuser. The entrance slit and the sun itself defined the beam geometry as shown in figure 6. In this case, we had to rely on the flux responsivity being sufficiently uniform over the 0.5 [deg] field of view without a diffuser. It was essential to confirm that this was the case by measuring the flux responsivity as a function of angle. This was done by using a small tungsten halogen lamp providing a beam entering the monochromator with an angular extent of 0.2 [deg] in one direction and of 0.6 [deg] perpendicular to this direction. $R_\Phi(\theta)$ was obtained by determining the output signal as a function of angle of tilt of the spectroradiometer. The result, shown in figure 8, was about the same for either orientation of the lamp. The responsivity was uniform around the peak to within 1 percent between about -0.25 [deg] and +0.25 [deg]. This meant that the standard should be confined to a 0.5 [deg] field of view, the angle subtended at the earth's surface by the sun. This was accomplished by positioning the approximately 14 [mm] × 36 [mm] standard

[1]Negligible is in reference to the overall or total uncertainty that we were striving to realize, which in these very difficult solar spectral measurements was about 5 or 10 percent.

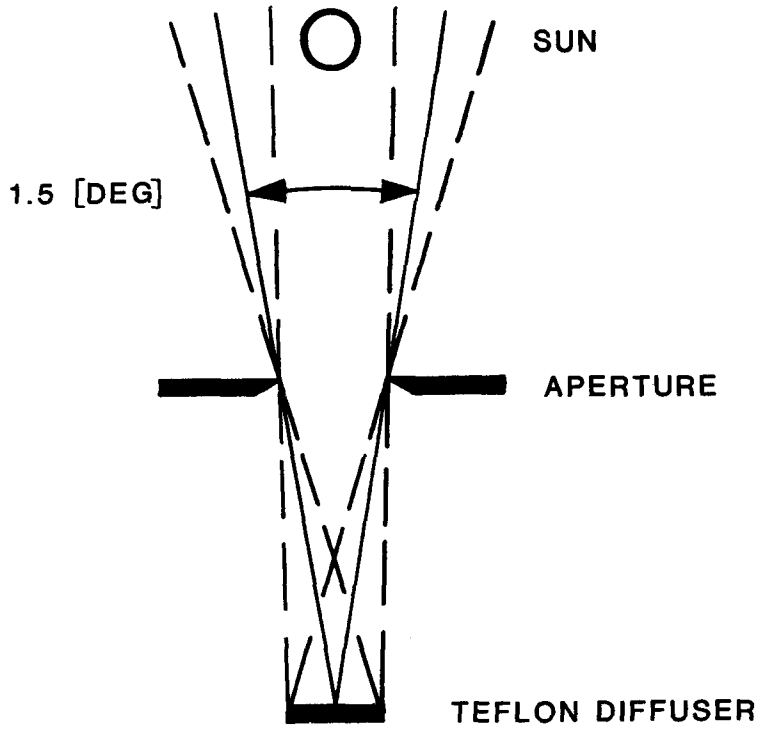

Figure 7. Measurement configuration with a diffuser.

lamp on the solar side of the tracker about 400 [cm] from the entrance slit of the spectroradiometer. It was also necessary that we be able to align and maintain the spectroradiometer orientation relative to the beam from the tracker to within 0.25 [deg]. For this purpose a mount was designed for the spectroradiometer which provided micrometer-type adjustments. The precision of the angular positioning was 10^{-3} [rad] (0.05 [deg]) and the translational positioning 0.1 [mm].

In addition to the above described check on the uniformity of the flux responsivity, we decided to confirm by direct measurement that not using a diffuser did not greatly degrade the accuracy. The confirmation could be made in the wavelength region between 305 [nm] and 340 [nm] where the spectroradiometer output signal was high even when the diffuser was used. We planned to make several sets of measurements in this region with and without the diffuser. If significant differences were found, we could then consider using these differences to correct the shorter wavelength data where the signal was too small to use the diffuser.

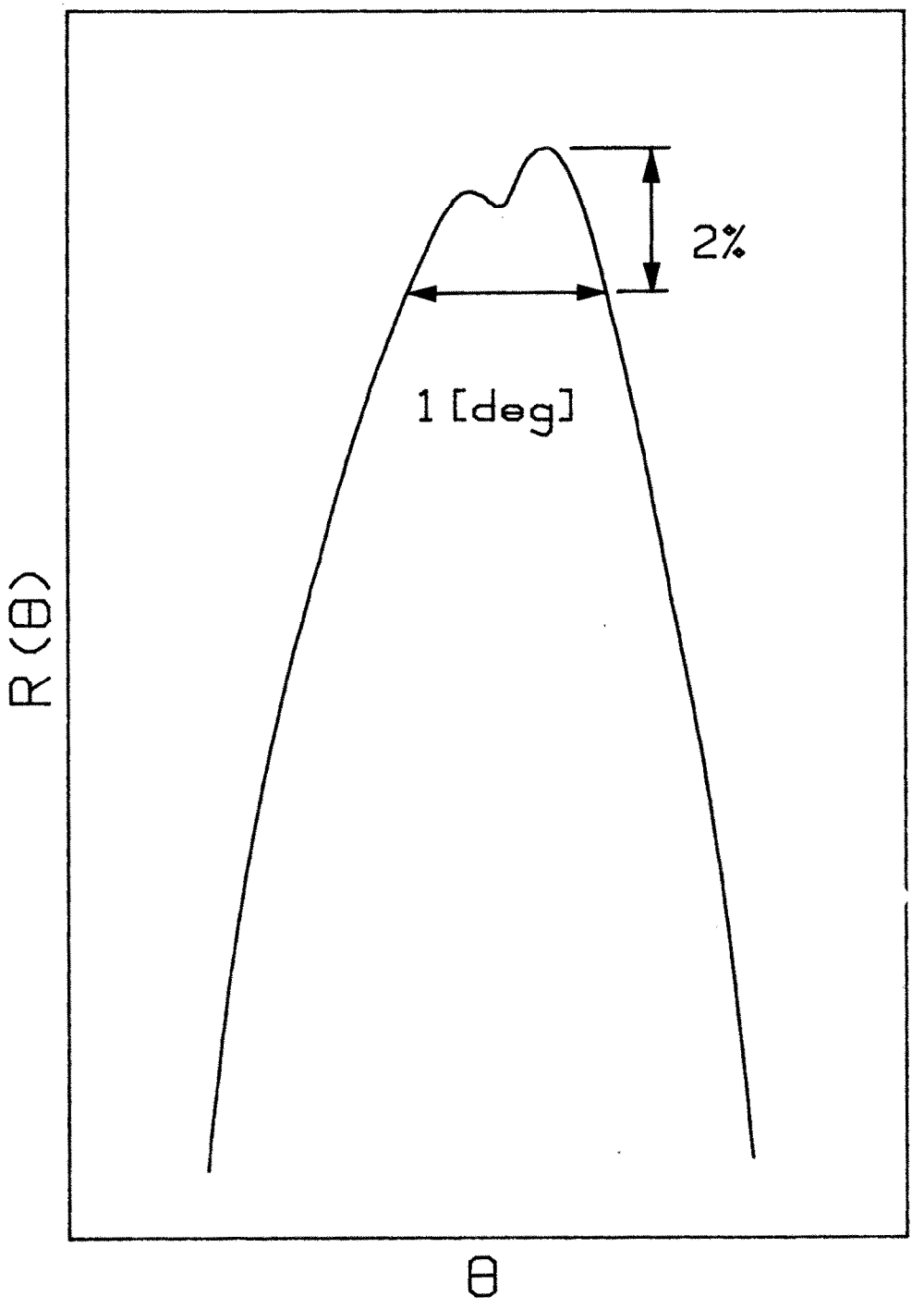

Figure 8. Angular responsivity function of NBS Solar Spectroradiometer (without diffuser).

Calibration standard. The spectral irradiance source standard usually used to calibrate spectroradiometers in the wavelength region in which we were working (287-340 [nm]) is a 1000 [W] clear tungsten halogen lamp. Figure 4 includes a wavelength plot of the spectral irradiance at 50 [cm] from such a standard. The spectral irradiance of this standard is quite different from that of the sun for most of the wavelength range of interest. Also the beam geometry (coiled-coil filament is about 5 [mm] × 25 [mm]) is different from that of the sun. This (standard) flux also has a polarization of about 3 percent while the sun is unpolarized. Differences between the optical radiation being measured and that of the standard are potential sources of error [8]. In characterizing the measuring instrument, which will be discussed later, the effects of such differences will have to be determined.

MEASUREMENT EQUATION. The general measurement equation for incoherent radiation including polarization effects (p. 23, 910-3) [9] is

$$S(\lambda_o) = \int_{\Delta\lambda}\int_{\Delta A}\int_{\Delta\omega} (R_{00}\cdot L_0 + R_{01}\cdot L_1 + R_{02}\cdot L_2 + R_{03}\cdot L_3)\cdot\cos\theta\cdot d\omega\cdot dA\cdot d\lambda. \qquad (1.3)$$

A similar equation is required for the standard which in our case would be located on the solar side of the aperture shown in figure 5. This equation is

$$S^s(\lambda_o) = \int_{\Delta\lambda}\int_{\Delta A}\int_{\Delta\omega^s} (R_{00}\cdot L_0^s + R_{01}\cdot L_1^s + R_{02}\cdot L_2^s + R_{03}\cdot L_3^s)\cdot\cos\theta\cdot d\omega\cdot dA\cdot d\lambda \qquad (1.4)$$

where the R_{0i} are the elements in the first row of a Mueller responsivity matrix representing a combination of the tracker and spectroradiometer responsivities; that is (Chapter 6, 910-3) [9],

$$\begin{pmatrix} L'_0 \\ L'_1 \\ L'_2 \\ L'_3 \end{pmatrix} = \begin{pmatrix} R_{00} & R_{01} & R_{02} & R_{03} \\ R_{10} & R_{11} & \cdot & \cdot \\ R_{20} & \cdot & \cdot & \cdot \\ R_{30} & \cdot & \cdot & \cdot \end{pmatrix} \cdot \begin{pmatrix} L_0 \\ L_1 \\ L_2 \\ L_3 \end{pmatrix} = \begin{pmatrix} \text{responsivity} \\ \text{matrix} \\ \text{for} \\ \text{spectroradiometer} \end{pmatrix} \cdot \begin{pmatrix} \text{responsivity} \\ \text{matrix} \\ \text{for} \\ \text{tracker} \end{pmatrix} \cdot \begin{pmatrix} L_0 \\ L_1 \\ L_2 \\ L_3 \end{pmatrix} \qquad (1.5)$$

where the L_i are the components of the Stokes vector associated with the sun or the standard, L^s. Since the sun is unpolarized $L_1 = L_2 = L_3 = 0$ and

$$S(\lambda_o) = \int_{\Delta\lambda}\int_{\Delta A}\int_{\Delta\omega} R_{00}\cdot L_0\cdot\cos\theta\cdot d\omega\cdot dA\cdot d\lambda. \qquad (1.6)$$

Clearly, if the usual 3 percent polarized standard lamp were used, we would have to concern ourselves with a more complex measurement equation for the standard, one involving other

R_{0i} and L_i^s. Therefore we chose to calibrate a frosted (unpolarized) tungsten halogen lamp by comparing it to a typical standard, using a (different) polarization-insensitive spectroradiometer, and use this unpolarized secondary standard in our solar measurements. The measurement equation for such an unpolarized $(L_1^s = L_2^s = L_3^s = 0)$ standard would then also be

$$S^s(\lambda_o) = \int_{\Delta\lambda}\int_{\Delta A}\int_{\Delta\omega^s} R_{00}\cdot L_0^s\cdot\cos\theta\cdot d\omega\cdot dA\cdot d\lambda. \tag{1.7}$$

Thus it appears that since both the sun and the standard lamp are unpolarized, there are no effects due to polarization. However, this is not the case. The first column of the responsivity matrix for the tracker in eq. (1.5) is a function of the tracker orientation [10] resulting in R_{00} also changing with tracker orientation. This orientation is determined by the time of day that the solar measurements are made. Therefore the (combined) measurement equation should be written

$$\frac{S(\lambda_o)}{S^s(\lambda_o)} = \frac{\int_{\Delta\lambda}\int_{\Delta A}\int_{\Delta\omega} R_{00}(T)\cdot L_0\cdot\cos\theta\cdot d\omega\cdot dA\cdot d\lambda}{\int_{\Delta\lambda}\int_{\Delta A}\int_{\Delta\omega^s} R_{00}(T)\cdot L_0^s\cdot\cos\theta\cdot d\omega\cdot dA\cdot d\lambda} \tag{1.8}$$

and the calibration must be obtained as a function of tracker orientation, expressed here in terms of the time (T) at which the instrument correctly points to the sun, so that the $R_{00}(T)$ corresponding to the time of the solar measurement is used. Figure 9 shows how R_{00} varies as a function of tracker orientation from 290 to 300 [nm]. From 300 to 340 [nm] the functional relationship is different than that at the shorter wavelengths and also varies with wavelength.

When the diffuser is used, calibrations need not be taken as a function of tracker orientation. In this case the spectroradiometer is unpolarized (all R_{ij} in the spectroradiometer's responsivity matrix, except R_{00}, are equal to zero), and since the R_{00}(tracker) varies only slightly (0.1 percent) with tracker orientation [10] so does R_{00}(spectroradiometer and tracker). In other words, although the tracker polarizes the incoming radiation, it doesn't change the flux level significantly. Therefore when the spectroradiometer is polarization insensitive (when using the diffuser), the responsivity is virtually independent of tracker orientation.

Since we wish to measure spectral irradiance, the measurement eq. (1.8) must be modified to include E_λ rather than L_λ. As discussed earlier, this requires that $R_{00}(T)$ be independent of the source solid angles $\Delta\omega$ and $\Delta\omega^s$. Then

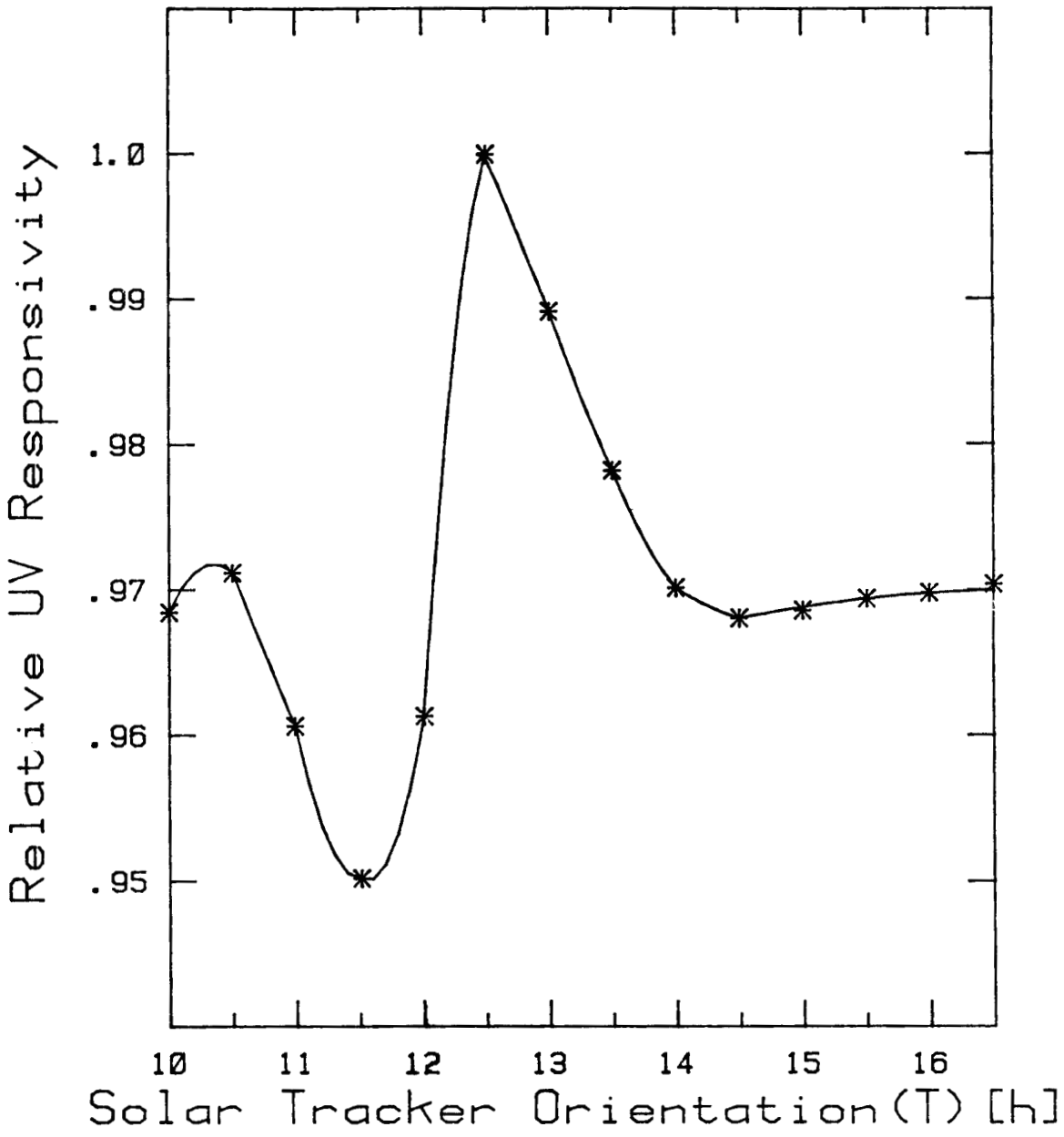

Figure 9. Relative system responsivity (without diffuser) as a function of tracker mirror orientation (T). (Time of day T is a convenient variable for designating the orientation of a mirror that is tracking the sun.)

$$\frac{S(\lambda_o)}{S^s(\lambda_o)} = \frac{\int_{\Delta\lambda}\int_{\Delta A} R_{00}(T)\cdot\left(\int_{\Delta\omega} L_0\cdot\cos\theta\cdot d\omega\right)\cdot dA\cdot d\lambda}{\int_{\Delta\lambda}\int_{\Delta A} R_{00}(T)\cdot\left(\int_{\Delta\omega_s} L_0^s\cdot\cos\theta\cdot d\omega\right)\cdot dA\cdot d\lambda} \tag{1.9}$$

and

$$\frac{S(\lambda_o)}{S^s(\lambda_o)} = \frac{\int_{\Delta\lambda}\int_{\Delta A} R_{00}(T)\cdot E_\lambda\cdot dA\cdot d\lambda}{\int_{\Delta\lambda}\int_{\Delta A} R_{00}(T)\cdot E_\lambda^s\cdot dA\cdot d\lambda}\,. \tag{1.10}$$

In our application, E and E^s are constant over the receiving aperture area ΔA to well within one percent so that

$$\frac{S(\lambda_o)}{S^s(\lambda_o)} = \frac{\int_{\Delta\lambda} E_\lambda\cdot\left(\int_{\Delta A} R_{00}(T)\cdot dA\right)\cdot d\lambda}{\int_{\Delta\lambda} E_\lambda^s\cdot\left(\int_{\Delta A} R_{00}(T)\cdot dA\right)\cdot d\lambda} \tag{1.11}$$

$$\frac{S(\lambda_o)}{S^s(\lambda_o)} = \frac{\int_{\Delta\lambda} E_\lambda\cdot R_E(T)\cdot d\lambda}{\int_{\Delta\lambda} E_\lambda^s\cdot R_E(T)\cdot d\lambda} \tag{1.12}$$

where $R_E(T)$ $[S\cdot W^{-1}\cdot m^2]$ is the irradiance responsivity expressed as a function of tracker orientation, T. Under certain conditions, which will be discussed later,

$$\frac{S(\lambda_o)}{S^s(\lambda_o)} = \frac{R_E^f(\lambda_o,T)\cdot\int_{\Delta\lambda} E_\lambda\cdot z(\lambda_o,\lambda,T)\cdot d\lambda}{R_E^f(\lambda_o,T_s)\cdot\int_{\Delta\lambda} E_\lambda^s\cdot z(\lambda_o,\lambda,T_s)\cdot d\lambda} \tag{1.13}$$

where $R_E^f(\lambda_o,T)$ $[S\cdot W^{-1}\cdot m^2]$ is the <u>irradiance responsivity factor</u>[1] at wavelength λ_o and

[1]In NBS Tech. Note 910-4 [6] (pp. 15 and 17), the responsivity factor r^f was defined in terms of the relative responsivity $r = z\cdot r^f$, and $R_E = K\cdot r = K\cdot z\cdot r^f$. In this chapter it is more appropriate to absorb K into the responsivity factor resulting in $R_E = z\cdot R_E^f$, where R_E^f is called the <u>irradiance responsivity factor</u>. Note that R_E, K, and R_E^f all have the same unit-dimensions $[S\cdot W^{-1}\cdot m^2]$, while r, r^f, and z are dimensionless. In general, the slit-scattering function is also a function of the polarization of the incident flux and therefore of the tracker orientation T, as indicated in eq. (1.13).

tracker orientation T, and where z is the slit-scattering function (p. 15, 910-4) [6]. When the diffuser is employed, R_E or R_E^f and z will be independent of tracker orientation T.

OTHER FACTORS in EXPERIMENTAL DESIGN

Scattering and distortion. For many spectroradiometric measurements, the error produced by assuming that E_λ is constant (so that it may be moved outside of the integral sign) in eq. (1.12) or eq. (1.13) is not great. This is not so in our case.

The biggest problem is the unwanted response to the large and extensive (relative to wavelength) spectral flux far from the wavelength setting of the spectroradiometer that is detected by the instrument (p. 24, 910-4) [6]. This is caused by the very long wavelength wing of the responsivity function (see figure 10). If this wing of the responsivity function is even 10^{-8} relative to its peak, a typical value for a high-quality double monochromator, calculations show that the amount of flux "leaked" or "scattered" at 290 [nm] for a spectral distribution similar to that in figure 1 is about equal to the actual spectral irradiance at 290 [nm]. The amount of leakage changes very little with monochromator wavelength setting. Thus we expected significant scattering below about 293 [nm] and would probably have to determine the wings of the responsivity function experimentally and deconvolute (p. 35, 910-4) [11] the numerator of eq. (1.12) if results accurate to 5-10 percent are desired at the short wavelengths.

In addition to the wings of the responsivity function producing an error or uncertainty due to scattering, the central portion can cause an error if the spectral irradiance being measured does not vary linearly with wavelength (p. 26, 910-4) [6]. This effect is referred to as distortion. Calculations show that the curvature[1] of the spectral distribution in figure 2 is sufficient to produce an error of about 20 percent when the spectral slitwidth is 1 [nm]. However, if one were only interested in the average spectral irradiance over a 1 [nm] interval, the error would be reduced to about 5 percent. Because of the structure actually present in the spectral distribution (figures 3 and 4), use of a narrower spectral slit width such as 0.18 [nm] does not reduce the distortion. Therefore, deconvolution calculations (Chapter 8, 910-4) [11] of some type will be required and for this purpose the central portion of the responsivity function will have to be determined experimentally.

Wavelength accuracy. A disadvantage of using a 1 [nm] spectral slit width as in figure 2 is that the wavelength uncertainty of the instrument would have to be limited to about 0.01 [nm]. The slope of the spectral distribution in figure 2 at 290 [nm] is about 100 percent per nanometer [nm]. The wavelength uncertainty of the best small- or medium-sized monochromators is usually 10 to 20 times larger than 0.01 [nm]. It appears that obtaining adequate wavelength accuracy will be a problem in this measurement. One solution would be to use a small spectral slit width and use the features of the spectral

[1]To see the extensive curvature one must replot the figure with a linear ordinate.

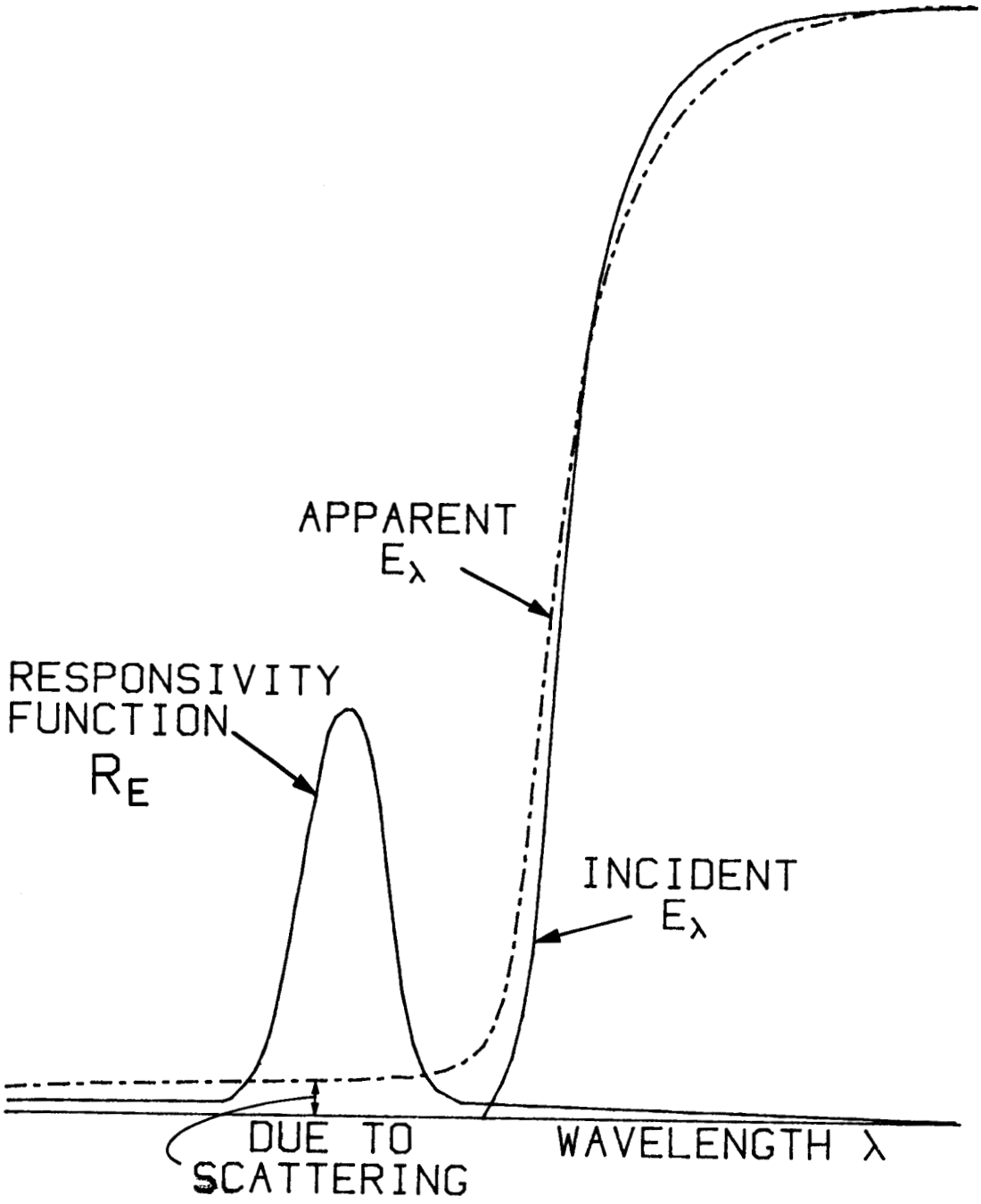

Figure 10. Response in the cut-off region showing the effect of the long wavelength wing of the responsivity function.

structure seen in figure 4 as a (wavelength) self-calibration to help reduce the wavelength uncertainty.

Computer control. Finally, careful analysis of the measurement configuration has shown that without a diffuser -- and this is the configuration required for the low spectral fluxes below 305 [nm] -- the responsivity function will depend on time (through tracker orientation) as indicated in eq. (1.12). In addition, temporal variations in atmospheric conditions (e.g., clouds) make it desirable to perform the measurements in as short a time as possible. On the other hand, the signal at the shortest wavelengths will be very small and probably require integrating for 5 or 10 [min]. The flexibility required to handle these various timing problems efficiently suggests utilizing a computer for controlling the time sequence in which data are taken and for storing and conveniently reducing these data.

DESCRIPTION of SPECTRORADIOMETER. After careful consideration of the various factors discussed in the previous sections, the spectroradiometer system shown in figure 5 was designed and developed. There are four major subsystems of the spectroradiometer consisting of the monochromator, the detection system, the amplification and counting system, and the computer control and data handling system.

The major monochromator specifications that were either required or highly desirable were:

(1) Wavelength reproducibility of 0.01 [nm].

(2) Spectral slit width of about 0.2 [nm] and possibly 1 [nm].

(3) A slit-scattering function that did not exceed 10^{-8} of its peak value at 50 [nm] from its peak wavelength.

(4) Angular aperture at least as large as that of an f/5 system.

(5) Spectral range at least from 280 [nm] to 370 [nm].

(6) Weight less than 1 [kg] and dimensions less than 25 [cm] × 25 [cm] × 50 [cm].

We were fortunate to find that Dr. William Fastie of Johns Hopkins University had recently designed a monochromator intended to meet or exceed these specifications. A few of these instruments had already been produced commercially.[1] We borrowed one of these monochromators and checked its performance relative to the above specifications. All specifications were satisfied except the wavelength reproducibility which was about five times poorer than desired. We made some design modifications that we thought had a good chance of improving the wavelength performance and let a contract for construction. The major features of the final design were:

(1) All Invar 36 construction and all optical materials of Cervit to assure thermal stability.

(2) Screw driven sine wavelength drive with stepping motor and encoder readout to 0.001 [nm] and setability to 0.005 [nm].

[1]Research Support Instruments, Inc., 10610 Beaver Dam Road, Cockeysville, MD 21030.

(3) Double Ebert-Fastie (dispersion cancelling) monochromator with focal length of approximately 125 [mm] and optical speed of f/5.

(4) Holographic gratings of 3600 [grooves per nm].

(5) All optical elements super polished and mirrors coated in such a way as to optimize high specular reflectance and low diffuse reflectance (scattering).

(6) Fixed (non-adjustable) slits with spectral slit widths of 0.2 [nm] and 1 [nm].

(7) Weight less than 4.5 [kg] and dimensions less than 15 [cm] × 15 [cm] × 30 [cm].

The cost was approximately $27,000 in 1980.

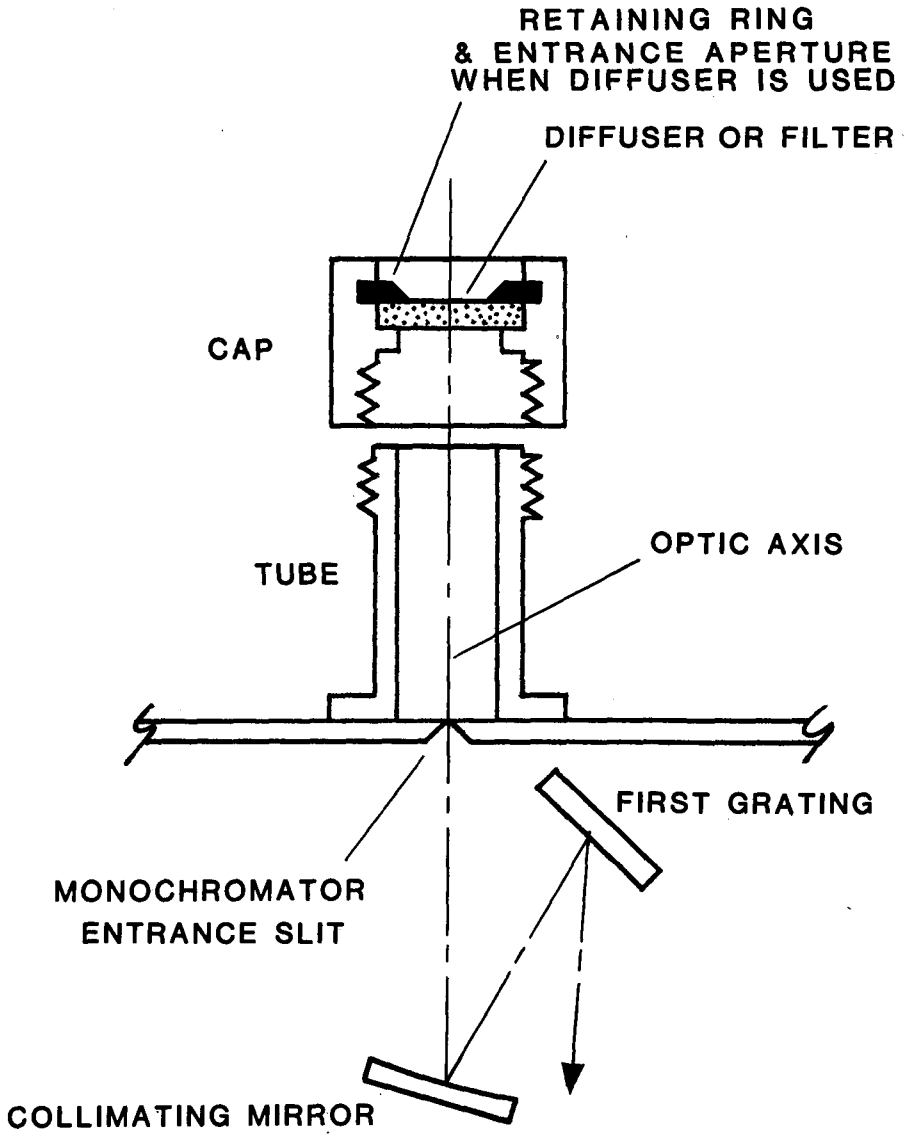

Figure 11. Schematic diagram of diffuser/filter system.

The above monochromator did not include a means for mounting diffusers or filters in front of the entrance slit or a cooled detector following the exit slit. These additions were designed and fabricated at NBS.

The diffuser/filter mounting system allowed for rapid, reproducible placement or interchange of filters and provided a means of easily locating the optic axis of the instrument for alignment purposes. Figure 11 is a schematic diagram of the system. The tube, shown in the figure, is mounted by screws onto the front (entrance-slit portion) of the monochromator in a position so that it is coaxial with the monochromator's optic axis.[1] The cap, when screwed tightly on the tube, conveniently insures good reproducibility in positioning filters. One normally would have as many caps as filters or combinations of filters.

A schematic diagram of the detection system is shown in figure 12. The quartz lens and photomultiplier are positioned so that the exit slit is defocused on the cathode of the photomultiplier. The larger area of irradiation minimizes the effects (noise and instability) of cathode non-uniformity and of small vibrations or motions.

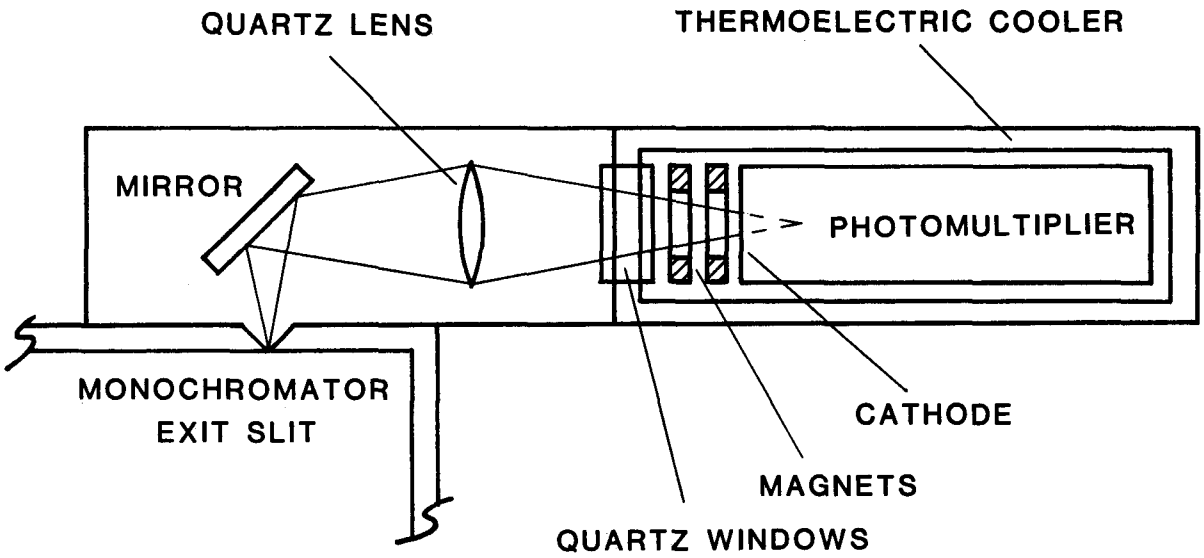

Figure 12. Detector system.

[1]The optic axis is the central ray of the full optical beam that can traverse the monochromator. Normally for a well-aligned monochromator, the optic axis passes through the centers of all the slits and the centers of all the optical elements. A small HeNe laser is useful for establishing the optic axis and the alignment of this axis relative to the tracker or external apertures.

The purpose of the ring magnets is to reduce the effective size of the cathode. The magnetic field produced by the rings permits only those thermal electrons that are emitted from about a 0.5 [in] diameter area of the cathode to strike the first dynode. This factor plus cooling to about -20°C with the thermoelectric cooler minimizes dark current (or dark counts) which is particularly important at the low flux levels at wavelengths below about 292 [nm].

The photomultiplier has a bialkali cathode and was selected for high quantum efficiency and low dark count. In order to reduce the amount of scattered signal detected, a Cs-Te (solar blind) cathode was considered. However, a bialkali cathode together with a "solar blind" filter (transmittance shown in figure 13) accomplishes the same thing but with a higher quantum efficiency at 290 [nm].

The output signal of a photomultiplier, resulting from an incident photon that has ejected a photo-electron, consists of a burst or pulse of electrons lasting only a few nanoseconds. When the photon rate (incident flux level) is high these occur too close together (may even be superimposed) for them to be detected individually. The average electron flow must be measured. This is the so-called current measuring mode which is used in most radiometric applications using photomultipliers. However, when the flux level is low, as in our case at the shorter wavelengths, these electron bursts or pulses are sufficiently separated so that they can be detected individually. This is the photon counting mode. Because the flux level at wavelengths below 295 [nm] is so low, we decided to use the photomultiplier in a photon counting rather than a current measuring mode.

The photon counting mode has a number of advantages over the current measuring mode. Noise and dark counts (signal counts when a shutter is in place so that the flux being measured is blocked or shuttered) can usually be reduced, relative to the current mode, because most pulses that are produced by sources other than incident photons (e.g. thermionic electrons and stray electrons from dynodes) have a smaller amplitude and can be rejected by proper setting of the threshold voltage in the discriminator (see figure 5). Noise from electronic components and connections, leakage currents, power lines, and external fields can be made insignificant or minimized through digital processing and counting procedures. The average signal in the current measuring mode is directly affected by all the above types of noise but the number of pulses per second in the photon counting mode is not. Another advantage in the photon counting mode is that the counting rate is not as highly sensitive to the dynode voltages as is the average signal in the current measuring mode. Thus, much less stability and control are required in the high voltage power supply used for supplying the dynode voltages.

One disadvantage of the photon counting mode is that, for very high photon fluxes, the observed counting rate S' [$c \cdot s^{-1}$] is not exactly proportional to the incident flux. This is because there is a significant probability of two photons arriving within the resolving time (dead time) of the instrument (pulse overlapping). Without this

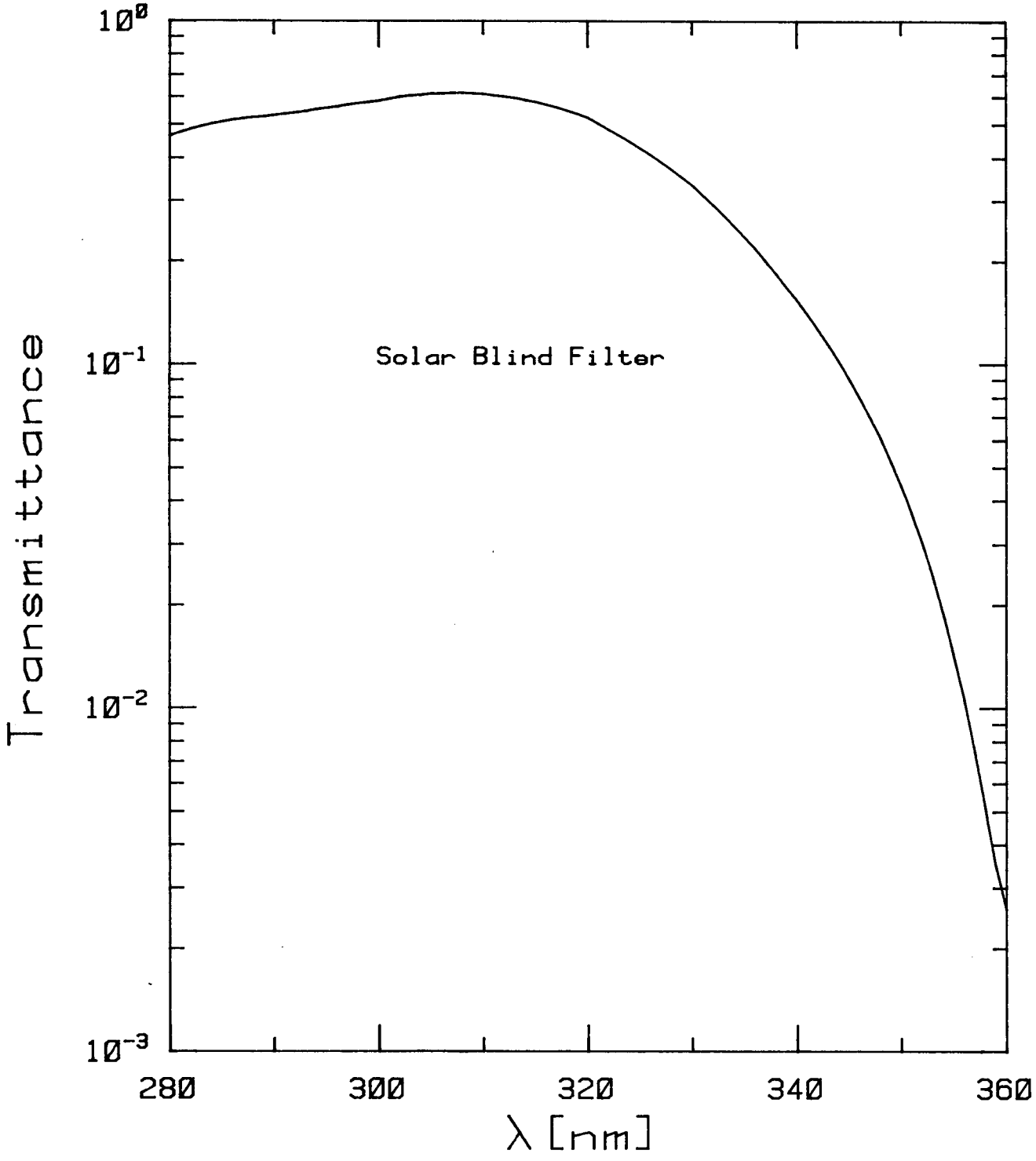

Figure 13. Spectral transmittance of solar blind filter.

proportionality (linearity), we can't do many of the things with the measurement equation that we would like to do.[1]

Fortunately there is an easy way of handling the non-linearity in the current problem. This is done by assuming that the flux responsivity is constant (linearity exists) and then correcting the observed output signal to what it would have been if this constancy had actually existed. Operationally one might think of the "detector" as consisting of the photomultiplier and associated electronics together with a computer or hand calculator which provides a correction from the indicated deficient rate S' to a quantity S that is exactly proportional to the actual incident photon flux. An approximate relationship between S' and S is [12]

$$S/S' = C(S') \cong 1 + t \cdot S' \tag{1.14}$$

where $C(S')$ is the "correction factor" for transforming the observed counting rate S' $[c \cdot s^{-1}]$ to the "correct" counting rate S, and t $[s \cdot c^{-1}]$ is the resolving time of the system. Differences between S' and S can be quite significant. For example, with $t = 10^{-7}$ $[s \cdot c^{-1}]$, a typical value, and $S' = 10^{6}$ $[c \cdot s^{-1}]$, the "correct" counting rate differs from the observed counting rate by 10 percent.

High quality photon counting systems are now available commercially as "shelf items." We selected one of these for this application. The major points to consider in this selection are over-all stability and ease of operation and required resolving time and integration time.

The computer control and data handling system is the remaining subsystem (figure 5) to be discussed. This subsystem consists of a 48K RAM microcomputer, dual floppy 8 [in] disk drive, terminal/video screen and printer. We purchased standard, readily available commercial items. The electronic circuitry (interfacing) required to couple the computer system to the rest of the spectroradiometer was designed and constructed at NBS. This is not a difficult task for a digital electronic engineer. It is also possible to obtain the interface electronics commercially.

The computer can be programmed to start measurements at a particular wavelength, integrate the counts for any time interval from a fraction of a second to hours and repeat this at any other wavelength or group of wavelengths. In addition to the

---

[1]When the measurement equation was first derived in Chapter 5 [4], we indicated that the assumed constancy of the flux responsivity with respect to the magnitude of the flux was a convenience. However, we have come to realize that it is a necessary assumption for much that we want to do when applying the measurement equation. Examples of this are in going from eq. (1.12) to eq. (1.13) and in the definition $R = K \cdot z \cdot r^{f}$. (See footnote on page 16.) An in-depth treatment of linearity is planned for a forthcoming chapter of this Manual.

wavelength, total signal counts, and counts per second, the ambient temperature, time, and date are also recorded. As data are obtained they may be viewed on the video screen, and/or printed and stored on a floppy disk. Printing the data is usually delayed until all observations for the day are complete because concurrent printing increases the time required to perform the experiment.

CHARACTERIZATION of SPECTRORADIOMETER. In order to minimize the errors or uncertainties of a radiometric measurement, the measuring instrument's responsivity should be determined as a function of each radiation parameter for which there are significant differences between the unknown radiant flux being measured and that of the standard. The pertinent radiation parameters were discussed in the sections on the measurement configuration and the measurement equation. The two radiation fluxes in this problem were the sun and a frosted 1000 [W] tungsten halogen lamp at 400 [cm]; the parameters for which the two fields differed significantly were magnitude (absolute value of the spectral irradiance) and spectral distribution.

Relative to magnitude. As pointed out earlier, the responsivity of photomultipliers when used as photon counters decreases at sufficiently high levels of incident photon flux in accordance with eq. (1.14). With the very large magnitude and variation of magnitude of the solar terrestrial irradiance in the spectral region of interest, these decreases (non-linearity) could be significant. This problem has been addressed by determining $C(S')$ of eq. (1.14) and using the "corrected" output signal $S = C(S')\cdot S'$ instead of the observed signal S' in the measurement equation. In this way linearity with all its desirable features is effectively maintained.

The correction $C(S')$ was obtained by first determining the spectral transmittance τ of a filter at a sufficiently low incident flux ϕ_i (and corresponding low observed counting rate S') where $C(S') = 1$ and then repeating the measurement of τ with higher incident flux levels up to the highest flux level or counting rate obtained in the solar measurements.[1] In order to achieve a more accurate approximation, the power series in S' [eq. (1.14)] was carried to one more term; i.e.,

$$C(S') \equiv S/S' = 1 + t\cdot S' + u\cdot S'^2. \qquad (1.15a)$$

---

[1]This technique can be used in the current problem because it is well established that for photomultipliers, when the counting rate is sufficiently low, $S' = R\cdot\Phi$ and therefore $\tau = \frac{\Phi_t}{\Phi_i} = \frac{S'_t}{S'_i}$. Otherwise, if the responsivity of a detector were such that $S' = R\cdot\Phi^n$ at low levels, S'_t/S'_i would still be constant as a function of S'_i at sufficiently low S'_i but equal to τ^n instead of τ. These filter measurements alone will not determine the value of the exponent n.

The transmittance τ of the filter referred to above would then be

$$\tau = C(S'_t) \cdot S'_t / [C(S'_i) \cdot S'_i] \tag{1.16a}$$

For S'_i sufficiently small $C(S'_i) = C(S'_t) = 1$ and $\tau = S'_t/S'_i$. For larger values of S'_i, substituting eq. (1.15a) into eq. (1.16a)

$$\tau = \left(S'_t + t \cdot S'^2_t + u \cdot S'^3_t\right) / \left(S'_i + t \cdot S'^2_i + u \cdot S'^3_i\right) \tag{1.16b}$$

and rearranging terms

$$\tau S'_i - S'_t = \left(S'^2_t - \tau \cdot S'^2_i\right) \cdot t + \left(S'^3_t - \tau \cdot S'^3_i\right) \cdot u. \tag{1.16c}$$

Measurements of τ, S'_i and S'_t were performed with the 253.7 [nm] spectral line from a temperature-stabilized low-pressure mercury-discharge lamp source from which the irradiance (flux) level was varied by the insertion of additional filters, taking care not to disturb the geometry of the beam incident on either the filter being measured or on the monochromator. Using these data, t and u were obtained from a least squares fit of eq. (1.16c). For values of S' as high as $2.5 \cdot 10^6$ $[c \cdot s^{-1}]$,

$$S/S' \equiv C(S') = 1 + 6.927 \cdot 10^{-8} \cdot S' + 7.174 \cdot 10^{-15} \cdot S'^2 \tag{1.15b}$$

where S is the "corrected" output signal and S' is the actually observed output signal in $[c \cdot s^{-1}]$.

There was another problem relative to the responsivity that we uncovered which is significant at very low counting rates. In our system, about once every 5 [min], we witnessed a burst of 50 to 100 counts. This means about a 1 percent error for a counting rate of 30 $[c \cdot s^{-1}]$ when integrating for 5 [min] and larger errors at lower counting rates. This effect was not significant down to 290 [nm] because the lowest counting rate at this and longer wavelengths was about 40 $[c \cdot s^{-1}]$. The effect was significant at shorter wavelengths because the lowest counting rate was about 5 $[c \cdot s^{-1}]$ at 289 [nm], 2 at 288, and 1 at 287. However, we did not try to solve this problem because scattering was a serious problem below 290 [nm], and, as you will see shortly, we were not able to correct for this scattering. So an additional error was immaterial. We were only able to satisfy our desired overall 5-10 percent uncertainty at wavelengths of 290 [nm] and higher.

Relative to spectral distribution -- wavelength accuracy. The most obvious concern relative to the large difference in spectral distribution between the standard source and the sun is that of wavelength accuracy. The spectral irradiance of the sun falls off at

a rate of about 1 percent per 0.01 [nm]. Therefore a wavelength uncertainty of 0.01 [nm] or less is desired.

The first step in characterizing the spectroradiometer relative to wavelength was to check its reproducibility. The 296.728 [nm] mercury spectral line from a low pressure mercury source was used for this purpose. With the spectral slit width of the instrument being 0.2 [nm], the "peak" of the line was too broad to utilize its position to check wavelength reproducibility to 0.01 [nm]. A wavelength reference which is orders of magnitude more sensitive than the peak of a spectral line is the steep sides of the line. When the spectral slit width is large compared to the spectral line width, this is really the side of the slit-scattering function. A suitable region to use is that part of the spectrally scanned line which is a factor of 10^{-2} less than the peak. The rate of change of signal with wavelength at 10^{-2} of the peak is at least 50 percent per 0.01 [nm] compared to about 0.5 percent per 0.01 [nm] at the peak.

We found that the wavelength reproducibility for our monochromator varied from 0.01 [nm] to about 0.05 [nm] depending on the prior (immediate) history of the wavelength drive and setting. The 0.01 [nm] figure relates to scanning repeatedly over a spectral line, covering a range of about 1 [nm] and taking a few minutes for each scan. The 0.05 [nm] reproducibility corresponds to scanning repeatedly over the line but covering a range of about 60 [nm] or 30 [min] for each scan. By cleaning, tightening, adjusting, and lubricating, it was possible to improve the 0.05 [nm] only slightly to 0.04 [nm]. It was clear that to achieve 0.01 [nm] wavelength uncertainty would require a data-taking schedule (short-term, small wavelength range repetitive scans) that was not practical in most cases. Another possiblity for realizing a 0.01 [nm] reproducibility was to use the solar structure shown in figure 4 to perform a wavelength self-calibration in each experimental run.

In addition to the short-term reproducibility just discussed, wavelength accuracy may also depend on somewhat longer term changes (few hours) caused by ambient temperature variations. The effect of instrument temperature on wavelength setting was checked and found to be only about 0.01 [nm] per 3 [°C] change in temperature. This was considered to be an insignificant factor in our case compared to the short-term reproducibility.

Wavelength accuracy is also affected by any lack of symmetry in the slit-scattering function, particularly when the wavelength determination is made by the technique (sides of slit-scattering function) described earlier. This will be discussed in the next section along with the effects of distortion and scattering.

Relative to spectral distribution -- distortion. The central portion of the slit-scattering function is required in order to ascertain and correct for the amount of distortion. We determined the central portion of the slit-scattering function down to about 10^{-2} of its peak value by spectrally scanning over various mercury lines between 289.4 and 365 [nm]. It was not possible to get lower than about 10^{-2} with a mercury line because of

the background radiation from other lines, particularly the 254 [nm] line. For values below 10^{-2}, we used a laser line at 290 [nm]. We obtained this UV line from a tunable CW dye laser operating at 580 [nm] by frequency doubling with an appropriate crystal. The laser beam was positioned along the optic axis of the monochromator with the diffuser in place. The size of the beam was adjusted so that the instrument was irradiated with about the same solid angle as that subtended by the sun. A spectral scan over these lines should be a good approximation to the central portion of the slit-scattering function (p. 20, 910-4) [6]. When irradiated on axis, the central portion was quite asymmetric. However, the degree of asymmetry changed with the direction of the beam entering the monochromator. It was possible to find a particular direction slightly off axis, for which good symmetry was realized. This was done and all solar measurements made without the diffuser were made with the solar beam incident from this direction. The asymmetry was also quite pronounced in the diffuse mode; that is, with the diffuser filled with optical radiation. However, by trial and error, it was possible to find an area on the diffuser (equal to about one-half the total area) which also resulted in a symmetric slit-scattering function.

Figure 14 shows an example at 296 [nm] of that portion of the slit-scattering function obtained with the mercury lines. Also shown are triangular and Gaussian functions having the same spectral slit width. These functions do a fair job of representing our measured slit-scattering function down to about 0.3 of its value. From 0.3 to about 10^{-5}, a much better representation is the following function:

$$z(\lambda_o,\lambda) = \exp[-126.38\cdot(\lambda_o-\lambda)^2] + \tfrac{1}{2}\exp[-2.983\cdot10^{-3}\cdot(\lambda_o-\lambda)^{-2} - 1.2037\cdot10^{4}\cdot(\lambda_o-\lambda)^{4}], \tag{1.17}$$

where λ_o is the monochromator setting and λ is the wavelength in nanometers [nm]. The slit-scattering function for values less than 10^{-5} is discussed in the next section. Incidentally, the spectral slit width varied slightly with wavelength from 0.183 [nm] at 289 [nm] to 0.165 [nm] at 312 [nm] and then back to 0.176 [nm] at 334 and 365 [nm].

Convolution calculations indicated that it was more important, relative to distortion effects, to know that the slit-scattering function was symmetric than to know its exact shape or width. Also, the existence of symmetry meant that wavelength calibrations could be performed by determining the average of the wavelengths on the two sides of the slit-scattering function where the value of the function is about 10^{-2} of its peak value.

Relative to spectral distribution -- scattering. In order to correct for scattered radiation that we anticipate to be significant below about 292 [nm], the long wavelength wing of the slit-scattering function is required. We tried to obtain these wings with our tuned UV laser, but the signal-to-noise ratio was too small to get lower than about 2×10^{-7},

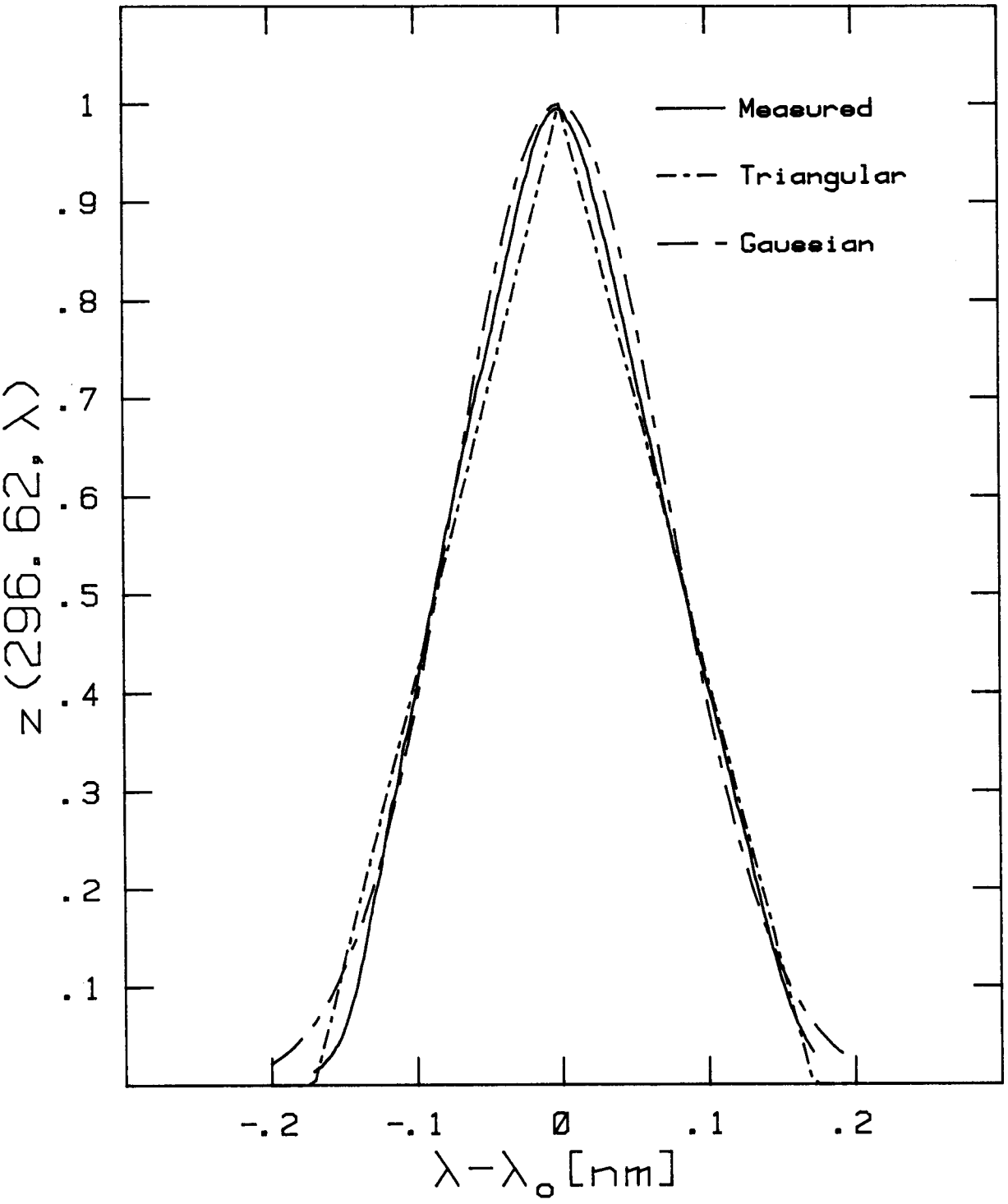

Figure 14. Measured slit-scattering function $z(\lambda_o,\lambda)$ at λ_o = 296.62 [nm] and triangular and Gaussian functions having the same spectral width.

even with an integrating time of one hour. The 2×10^{-7} was the value at about 1.8 [nm] from the peak. We obtained a rough idea of the magnitude of the more distant wing by scanning over the short wavelength portion (p. 22, 910-4) [6] of the 253.7 [nm] spectral line from a very intense low pressure mercury source using suitable filters to remove radiation other than that scattered from the 253.7 [nm] line itself. At 200 [nm] the result was 1.4×10^{-8}. Thus the slit-scattering function at +53.7 [nm] (i.e., 253.7-200) from the peak is about 10^{-8} when the monochromator is irradiated with highly incoherent radiation that fills the f/5 field of view.

So, much to our disappointment, we were not able to obtain an accurate (5 or 10 percent) determination of the distant wing of the slit-scattering function and would not be able to accurately correct for scattering. This will be possible when a tunable laser is available with about 10 [mW] of power at 290 [nm]. Until then, the short wavelength limit for our accurate measurements will be determined by the wavelength at which scattering begins to be significant. The solar data itself will reveal this wavelength, as will be shown shortly.

DATA TAKING. In this section we discuss not only details of the actual data taking but also alignment of the monochromator relative to the sun, alignment of the tungsten lamp standard, and calibration using the standard.

Monochromator alignment. Careful alignment of the monochromator was essential prior to making any solar measurements, particularly when the diffuser was not used. Figure 8 shows that an angular misalignment of a degree would result in a significant error. Also, as mentioned in the previous section, an angular misalignment would destroy the spectral symmetry of the slit-scattering function reducing wavelength accuracy and increasing distortion.

The monochromator was aligned in the following manner. A low-power He/Ne laser was set up in the laboratory and aligned so that its beam passed upward approximately through the center of the solar tracker. Then the laser was fine-adjusted in position and orientation so that its beam (see figure 15) did not move relative to the upper aperture when the tracker followed the sun. This meant that the laser beam was striking each tracker mirror at the intersection of the plane of the mirror with the vertical and horizontal axes of rotation, as indicated in figure 15. After this condition was realized, the upper aperture was positioned and secured so that the laser beam passed through its center. The 5 [in] diameter lower aperture was also positioned so that the laser beam passed through its center. Next the laser was set up on the roof and again aligned so that its beam went downward through the centers of both apertures. The monochromator was then positioned and oriented so that the laser beam struck the center of the entrance slit and coincided with the optic axis. This was easy to accomplish because the tube of the diffuser/filter system had been made and mounted so that its top surface was perpendicular to the optic axis. A microscope cover glass placed on this surface was therefore perpendicular to the optic axis and the monochromator was rotated

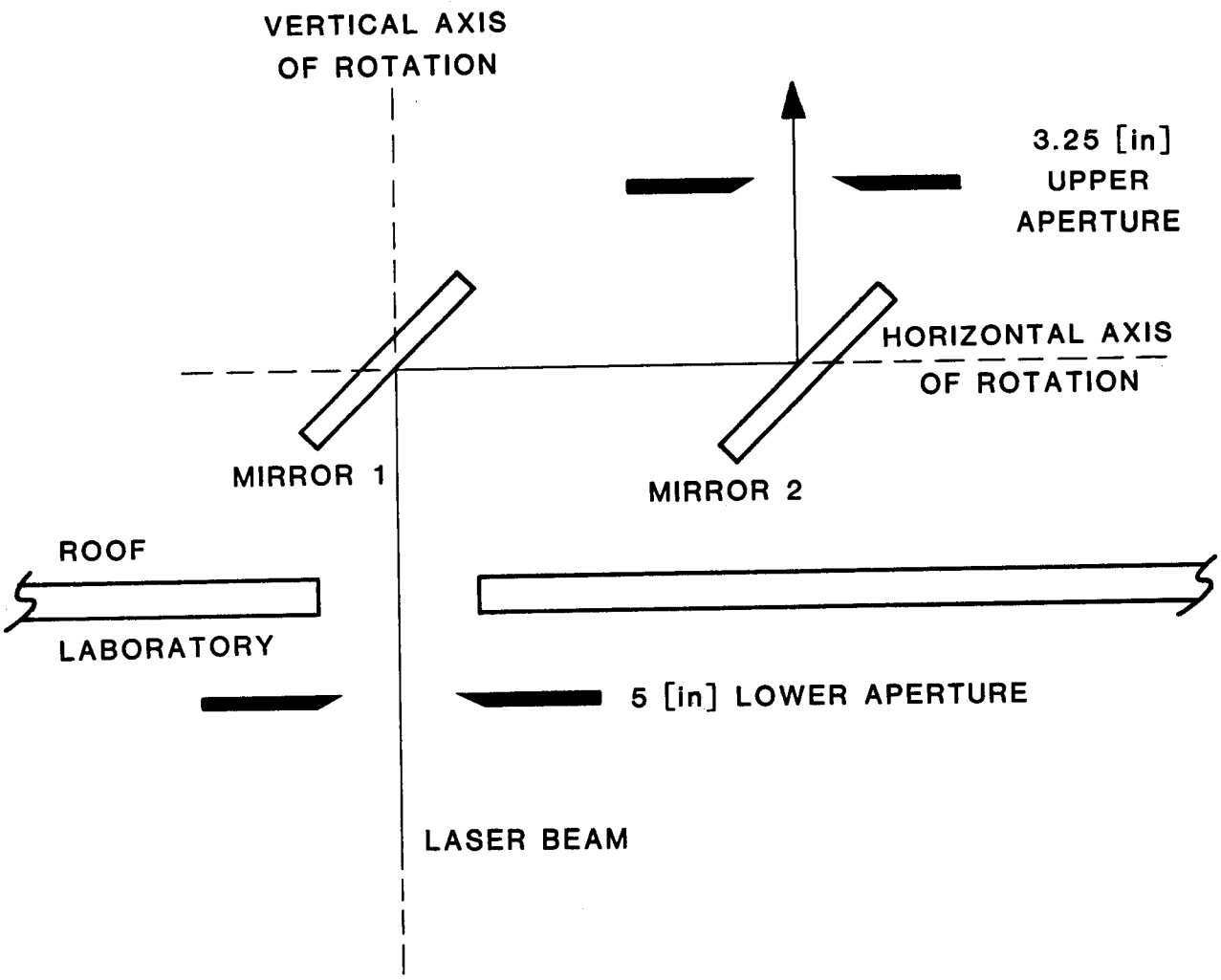

Figure 15. Use of a laser beam to find the axes of the solar tracker.

until the laser beam retroreflected back on itself (or the center of the 5 [in] aperture). Finally, the monochromator was rotated about its entrance slit by the amount required (0.4 [deg]) for a spectrally symmetric slit-scattering function.

In performing the above alignments it was essential to use a heavy, stable, laser mount with micrometer adjustments for translation and two orthogonal rotations about axes perpendicular to the laser beam. In addition, it was convenient to use circular aluminum inserts each with a translucent "button" with a small hole drilled through the center as shown in figure 16. The insert could be placed in the aperture and used as a convenient indicator of the aperture center while adjusting the laser beam.

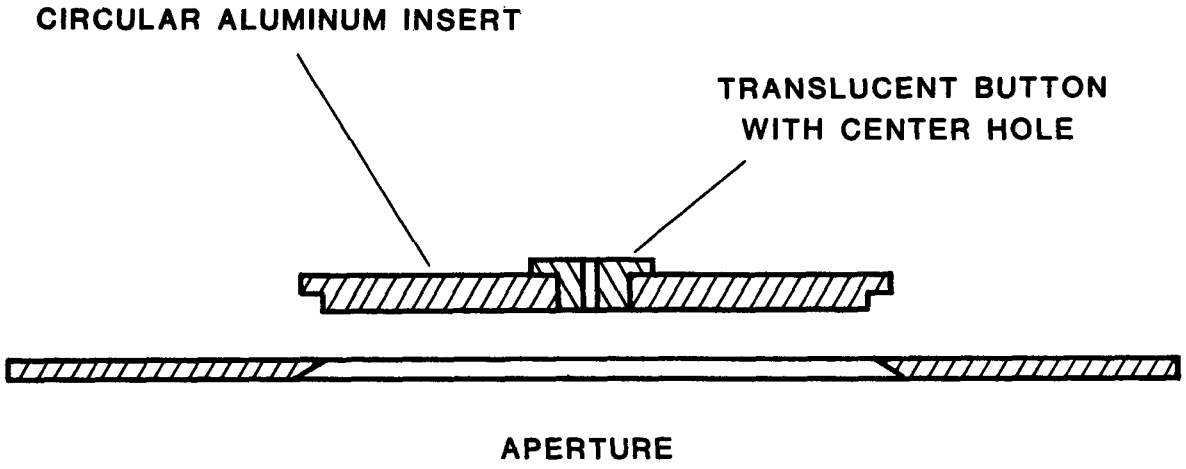

Figure 16. Inserts used to indicate the centers of the tracker apertures.

Alignment of standard. For the spectroradiometer calibration it was necessary to position the standard lamp precisely. The procedure was as follows. The He/Ne laser was mounted on the roof above the tracker and aligned until the laser beam went through the center of the button in the upper aperture insert (see figure 16) and was incident on the center of the monochromator entrance slit. Another insert similar to that in figure 16 was fitted into a rectangular piece of aluminum and positioned in the lower aperture as indicated in figure 17 so that the laser beam traversed its button also. The laser was then set up in the laboratory and aligned so that its beam traversed the buttons in the lower and upper apertures in the opposite direction. Then, the tungsten standard was mounted on the roof tracker so that its center was irradiated by the laser beam. The lamp mount was an aluminum tubular structure of sufficient lightness not to limit the smooth motions of the tracker and of sufficient rigidity so that the lamp was stably positioned relative to the 3.25 [in] tracker aperture. The distance between the entrance slit and the lamp was selected, as mentioned earlier, so that the lamp's largest dimension subtended about 0.5 [deg] (same as the sun) at the entrance slit. The actual distance was measured to be 396.3 [cm] with an uncertainty of about 0.5 [cm].

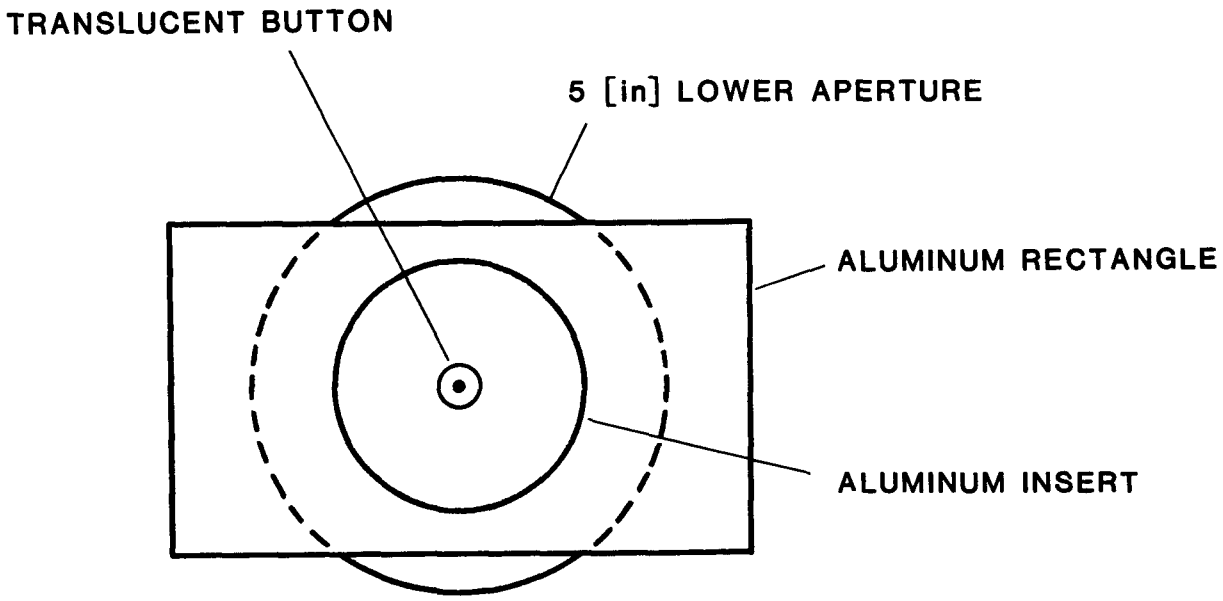

Figure 17. Looking down from mirror 1 in tracker at aluminum pieces and button used in lamp adjustment.

Spectral irradiance calibration. The standard lamp calibrations had to be frequent enough and extensive enough relative to wavelength, tracker position and filters so that a sufficiently accurate calibration was available for any time, wavelength and measurement configuration (tracker position or filter) for which solar data was taken.

Relative to time, calibrations were performed as often as practical, primarily whenever weather permitted. This turned out to be at least every other night during the period in which good solar data were obtained. Successive calibrations taken about 48 hours apart differed by a maximum of a few percent. Relative to wavelength, standard lamp calibrations were obtained between 340 and 280 [nm] at 5 [nm] intervals. Previous experience had shown this to result in a least squares fit with a standard deviation of the fit of a few tenths of a percent. To confirm that 5 [nm] intervals were adequate, one run was also taken at 1 [nm] intervals. To obtain the effect of tracker position, the 340-280 [nm] runs were obtained for about every half hour of tracker position between 10:00 and 16:30 EST. Figure 9 is a typical example of a relative tracker calibration. Though a complete calibration relative to the tracker was not performed every evening during which calibrations were performed, sufficient data were taken to show any changes in the relative tracker calibration over the eight days of data taking. No significant change was detected. Sufficient standard lamp data were also taken with the neutral density and solar blind filters and the diffuser to determine their transmittances and to detect any changes in their transmittances over the eight days of operation. None were observed. The spectral transmittances of each of these optical elements were obtained in the wavelength range in which they were used (neutral density filter and diffuser, 340-305 [nm]; solar blind, 296-287 [nm]). For optimum accuracy, it was necessary to obtain this transmittance with the same measurement beam configuration that was used in taking the solar data (as opposed, e.g., to using a general purpose spectrophotometer to determine the transmittances). This eliminated the need for a tedious characterization of the filters and the optical beam relative to uniformity and direction.

Wavelength calibration. Wavelength calibrations were made every morning and late afternoon. Five mercury spectral lines at 289.360, 296.728, 312.566, 334.148, and 365.015 [nm] from a low pressure pen ray lamp were used. The lamp was used with a 5 [mm] aperture in front of it and with the aperture at a distance of about 573 [mm] from the slit, so that the largest plane angle subtended by that aperture at the slit was 0.5 [deg]. The mercury lamp and its aperture were also positioned so that the path of this beam through the monochromator was the same as that of the solar beam. As discussed earlier, the wavelength encoder readout for each scanned spectral line was taken to be the average of the readouts on each side of the peak where the signal was exactly equal to 10^{-2} that of the peak (10^{-1} for the 289.36 [nm] line). To obtain an estimate of the wavelength hysteresis effects that had been observed, wavelength calibrations were performed starting at about 289 [nm] and going to about 365.4 [nm] and then back to 289 [nm].

Wavelengths for each of the five lines were always obtained in a spectral scan that was decreasing in wavelength. This was the case even when performing calibrations starting

with the 289 [nm] line and ending with the 365 [nm] line. Each line in this sequence was still scanned in decreasing wavelength to minimize backlash errors. A typical calibration correction curve is shown in figure 18 where the difference between the published wavelength of a line and the corresponding wavelength encoder readout is plotted against wavelength. The largest wavelength hysteresis usually observed was 0.04 [nm]. The dashed line in the figure, the mean of the calibrations in the two wavelength directions (indicated by arrows), was used as the calibration for the time these wavelength data were obtained.

Solar measurements. Solar data were taken in Gainesville, Florida between June 11, 1980 and June 18, 1980 whenever the sky was sufficiently clear. This meant that there were no visible clouds in the sun's line of sight. Four types of data were obtained for four different purposes. These were (1) short wavelength cut-off data (287-296 [nm] at 1 [nm] intervals), (2) data for ozone determinations (294.7 - 305.2 [nm] at a sufficient number of wavelengths so that the spectral structure could be used to obtain at least 5 spectral irradiances for which the wavelength uncertainty was not greater than 0.01 [nm]), (3) data for ozone determination at the "Dobson wavelengths" (305.5 - 340) [nm] and (4) data at various wavelength intervals of 0.1 [nm] to 2 [nm] over the wider spectral interval of the solar spectral irradiance which would be required for deconvolution calculations (295 - 340) [nm]. In all, eighty-one different experimental runs were carried out.

The electronic components of the spectroradiometer were left on continuously for the entire 8 days of data taking. The anode to cathode voltage on the photomultiplier was maintained at 1500 [V]. The discriminator voltage was set to produce a dark count rate of about 0.3 $[c \cdot s^{-1}]$.

Before starting an experimental run, a check was made to insure that the shadow of the 3.25 [in] tracker aperture was concentric with the diffuser/filter system. If the shadow was not centered, it was made so by overriding the computer control of the tracker stepping motors with a manually operated control. Next, the appropriate filter or diffuser cap was inserted and a computer program selected for one of the four types of data runs. In order to observe, during each run, all parts of the spectrum under closely similar atmospheric conditions and solar paths, integration times were limited to about 1 [s] or to that required to obtain about 10,000 [c]. An experimental run required between 3 and 30 [min] with most of them about 5 [min]. In order to minimize this run time, data being taken were usually stored on the computer disk, and a hard copy made at end of day. Continuous visual monitoring of the sun was maintained during the run to insure that no visible clouds were in line of sight of the sun. Notes were taken during the experimental run describing environmental conditions and commenting on anything that occurred that was considered potentially useful. As many of the measurements as possible were made within one hour of high noon ($\sim$12:30 EST). When comparisons were to be made; e.g., comparing the Dobson and "Sharp Cut-Off" ozone determinations, one type of run was made twice, and it bracketed the other type in time; and all runs were made in as short a

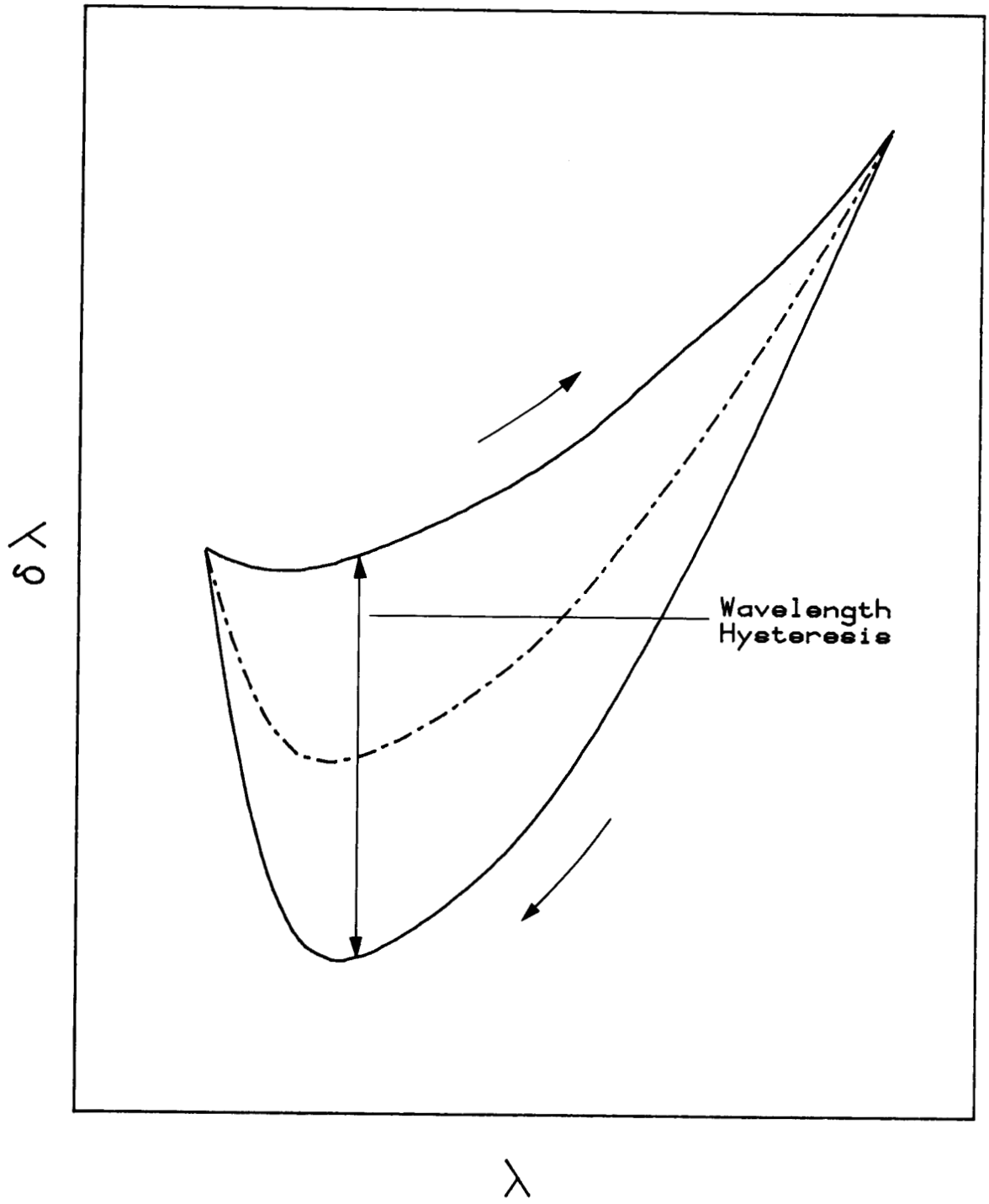

Figure 18. Typical correction curve for the monochromator wavelength readout. Maximum observed wavelength hysteresis was about 0.04 [nm].

time as possible. In this way, atmospheric changes were less likely to occur during the comparison, and if they did occur, would be more likely to be detected. Data taking was automatically interrupted via the computer program when a filter or diffuser had to be inserted. Ambient temperature control was limited to manual control of window air conditioners but the air temperature near the monochromator was taken and automatically recorded about once per minute. Barometric pressure readings were obtained continuously. Records for the weather parameters such as humidity, visibility, temperature, and wind, taken each hour, were available from the Gainesville Weather Station. Table 1 is an example of a typical computer printout of data obtained in one short run.

Table 1. Typical computer printout for a short run of data.

DATA FILE NAME- B:WSOLB1 **TIME 11:51:25 EST**
DATE 6/18/80

TEMPERATURE 25.039 [°C]

WAVELENGTH	PHOTON COUNT	COUNTING RATE [cps]
296.002	319828	159914.00
295.000	93692	46846.00
294.001	52306	26153.00
293.002	256625	8554.17
292.002	119052	3968.40
TIME- 11:53:52 EST	TEMPERATURE 25.097 [°C]	
291.000	26241	874.70
289.998	17264	287.73
288.998	6177	51.48
287.999	1278	10.65
287.000	3029	5.05
TIME- 12:09:25 EST	TEMPERATURE- 23.030 [°C]	

DATA REDUCTION and UNCERTAINTIES. Data reduction means obtaining the solar spectral irradiance E_λ at the wavelengths of interest or the average of E_λ weighted by the slit-scattering function. In this problem, because the spectral slit width is so much greater (0.18 [nm]) than the wavelength differences for which large changes occur in the solar spectrum (<0.01 [nm]), we must be satisfied with a weighted average of E_λ.

In reducing and analyzing the data, we start with the measurement equation, eq. (1.12),

$$\frac{S(\lambda_o,t,T)}{S^s(\lambda_o,t,T_s)} = \frac{C(S')\cdot S'(\lambda_o,t,T)}{C(S'^s)\cdot S'^s(\lambda_o,t,T_s)} = \frac{\int_{\Delta\lambda} E_\lambda(\lambda,t)\cdot R_E(\lambda_o,\lambda,t,T)\cdot d\lambda}{\int_{\Delta\lambda} E^s_\lambda(\lambda,t)\cdot R_E(\lambda_o,\lambda,t,T_s)\cdot d\lambda}, \tag{1.18}$$

where the independent variables λ_o (wavelength setting of the monochromator), t (time at which S' was obtained), and T (tracker orientation indicated by time) have been inserted to emphasize that the responsivity is a function of these variables. The irradiance responsivity may be written

$$R_E(\lambda_o,\lambda,t,T) = \tau(\lambda,t)\cdot z(\lambda_o,\lambda,T)\cdot R^f_E(\lambda_o,t,T), \tag{1.19}$$

where $\tau(\lambda,t)$ is the spectral transmittance at time t of any filter, including the diffuser, $z(\lambda_o,\lambda,T)$ is the slit-scattering function (p. 15, 910-4) [6][1], and $R^f_E(\lambda_o,t,T)$ is the responsivity factor for tracker orientation T. When we substitute eq. (1.19) into the measurement equation, eq. (1.18), we have

$$\frac{S'(\lambda_o,t,T)}{S'^s(\lambda_o,t,T_s)} = \frac{C(S'^s)\cdot R^f_E(\lambda_o,t,T)\cdot\int_{\Delta\lambda} E_\lambda(\lambda,t)\cdot\tau(\lambda,t)\cdot z(\lambda_o,\lambda,T)\cdot d\lambda}{C(S')\cdot R^f_E(\lambda_o,t,T_s)\cdot\int_{\Delta\lambda} E_\lambda(\lambda,t)\cdot z(\lambda_o,\lambda,T_s)\cdot d\lambda}, \tag{1.20}$$

where τ for the case of the calibration signal, S'^s, has been set equal to one because no filters were normally used in obtaining S'^s. The unknowns in this equation are $E_\lambda(\lambda,t)$ and z. We have reliable measurements for the central part of z, approximately ± 0.4 [nm] on either side of the peak, and we have an upper limit to the magnitude of z at +50 [nm] from the peak. This is about 10^{-8}. Roughly sketching in the intermediate values of z and then using this slit-scattering function in a simple deconvolution (p. 38, 910-4) [11] on spectral runs for which data were obtained to 287 [nm], we found that the computed scattering was about 100 times more than the observed signal count rate S' at 287 [nm]. The only explanation we have for this huge discrepancy is that the long

[1] In TN 910-4 [6], the slit-scattering function has the functional form $z(\lambda_o-\lambda)$. It is not necessary to restrict it to that form in this investigation, and we define it here more generally as

$$z(\lambda_o,\lambda,T) = \frac{R_E(\lambda,\lambda_o,t,T)}{R^f_E(\lambda_o,t,T)}.$$

wavelength wing of the slit-scattering function for our instrument when observing the sun without a diffuser[1] is about 10^{-10} rather than 10^{-8}. Calculations show that with a slit-scattering function equal to 10^{-10} in the long wavelength wing, scattering would be negligible down to 290 [nm]. This is experimentally confirmed by comparing S'(287), which is about equal to or greater than the scattered signal at 287 or 290 [nm], to S'(290). Since there is not enough power in the UV in available CW lasers to determine the distant wings of z accurately, the lower wavelength limit for accurate data reduction is about 290 [nm]. And since scattering is insignificant for $\lambda \geq 290$ [nm], we may limit $\Delta\lambda$ to only the central portion of z. Trial convolutions showed that it was sufficient for $\Delta\lambda$ to be equal to 0.44 [nm]; that is, 0.22 [nm] on either side of the peak of z.

For the wavelength range $\lambda_o \pm 0.22$ [nm], eq. (1.20) can be simplified as follows

$$\frac{S'(\lambda_o,t,T)}{S'^{s}(\lambda_o,t,T_s)} = \frac{C(S'^{s})\cdot\tau(\lambda_o,t)\cdot R_E^f(\lambda_o,t,T)\cdot\int_{\lambda_o-0.22}^{\lambda_o+0.22} E_\lambda(\lambda,t)\cdot z(\lambda_o,\lambda,T)\cdot d\lambda}{C(S')\cdot E_\lambda^s(\lambda_o,t)\cdot R_E^f(\lambda_o,t,T_s)\cdot\int_{\lambda_o-0.22}^{\lambda_o+0.22} z(\lambda_o,\lambda,T_s)\cdot d\lambda}. \qquad (1.21)$$

$$\frac{\int_{\lambda_o-0.22}^{\lambda_o+0.22} E_\lambda(\lambda,t)\cdot z(\lambda_o,\lambda,T)\cdot d\lambda}{\int_{\lambda_o-0.22}^{\lambda_o+0.22} z(\lambda_o,\lambda,T_s)\cdot d\lambda} \equiv \bar{E}_\lambda^z(\lambda_o,t) = \frac{C(S')\cdot S'(\lambda_o,t,T)\cdot E_\lambda^s(\lambda_o,t)}{C(S'^{s})\cdot S'^{s}(\lambda_o,t,T_s)\cdot\tau(\lambda_o,t)\cdot P}, \qquad (1.22)$$

where

$$P = \frac{R_E^f(\lambda_o,t,T,)}{R_E^f(\lambda_o,t,T_s,)} \qquad (1.23)$$

is the polarization correction required when the calibration data S'^{s} are obtained with tracker orientation T_s and solar data S' with tracker position T. Calculations involving eqs. (1.20) and (1.21) show that this simplification produces a negligible error (<0.3 percent). From previous experience, we expect that the difference between $z(\lambda_o,\lambda,T$

[1]Because the terrestrial sun is confined to such a small angle (0.5 [deg]), its irradiance on the entrance slit of the spectroradiometer is highly coherent. Calculations of the type described by Shumaker [26] show that for the f/5 spectroradiometer that we used the distant wings of the slit-scattering function could be reduced by this order of magnitude.

and $z(\lambda_o,\lambda,T_s)$ for $\lambda_o \pm 0.22$ [nm] is small, and we assume the effect of this difference in eq. (1.22) is insignificant.

All the data and the equations resulting from the various fits were stored on floppy disks. It was therefore a simple matter to write a program to compute $\bar{E}^z_\lambda(\lambda_o,t)$. This was done and $\bar{E}^z_\lambda$ was computed for all wavelengths in the 81 experimental runs. Examples of the data and results printed out from these computations are shown in tables B-1 through B-7, in Appendix 1B. Keep in mind that these results have not been corrected for scattering. However, we believe this to be significant only <u>below</u> 290 [nm]. Also, they have not been corrected for possible differences between using and not using a diffuser, which will be addressed later.

In order to estimate the uncertainty in our determination of $\bar{E}^z_\lambda$ [eq. (1.22)], we shall address the way in which each independent and dependent variable in this simplified equation was obtained.

The first variable is λ_o, which is the (corrected) wavelength setting of the spectro--radiometer. This is actually the peak or center wavelength of our slit-scattering function. The wavelength calibrations that were taken every morning and late afternoon, one of which is shown in figure 18, were generally used to obtain λ_o. The data represented by the dashed curve in the figure was fitted to a cubic equation in λ. A linear interpolation in time between the morning and afternoon calibrations was used to determine the wavelength correction at any time t. These wavelength calibrations were estimated to have an uncertainty ranging from ± 0.02 [nm] at 290 [nm], ± 0.03 [nm] at 295 [nm], ± 0.03 [nm] at 305 [nm] to ± 0.02 [nm] at 340 [nm]. A smaller wavelength uncertainty, estimated to be ± 0.01 [nm], was obtained in the data taken for ozone determinations by using the spectral structure shown in figure 4. In this case, during a solar run, about five data points were taken at 0.02 [nm] intervals through 5 or 6 of the troughs in figure 4. The observed trough wavelengths were then compared with those obtained by convolution of $E_\lambda(\lambda,t)$, where $E_\lambda(\lambda,t)$ was obtained in the manner described in Appendix A. The $\bar{E}^z_\lambda$ uncertainties associated with these various wavelength uncertainties vary with wavelength and are shown in table 2 along with the other uncertainties to be discussed in this section.

The time (Eastern Standard), t, was provided by a clock in the computer and was accurate to about one second. Time was stored along with the data at intervals of about one minute. The time parameter was used to compute the orientation of the tracker for polarization corrections and for linear interpolations of the standard lamp calibration, S'^s and introduced negligible uncertainty in $\bar{E}^z_\lambda$.

The signal counting rate, S', for solar photons was obtained with an integration time varying from one second to 10 minutes, chosen to realize a standard deviation for S' of 1 percent or less. In photon counting, the standard deviation of the signal is approximately equal to the square root of the total counts. The dark count rate was always set to about 0.3 $[c \cdot s^{-1}]$ by adjusting the discriminator voltage and was subtracted from the observed signal rate when significant. Time intervals for integrations

Table 2. Individual and Total Estimated Uncertainties (percent of solar terrestrial spectral irradiance).

Source of Uncertainty \ Wavelength	290 nm	295	305	340
Wavelength				
Calibration from mercury lines	4% (.02 nm)	3% (.03 nm)	.6% (.03 nm)	negligible (.02 nm)
Self-calibration from solar spectrum		1% (.01 nm)	.2% (.01 nm)	
Noise--solar measurements S'	←		1%	→
Solar tracking malfunction	←		2%	→
Inability to resolve all photon counts C(S')			← 1% →	
Spectral irradiance standard lamp E_λ^s	←		3%	→
Noise, alignment & changes in tracker mirrors--calibration with lamp S'^s	←		2%	→
Transmittance of filters	← Solar blind filter 3% →		← Diffuser 2% →	
			← Neutral density filter 1% →	
Polarization correction	←		2%	→
Linear interpolation relative to time of roof calibration	←		2%	→
Correction for difference between using & not using diffuser	←		2%	→
Total (square root of sum of squares of individual uncertainties)	← 7.4%	to	5.7%	→

were determined by the computer with negligible uncertainty. Time was the basis for automatic control of the tracker orientation such that the solar beam remained centered relative to the entrance slit of the spectroradiometer. This automatic mechanism malfunctioned rather frequently during the runs, requiring manual control. We have assigned a 2 percent uncertainty for this malfunctioning as indicated in table 2.

The correction C(S') (for not being able to resolve all the photon counts) given in eq. (1.15b) is considered uncertain by about 1 percent for counting rates from 5×10^5 [c·s^{-1}] to the highest observed. At lower counting rates, its uncertainty is estimated to decrease monotonically to a few tenths of one percent at 10^5 [c·s^{-1}].

The spectral irradiance of the 1000 [W] frosted tungsten halogen standard $E^s_\lambda(\lambda,t)$ was obtained by a comparison calibration with three NBS spectral irradiance 1000 [W] standards before and after the eight-day period of solar observations. This was performed at the normal distance of 50 [cm] and at 5 [nm] intervals for the wavelength range 280-350 [nm]. No significant change was observed in the two calibrations obtained 8 days apart. The spectral irradiance of the frosted lamp at the distance used, 396.3 [cm] without diffuser and 384.8 [cm] with diffuser, was calculated assuming an inverse square law dependence relative to 50 [cm]. From previous experience, the uncertainty of this procedure for obtaining E^s_λ of this type lamp at the above distances does not exceed 0.5 percent. In order to obtain the spectral irradiance at wavelengths other than the 5 [nm] intervals at which data was taken, a least squares fit was performed to the expression

$$E^s_\lambda(\lambda) = (A_1 + A_2\cdot\lambda + A_3\cdot\lambda^2 + A_4\cdot\lambda^3 + A_5\cdot\lambda^4)\cdot\lambda^{-5}\cdot e^{[a+(b/\lambda)]} \qquad (1.24)$$

with weights of $1/(E^s_\lambda)^2$ (NBS Tech Note 594-13) [13]. If only a <u>linear</u> least squares computer program is available, one can determine the quantities a and b from a fit of

$$\ell n(E^s_\lambda\cdot\lambda^5) = a + (b/\lambda) \qquad (1.25)$$

with weights of 1. Then with a and b determined, one obtains the A_i from a fit of eq. (1.24) with weights $1/(E^s_\lambda)^2$. The uncertainty of E^s_λ at the distances and wavelengths used in this experiment is estimated to be 3 percent.

The standard lamp calibration data S^s were obtained as a function of wavelength by fitting an equation similar to eq. (1.24) but without the cubic and quartic terms (these terms were not significant in the S^s fits) and with a weighting of $1/(\Delta t\cdot S^s)$ where Δt is the integration time in seconds. In linear least squares fitting, the weights are proportional to the reciprocals of the variances. Total counts varied from about 10^4 [c] at 280 [nm] to 3×10^5 [c] at 350 [nm] when an integrating time of 5 [s] was used (no filters or diffuser). Fits performed with both 1 [nm] and 5 [nm] interval data

demonstrated that the 5 [nm] interval spacing was sufficiently close. Successive calibrations taken 48 hours apart differed by a maximum of about 2 percent which was attributed to imprecision (noise), alignment errors, and changes in the tracker mirrors. The calibration used for any particular solar measurement was obtained by linear interpolation, with respect to time, between the 48-hour calibrations. The uncertainty of S^s was estimated to be 2 percent as indicated in table 2.

Spectral transmittance data of the solar blind filter and diffuser were fitted with a quadratic function of wavelength with an insignificant (<0.5 percent) standard deviation for the fits. The solar blind filter had significant non-uniformities and the reproducibility in positioning this filter was about 2 percent. This problem did not exist for the diffuser. The neutral density filter had a constant transmittance as a function of wavelength to within the precision of the measurements of 1 percent. It did not possess significant non-uniformities. None of the filters showed any change in transmittance over the five nights of calibration. There was no reason to expect the solar blind or neutral density filter to be dependent on tracker orientation, and this was confirmed experimentally. Since the output signal of the spectroradiometer was not a function of tracker orientation with the diffuser in place, but without it, the output signal did vary with tracker orientation, the effective transmittance of the diffuser was always determined relative to one particular tracker orientation. This was taken to be the orientation at 12:30 EST. The uncertainties assigned these filters were 3 percent for the solar blind filter, 2 percent for the diffuser, and 1 percent for the neutral density filter.

The polarization correction for tracker orientation was obtained by two quadratic spline[1] "fits." The first fit was used to interpolate relative to tracker orientation for each of the 5 [nm] lamp calibration data. Since $R_E^f(\lambda_o,t,T_s)$ is proportional to

---

[1]A spline "fit" is a manner of interpolating non-linearly between a large number of data points. The procedure is to determine the coefficients of an nth order (usually n = 2 or 3) polynomial that "goes through" the first n + 1 data points, then the coefficients of the same order polynomial that "goes through" the second to n + 2 data points, and so on until all the data points are used. Then these polynomials are used to calculate the interpolated values. Since two or more polynomials can be used for calculating the same interpolated point, a standard format is set up which selects a particular polynomial. For example, if n = 3, a typical format would be to use the first polynomial for interpolating between the first 3 data points and the last polynomial for interpolating between the last 3 data points. Each of the remaining polynomials is used for interpolating between the 2nd and 3rd point used in determining that polynomial. Once a computer program has been written to accomplish all this, it is a simple, fast procedure to carry out. We have often used spline "fits" when we wanted data at equal intervals of the independent variable but the data wasn't taken at these intervals, and we did not know an appropriate equation to use for a least-squares fit.

$S'^{S}(\lambda_o,t,T_s) \cdot C(S'^{S})$, these data could be used to interpolate relative to the 10:00 to 17:00 tracker orientations (T). Curves similar to that shown in figure 9 were computed and stored on a floppy disk for each of the 5 [nm] runs from 340 to 280 [nm]. The tracker polarization correction P eq. (1.23) was determined by obtaining the ratio

$$\frac{S'^{S}(\lambda_o,t,T)}{S'^{S}(\lambda_o,t,T')}$$

where T is the tracker time for which the particular solar data S' was obtained and T' is the closest tracker time to T for which a lamp calibration was obtained. These ratios were determined for each of the 5 [nm] data and a 2nd quadratic spline fit was performed as a function of wavelength. The uncertainty of P was estimated to be 2 percent.

In order to detect any changes or drifts with respect to time in the spectroradiometer responsivity function, the standard lamp was set up in the laboratory and observed each morning before solar measurements began and in the late afternoon after solar measurements for that day had ended. The major differences between these lamp observations and the roof calibrations were that the former did not include the tracker and did not have to be made at night in an outdoor environment. These made the "lamp observations" more precise and they could be obtained more frequently. In order that corrections C(S') for high count rates be negligible, the neutral density filter was employed. Figure 19 is a plot of these results and the roof calibrations (S'^{S}) for 330, 335 and 340 [nm]. The "inside-laboratory" calibration had the same long-term drift as the roof calibration. However, short-term changes were different. We do not know the reason for this, but it is conceivably due to laboratory temperature changes. We attributed an uncertainty of 2 percent to this effect, referring to it in table 2 as "linear interpolation relative to time of roof calibration".

As mentioned earlier, we had planned to take several sets of data at the longer wavelengths with and without a diffuser to determine directly any differences between these two approaches. The set of runs 42, 43, and 44 in tables B-5, B-6, and B-7, respectively, is one such example. All these comparisons showed that there was a difference of about 5 percent, independent of wavelength, between the "diffuser" and "no-diffuser" runs with the latter resulting in higher values of spectral irradiance. We have not been able to determine the cause of this difference, but our suspicion is that it is due to differences in the beam geometry of the sun and standard lamp and lack of sufficient uniformity in the flux responsivity. We believe the diffuse data is correct and therefore must reduce all the data taken without a diffuser (virtually all below 305 [nm]) by the 5.3 percent difference observed. This correction has not yet been applied to the non-diffuser data in tables B-1 to B-7 in Appendix 1B. The uncertainty of such a correction

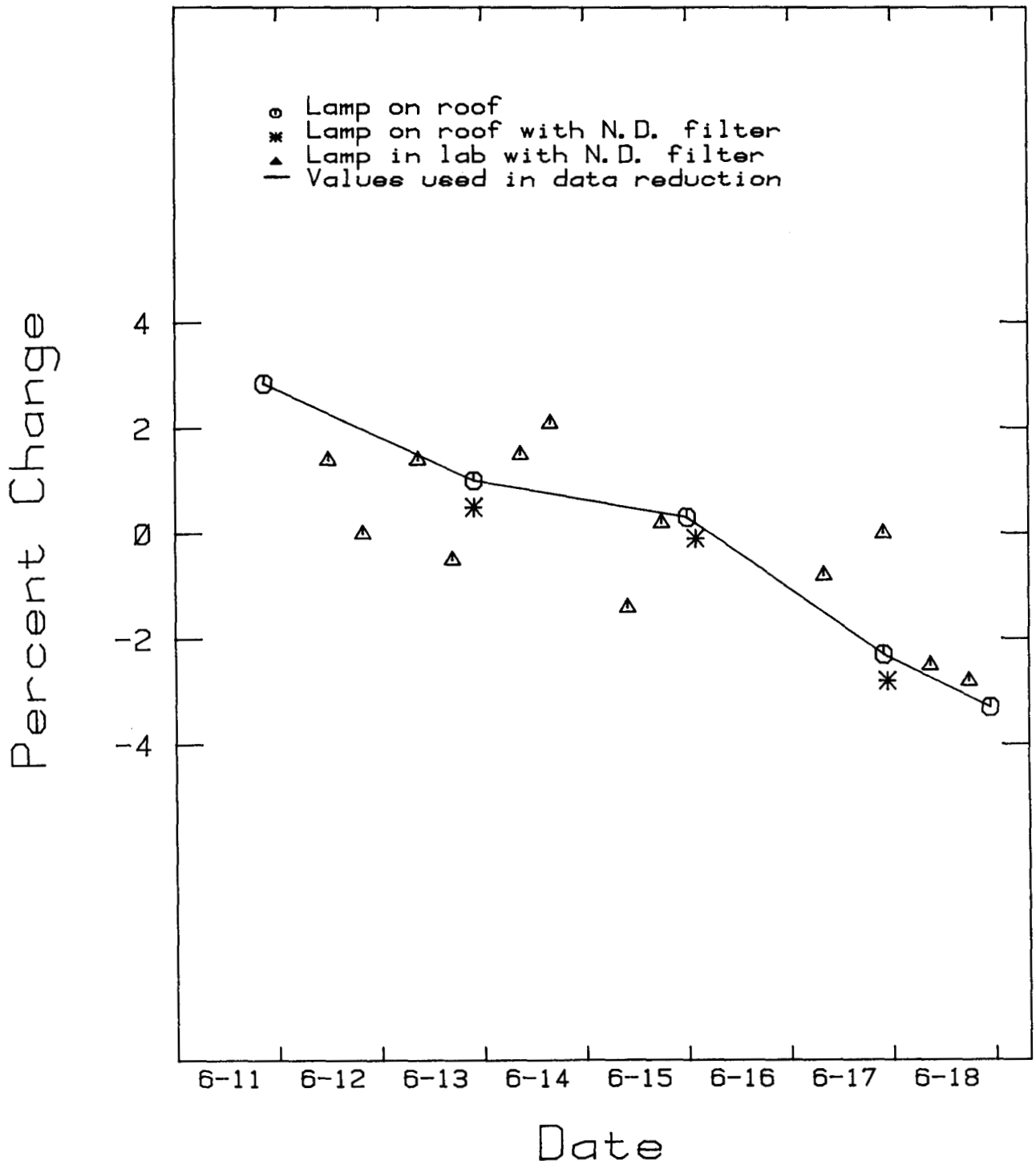

Figure 19. Change with time of direct mode lamp calibrations (S'^{S}) for 300, 335, and 345 [nm] data.

has been estimated, from the precision of the diffuser/no-diffuser comparisons, to be about 2 percent. This is the last item in the uncertainties of table 2.

It is common practice to make an estimate of the overall or total uncertainty of experimental measurements by combining in quadrature (square root of the sum of the squares) all the individual, independent uncertainties such as those listed in table 2. This has been done, and the result, given at the bottom of table 2, varies from 7.4 percent at short wavelengths to 5.7 percent at long wavelengths.

There are applications of solar terrestrial spectral irradiance measurements where only the ratio of values at wavelength intervals of 2 or 3 [nm] are needed. Many of the uncertainties in table 2 are significantly less for such relative spectral measurements, particularly when the data from which the ratio is to be determined have been obtained in time intervals of a few minutes. We estimate that the total uncertainty for such relative spectral measurements is about 3 percent or roughly half that shown in table 2. The component uncertainties contributing to this smaller uncertainty are wavelength--2 percent, noise (S')--1 percent, C(S')--1 percent, noise (S'^{S})--1 percent, E_{λ}^{S}--1 percent, and polarization--1 percent.

The repeatability of non-diffuser experimental runs taken at 10 to 30 minute intervals is not as good as predicted by our uncertainty estimates. Comparing such data when viewing conditions were good and wavelength uncertainties negligible, we found systematic differences that averaged 4 percent in successive runs. We did not see this large a difference when the diffuser was used. However, we only had one appropriate set of diffuser runs for checking this repeatability. In this case, there was a difference of only 1 percent. The only factor of which we are aware that could cause the lack of repeatability of 4 percent for the non-diffuser runs is improper alignment relative to the peak of the responsivity function (see figure 8). In this case, systematic errors of about 1/2 deg in solar tracking during a run would account for the results observed. The tracking malfunction uncertainty in table 2 addresses this type of behavior. However, the amount assigned this uncertainty (in table 2) accounts for only half the non-repeatability observed, and we would expect this uncertainty to reflect itself in a somewhat less systematic manner. As a result of this unaccountable behavior of our data, we add another 2 percent uncertainty to the totals in table 2 resulting in about 10 percent at the short wavelengths and 8 percent at the long wavelengths.

The question arises of whether or not a significant reduction of uncertainty in these solar terrestrial spectral irradiance measurements is likely without a major improvement in the spectroradiometer and standard. We believe the answer is yes if the existing mirror tracker were eliminated and the monochromator were located on the roof and itself mounted on a very accurate solar tracker. Arrangements also would have to be made for proper temperature control of the spectroradiometer. With such an arrangement, the solar tracking malfunction uncertainty, the systematic differences referred to in the last paragraph, the polarization correction and its uncertainty, and half the uncertainty associated with the standard lamp signal S'^{S} would be eliminated. In addition, we

believe the uncertainty associated with the lack of uniformity of the filters and with their transmittance measurements could be reduced by a factor of about two. Furthermore, whenever possible, one should use a diffuser. This is no problem for wavelengths greater than 305 [nm]. Between 295 and 305 [nm] it is possible only when integration times of 100 to 10 [s], respectively, can be employed. In all, it should be possible to realize a total uncertainty as computed in table 2 of about 6 percent at 290 [nm] and 4 percent between about 300 and 340 [nm].

FUTURE INVESTIGATIONS. There are three investigations or areas of research to which we would give a high priority in any future efforts in UV solar terrestrial radiometry.

The first investigation is a direct test of the effect of coherence of the solar flux on spectral scattering. We found negligible scattered signal at 290 [nm] which we attributed to the high coherence of the flux when the sun itself and the entrance slit defined the solar beam (solid angle at entrance slit of approximately 10^{-4} [sr]). This reason for the low scattering could be confirmed easily by first spectrally scanning between 295 and 290 [nm] with a low scattering, double monochromator under our viewing conditions and, immediately afterward, performing another scan with an appropriate lens inserted so that the entrance slit was irradiated with a much larger solid angle (e.g., the collimator of an f/5 instrument being filled or a solid angle of approximately 0.03 [sr]). If coherence is responsible for the significantly lower scattering, S(295)/S(290) from the two scans should differ by a factor of between about 50 and 100.

The second area of research in UV solar terrestrial radiometry that we believe should receive high priority is extending the measurements of the sun itself described in this chapter to measurements of the sun and sky; that is, hemispherical viewing. In the UV, the solar terrestrial hemispherical spectral irradiance is about twice that of the spectral irradiance of the sun itself [14]. Ultraviolet measurements of the sun itself, as described in this chapter, are of major interest for ozone and aerosol determinations. Hemispherical measurements are of interest in studies of biological effects. The usual way in which hemispherical measurements are made is with a diffuser that obeys the cosine law. Development and accurate characterization of a suitable diffuser would constitute the major effort in this investigation. Because of the signal attenuation of about 10^3 when using a diffuser, measurements will probably not be practical below about 292 or 293 [nm]. Even down to these wavelengths, the spectral slit width will have to be increased to 1 [nm] and the entrance slit area to about 1 [mm^2]. Because the ratio of hemispherical spectral irradiance to solar spectral irradiance changes orders of magnitude less relative to wavelength than the hemispherical quantity itself [14], the direct measurement of the ratio should be considered. If the need for going to shorter wavelengths is sufficiently great, development of a lens or optical system capable of hemispherical viewing and cosine law response might be attempted. Even if this were successful and the signal/noise problem down to 290 [nm] were solved, the difficult problem of accurately correcting for scattered flux would remain.

Finally, any extensive research in UV solar terrestrial radiometry should consider an instrument in which the spectral irradiances at all wavelengths of interest can be measured simultaneously. Changes in atmospheric conditions, often in a relatively short time, make this feature highly desirable. Fourier transform spectroradiometers, multi-channel spectroradiometers, and spectrographs are obvious examples. However, in order to make accurate measurements below about 300 [nm], this instrument must have a slit-scattering function comparable to that of a high quality double monochromator, and, to the best of our knowledge, this has not yet been realized.

SUMMARY of CHAPTER 1. This chapter addresses the difficult problem of measuring the solar terrestrial spectral irradiance from about 290 [nm] to 340 [nm]. It includes an account of the experimental design and measurements that were carried out in Gainesville, Florida, in June 1980. The major reasons for these measurements were to (1) apply current state-of-the-art radiometric instruments and techniques to UV solar terrestrial measurements and present the results in this Manual as a first applications chapter and (2) explore the potential of using solar data at wavelengths below 305 [nm] for determining atmospheric ozone thicknesses. Item 1 is the subject of this chapter. Item 2 is being developed for submission to Applied Optics.

The chapter begins with estimates of the spectral irradiances of the sun (not including sky) as seen from the surface of the earth. These are calculated using the equations developed in Appendix 1A. The results of the calculations are shown in figures 2 through 4. Figure 3 shows that with a spectral slit width of 0.003 [nm] considerable spectral structure appears. Therefore if spectral slit widths of 0.1 [nm] to 1.0 [nm] are used, as is common in radiometry, the measurements will provide only a weighted average spectral irradiance, weighted by the slit-scattering function of the spectroradiometer.

The measurement configuration that we used in this problem is shown in figures 5 through 7. The advantages of the common practice in irradiance measurements of using a diffuser as the first element of the spectroradiometer are reviewed. However, a signal reduction factor of about 1000 makes the diffuser impractical to use below about 305 [nm] where measurements for ozone determinations are to be concentrated. It is demonstrated that if a diffuser is not used, the flux responsivity function must be sufficiently uniform over the angular extent of both the sun and the lamp standard used in calibrating the spectroradiometer.

The general measurement equation for incoherent radiation (p. 23, 910-3) [9],

$$S(\lambda_o) = \int_{\Delta\lambda}\int_{\Delta A}\int_{\Delta\omega} (R_{00}\cdot L_0 + R_{01}\cdot L_1 + R_{02}\cdot L_2 + R_{03}\cdot L_3)\cdot\cos\theta\cdot d\omega\cdot dA\cdot d\lambda \qquad (1.3)$$

is applied to viewing both the sun and the standard lamp resulting in

$$\frac{S(\lambda_o)}{S^s(\lambda_o)} = \frac{R_E^f(\lambda_o,T) \cdot \int_{\Delta\lambda} E_\lambda \cdot z(\lambda_o,\lambda,T) \cdot d\lambda}{R_E^f(\lambda_o,T_s) \cdot \int_{\Delta\lambda} E_\lambda^s \cdot z(\lambda_o,\lambda,T_s) \cdot d\lambda} \tag{1.13}$$

where $R_e^f(\lambda_o,T)$ is the irradiance responsivity factor at wavelength λ_o and tracker orientation T; and where z is the slit-scattering function (p. 15, 910-4) [6].

The estimated irradiances, measurement configuration, and measurement equation are used to arrive at the specifications of the monochromator required for these measurements so that their uncertainty is less than 10 percent. These include a wavelength uncertainty of 0.01 [nm] or less, spectral slit widths varying from about 0.2 to 1 [nm], very low ($\leq 10^{-8}$) wings on the slit-scattering function and as large a geometrical throughput as available. A block diagram of the complete spectroradiometer selected is shown in figure 5, and detailed specifications for the instrument are also presented.

In order to minimize errors in the radiometric measurements, the flux responsivity of the spectroradiometer is characterized for the parameters for which a significant difference exists between the spectral irradiance of the sun and that of the lamp used as a calibration standard. The parameters involved are magnitude of the flux and spectral distribution.

For magnitude, the following correction to the output signal is experimentally obtained:

$$\frac{S}{S'} \equiv C(S') = 1 + 6.927 \cdot 10^{-8} \cdot S' + 7.174 \cdot 10^{-15} \cdot S'^2 \tag{1.15b}$$

where S is the "corrected" output signal and S' is the output signal actually observed.

The rapid fall-off in solar terrestrial spectral irradiance below 305 [nm] and the extensive structure require a maximum wavelength uncertainty of about 0.01 [nm] if wavelength accuracy is not to be a significant factor. It is found that this 0.01 [nm] uncertainty is realizable with this best available portable instrument only by using the spectral structure of the sun itself in a wavelength self-calibration while taking solar data. In order to obtain the calibration wavelengths in this observed spectral structure (by evaluating eq. (1.13) as a function of wavelength) the central portion of the slit-scattering function is required. It is obtained from spectral scans of various mercury and laser lines.

An accurate determination of the distant wings (to values of 10^{-8} or less) of the slit-scattering function is required in order to perform a deconvolution of eq. (1.13) to obtain a correction for scattering. This has not been possible because of insufficient power ($<<$ 10 [mw]) in available lasers. However, an estimate of the required long wavelength wing has been obtained using the strong 253.7 [nm] mercury line. The result is $2 \cdot 10^{-8}$ at 53 [nm] from the peak, with an uncertainty of about a factor of two.

The detailed manner in which the solar measurements were made is presented. This included an accurate optical alignment using a laser (required because a diffuser was not used for most of the measurements), frequent spectral irradiance and wavelength calibrations, selection of integration times and total time for experiments, visual monitoring, temperature control, weather conditions and computer usage, including control. Four types of data were obtained. These consisted of (1) sharp ozone cut-off data ($\lambda < 295$ [nm]), (2) data for the new-type ozone determinations ($295 < \lambda < 305$), (3) data for Dobson type ozone determinations ($305 < \lambda < 340$), and (4) data required for performing convolutions. Examples of these four types of data are shown in tables B-1 through B-7 in Appendix 1B.

For reducing the data and estimating the uncertainty of the measurements, the measurement equation is reduced to

$$\frac{\int_{\lambda_o-0.22}^{\lambda_o+0.22} E_\lambda(\lambda,t)\cdot z(\lambda_o,\lambda,T)\cdot d\lambda}{\int_{\lambda_o-0.22}^{\lambda_o+0.22} z(\lambda_o,\lambda,T_s)\cdot d\lambda} \equiv \bar{E}_\lambda^z(\lambda_o,t) = \frac{C(S')\cdot S'(\lambda_o,t,T)\cdot E_\lambda^s(\lambda_o,t)}{C(S'^s)\cdot S'^s(\lambda_o,t,T_s)\cdot\tau(\lambda_o,t)\cdot P}, \qquad (1.22)$$

where

$$P = \frac{R_E^f(\lambda_o,t,T,)}{R_E^f(\lambda_o,t,T_s,)} \qquad (1.23)$$

is the polarization correction required when the calibration data S'^s are obtained with tracker orientation T_s and solar data S' with tracker orientation T. E_λ^s is the spectral irradiance of the standard lamp as used in the calibration and τ is the transmittance of any filters inserted in the optical path for solar measurements but not inserted for the lamp calibrations. The manner of obtaining each independent variable in eq. (1.22) and its uncertainty is discussed. These uncertainties are summarized in table 2. Measurements made at wavelengths greater than 305 [nm], where it is possible (with good signal-to-noise ratio) to use a diffuser, showed a difference of 5.3 percent between using and not using a diffuser. The diffuser data are believed to be more accurate, and therefore all non-diffuser data will be corrected (multiplied by 0.947). This correction has not yet been made for the data shown in tables B-1 to B-7 in Appendix 1B.

Spectral scattering is found to be insignificant down to 290 [nm]. This requires the distant wings of the slit-scattering function to be about 10^{-10}. It is believed that this value was realized in our non-diffuser measurements because the irradiation of the slit of the monochromator, in this case, was quite coherent.

The uncertainty associated with each dependent and independent variable in eq. (1.22) is discussed and estimated. The overall or total uncertainty is obtained by taking the square root of the sum of the squares of the individual uncertainties in table 2. This total uncertainty varies from 7.4 percent at the short wavelengths to 5.7 percent at 305 [nm] and longer wavelengths.

Comparison of a number of experimental runs shows that the repeatability is not as good as the uncertainty estimates predict. An additional uncertainty of 2 percent is added to the totals given above to take account of this.

Means that can be taken to reduce these uncertainties are discussed. An improvement of about one third is considered feasible if the mirror solar tracker can be eliminated and the monochromator itself mounted on a precision solar tracker.

In some applications in which these measurements will be used, only ratios of solar terrestrial spectral irradiance at wavelength intervals of only 2 or 3 [nm] are required. These are estimated to have much lower uncertainties -- about 3 percent.

Various suggestions are made for further research in UV solar terrestrial spectral irradiance measurements. These include (1) direct confirmation of the effect of coherence on scattering, (2) extension of the solar measurements to include global (sun plus sky) measurements, and (3) the development of an instrument in which data for all wavelengths of interest are obtained virtually simultaneously.

Appendix 1A (Part III)

Computation of Solar Terrestrial Spectral Irradiance between 280 and 310 [nm][1]

[1]The purpose of this Appendix is to present our currently recommended procedure for computing the solar terrestrial spectral irradiance in the 280 to 310 [nm] region. It should be emphasized, however, that the accuracy of this recommended procedure has not yet been critically evaluated.

In irradiance calculations, as in most calculations involving radiometric quantities, there is less chance of error if one begins with the quantity radiance. The solar spectral radiance at the earth's surface, L_λ, is equal to the product of the solar spectral radiance outside the earth's atmosphere (extraterrestrial) L^e_λ and the spectral transmittance of the atmosphere $\tau(\lambda)$ along the path associated with this radiance (p. 38, 910-1) [15]; that is

$$L_\lambda = L^e_\lambda \cdot \tau(\lambda) \quad [W \cdot m^{-2} \cdot sr^{-1} \cdot nm^{-1}]. \tag{A-1}$$

The two spectral radiances in eq. (A-1) are shown in figure A-1 along with the major constituents of the atmosphere -- ozone, aerosol, and air -- that absorb or scatter the solar flux in the region between 280 and 340 [nm]. The spectral transmittance associated with each of these constituents is, by the familiar exponential law of transmittance,

$$\tau_i(\lambda) = e^{-q_i(\lambda) \cdot seq_i\theta} \tag{A-2}$$

where $q_i(\lambda)$ is the optical depth[1] of the i^{th} constituent for a vertical path (zenith angle $\theta = 0$). $Seq_i\theta$ is the ratio of the length of the actual path of the direct solar flux to that of the vertical path. The optical depth q_i can also be written as $n_i\sigma_i W_i$ or $k_i W_i$ where n_i [$cm^{-3} \cdot atm^{-1}$] is the number density, σ_i [cm^2] is the attenuation (or absorption) cross section, W_i [cm·atm] is the thickness, and k_i [$cm^{-1} \cdot atm^{-1}$] is the attenuation (or absorption) coefficient.[2] The overall transmittance, $\tau(\lambda)$, of the atmospheric model shown in figure A-1 is

---

[1]The usual symbol for the optical depth in the literature on atmospheric optics is τ. However, we have already used τ throughout the rest of this Manual for transmittance. Accordingly, we have adopted here the symbol q for optical depth, writing $q_i(\lambda)$ instead of $\tau_i(\lambda)$. Incidentally, don't confuse this with the unit of photon flux, the quantum [q], which we always enclose in square brackets, as with all unit-dimension symbols.

[2]The CIE-IEC International Lighting Vocabulary (3rd ed.) calls this the linear attenuation (or absorption) coefficient.

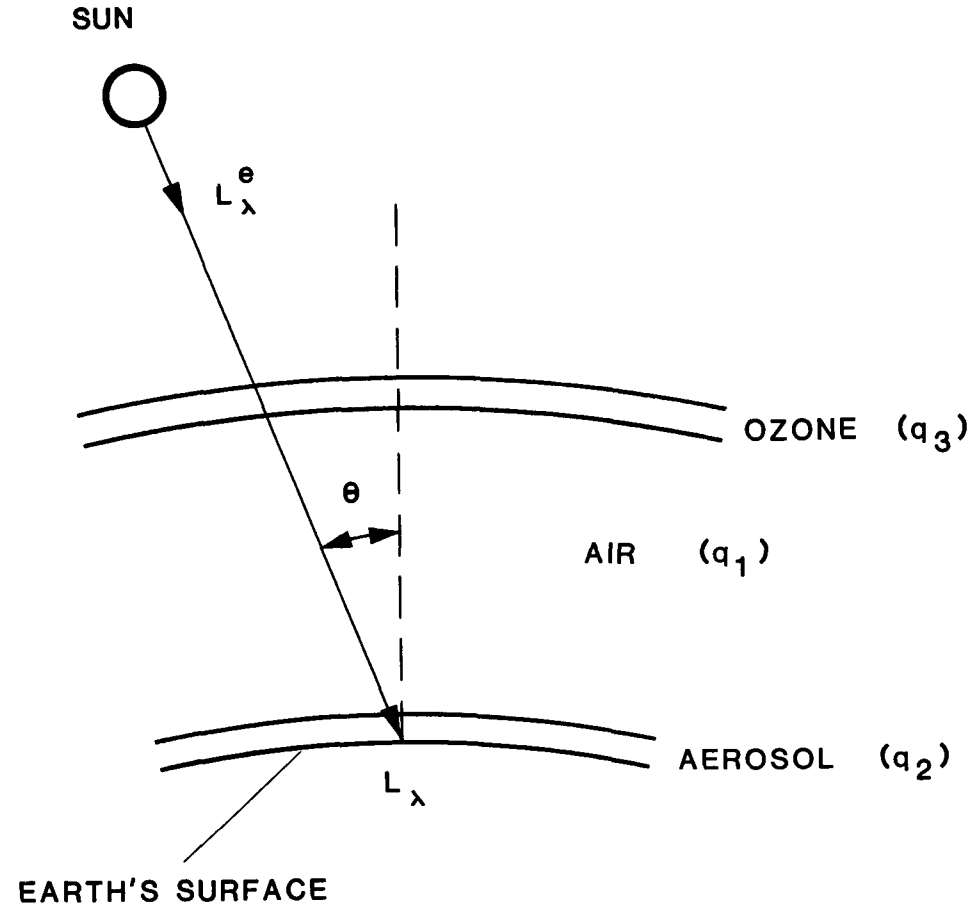

Figure A-1. Simple model of earth's atmosphere showing the major constituents that absorb or scatter solar flux in the UVB and the solar terrestrial spectral radiance L_λ and solar extraterrestrial spectral radiance L_λ^e. q_i is the vertical optical depth of the ith constituent.

$$\tau(\lambda) = \tau_1(\lambda)\cdot\tau_2(\lambda)\cdot\tau_3(\lambda) = e^{-q_1\cdot seq_1\theta}\cdot e^{-q_2\cdot seq_2\theta}\cdot e^{-q_3\cdot seq_3\theta} \tag{A-3}$$

$$\tau(\lambda) = e^{-(q_1\cdot seq_1\theta + q_2\cdot seq_2\theta + q_3\cdot seq_3\theta)} \tag{A-4}$$

and substituting eq. (A-4) into eq. (A-1), we obtain

$$L_\lambda = L_\lambda^e\cdot e^{-(q_1\cdot seq_1\theta + q_2\cdot seq_2\theta + q_3\cdot seq_3\theta)} \tag{A-5}$$

where q_1, q_2, and q_3 represent the vertical optical depth for air, aerosol and ozone, respectively.

To obtain the solar terrestrial spectral irradiance E_λ from the solar terrestrial spectral radiance L_λ we apply the equation (p. 12, 910-2) [16]

$$E_\lambda = \int_\omega L_\lambda\cdot\cos\theta'\cdot d\omega \tag{A-6}$$

to the configuration shown in figure (A-2). Since θ' does not exceed about 0.25 [deg],

$$E_\lambda = \int_\omega L_\lambda\cdot d\omega \tag{A-7}$$

to a very high accuracy. Substituting the expression for L_λ in eq. (A-5) into eq. (A-7), we obtain

$$E_\lambda = \int_\omega L_\lambda^e\cdot e^{-(q_1\cdot seq_1\theta + q_2\cdot seq_2\theta + q_3\cdot seq_3\theta)}\cdot d\omega. \tag{A-8}$$

Since each of the q_i and $seq_1\theta$ vary only slightly over ω

$$E_\lambda = e^{-(q_1\cdot seq_1\theta + q_2\cdot seq_2\theta + q_3\cdot seq_3\theta)}\cdot\int_\omega L_\lambda^e\cdot d\omega\ [W\cdot m^{-2}\cdot nm^{-1}]. \tag{A-9}$$

The solid angle ω subtended by the sun at the earth's surface is insignificantly different from that subtended by the sun at the top of the earth's atmosphere. Therefore

$$E_\lambda = e^{-(q_1\cdot seq_1\theta + q_2\cdot seq_2\theta + q_3\cdot seq_3\theta)}\cdot E_\lambda^e \tag{A-10}$$

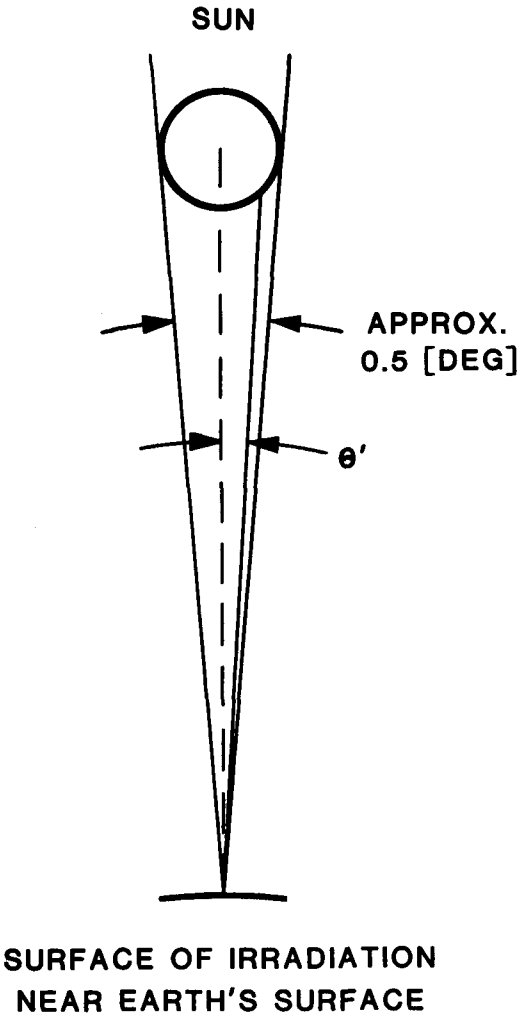

Figure A-2. Geometry involved in relating, through eq. (A-6), the solar terrestrial spectral radiance and solar terrestrial spectral irradiance.

where E_λ^e is the solar extraterrestrial spectral irradiance and E_λ is the solar terrestrial spectral irradiance.

The expression that we have used for the vertical optical depth for air q_1 is [17]

$$q_1 = \frac{1.0456 \cdot P}{1013} \cdot \left(\frac{300}{\lambda}\right)^4 \cdot e^{0.1462 \cdot (300/\lambda)^2} \qquad \text{(A-11)}$$

where P is the atmospheric pressure in millibars [mb] at the point for which E_λ is being determined and λ is the wavelength in nanometers [nm].

The vertical optical depth for aerosol q_2 for the limited range of 290 to 340 [nm] may be expressed [3] as

$$q_2 = q_{20} - S_{20} \cdot (\lambda - 300) \qquad \text{(A-12)}$$

where q_{20} and S_{20} are constants. The constants used in the computation of E_λ in figure 2 through figure 4 were representative values obtained in our 1980 Gainesville measurements ($q_{20} = 0.5$ and $S_{20} = 0.0033$ [nm^{-1}]).[1]

The vertical optical depth for ozone q_3 may be written

$$q_3(y) = k_3(y) \cdot W_3(y) \qquad \text{(A-13)}$$

where $k_3(y)$ [$cm^{-1} \cdot atm^{-1}$] is the ozone absorption coefficient and $W_3(y)$ [cm·atm] is the ozone vertical thickness at a point at an altitude y [km] where E_λ is being computed. The absorption coefficient k_3 is also a function of temperature. At wavelengths between 245 [nm] and 311 [nm], which includes the wavelengths with which this investigation is primarily concerned, this functional dependence is not great and may be represented by [17]

$$k_3(\lambda,t) = k_3(\lambda,t_o) \cdot \left[1 + \left\{\left[(t-t_o)/642\right] + \left[(t-t_o)/395\right]^2\right\} \cdot e^{(\lambda-300)/40}\right] \qquad \text{(A-14)}$$

where t and t_o are in degrees Celsius [°C] and λ is in nanometers [nm]. For our calculations, values of $k_3(\lambda,t_o)$ were obtained from measurements by Bass [18].

To take account of the variation of k_3 in the earth's atmosphere due to the variation of ozone temperature and number density, the following procedure was followed. A differential element of ozone optical depth dq_3 at an altitude y where the temperature is t may be written as

---

[1]Those interested in how q_{20} may vary for different types of aerosols and in analytical expressions covering a much larger wavelength range are referred to Green and Schippnick [17].

$$dq_3 = k_3(t) \cdot dW_3(y). \tag{A-15}$$

The total ozone optical depth is

$$q_3 = \int_0^{W_3(y)} k_3(t) \cdot dW_3(y), \tag{A-16}$$

where $W_3(y)$ is the thickness of ozone above altitude y. In eq. (A-16) we are integrating from the top of the atmosphere ($y = \infty$) where $W_3 = 0$ to a point in the atmosphere where the altitude is y and ozone thickness above y is $W_3(y)$. If W_{30} is the total thickness of ozone $W_{30} \equiv W_3(0)$ and $N(y)$ is the fraction of this thickness above altitude y,

$$dW_3(y) = W_{30} \cdot dN(y) = W_{30} \cdot \left(\frac{dN}{dy}\right) \cdot dy \tag{A-17}$$

and from eq. (A-16)

$$q_3(y) = \int_0^{N(y)} k_3(t) \cdot W_{30} \cdot dN \tag{A-18}$$

$$q_3(y) = \int_\infty^{y} k_3(t) \cdot W_{30} \cdot \left(\frac{dN}{dy}\right) \cdot dy. \tag{A-19}$$

Substituting eq. (A-14) into eq. (A-19), we obtain

$$q_3(y) = \int_\infty^{y} \left[1 + \left\{\left[(t-t_o)/642\right] + \left[(t-t_o)/395\right]^2\right\} \cdot e^{(\lambda-300)/40}\right] \cdot k_3(t_o) \cdot W_{30} \cdot \left(\frac{dN}{dy}\right) \cdot dy. \tag{A-20}$$

$$q_3(y) = -k_3(t_o) \cdot W_{30} \cdot \int_y^{\infty} \left[1 + \left\{\left[(t-t_o)/642\right] + \left[(t-t_o)/395\right]^2\right\} \cdot e^{(\lambda-300)/40}\right] \cdot \left(\frac{dN}{dy}\right) \cdot dy. \tag{A-21}$$

The total ozone optical depth $q_3(0)$ which we designate simply q_3 is

$$q_3(0) = q_3 = -k_3(t_o)\cdot W_{30}\cdot\left[\int_o^\infty \left(\frac{dN}{dy}\right)\cdot dy + \int_o^\infty \left\{\left[(t-t_o)/642\right] + \left[(t-t_o)/395\right]^2\right\}\cdot e^{(\lambda-300)/40}\cdot\left(\frac{dN}{dy}\right)\cdot dy\right]. \quad \text{(A-22)}$$

$$q_3 = -k_3(t_o)\cdot W_{30}\cdot\left[-1 + e^{(\lambda-300)/40}\cdot\int_o^\infty \left\{\left[(t-t_o)/642\right] + \left[(t-t_o)/395\right]^2\right\}\cdot\left(\frac{dN}{dy}\right)\cdot dy\right]. \quad \text{(A-23)}$$

For ozone, $N(y)$ may be written [19]

$$N(y) = \frac{0.1307}{2.350 + e^{y/2.66}} + \frac{0.9709}{1 + e^{(y-22.51)/4.920}} \quad \text{(A-24)}$$

where the altitude y is in kilometers [km]. Differentiating eq. (A-24), we obtain

$$\frac{dN}{dy} = -\frac{0.04914\cdot e^{y/2.66}}{\left(2.350 + e^{y/2.66}\right)^2} - \frac{0.1973\cdot e^{(y-22.51)/4.92}}{\left(1 + e^{(y-22.51)/4.92}\right)^2} \quad \text{(A-25)}$$

and substituting this into eq. (A-23)

$$q_3 = k_3(t_o)\cdot W_{30}\cdot\left[1 + C\cdot e^{(\lambda-300)/40}\right], \quad \text{(A-26)}$$

where

$$C = \int_0^\infty \left\{\left[(t-t_o)/642\right] + \left[(t-t_o)/395\right]^2\right\} \cdot\left(\frac{0.04914\cdot e^{y/2.66}}{\left(2.350 + e^{y/2.66}\right)^2} + \frac{0.1973\cdot e^{(y-22.51)/4.92}}{\left(1 + e^{(y-22.51)/4.92}\right)^2}\right)\cdot dy. \quad \text{(A-27)}$$

The constant C may be numerically evaluated for a particular t_o using tables giving atmospheric temperature t as a function of altitude y [20]. These tables depend on the latitude and the time of year (month). For $T_o = 18$ [°C] and a latitude of 30°N in

July, $C = -0.0714$. For the same latitude but the month of January, C changes only slightly to -0.0745. For $T_o = 25$ [°C] and a latitude of 30°N in July, $C = -0.0762$.

For $\lambda < 310$ [nm], the absorption coefficient for ozone at a particular temperature t_o may be approximated by the expression [17]

$$k_3(t_o,\lambda) = \frac{\alpha}{\beta + e^{(\lambda-300)/\gamma}} . \qquad \text{(A-28)}$$

Performing a non-linear least squares fit of Bass' data [18] from 288 to 305 [nm] to this expression results in

$$\alpha = 11.1419$$
$$\beta = 0.04928$$
$$\gamma = 7.1231$$

where $k_3(t_o,\lambda)$ has the units of $[cm^{-1} \cdot atm^{-1}]$.

Expressions used for $seq_i\theta$ in eq. (A-10) are [21]

$$seq_i(\theta,y_i) = \left(1 - \frac{\sin^2\theta}{r_i}\right)^{-\frac{1}{2}} , \qquad \text{(A-29)}$$

where

$$r_i = [1 + (y_i/R)]^2, \qquad \text{(A-30)}$$

and where θ is the solar zenith angle, R [km] is the earth's radius (6371 [km]) and where y_i [km] is the effective altitude for the ith species. We used [21]

$$y_1(\text{air}) = 5.69 \text{ [km]}$$
$$y_2(\text{aerosol}) = 1 \text{ [km]}$$
$$y_3(\text{ozone}) = 23.5 \text{ [km]}.$$

For small θ, $seq_i(\theta_i,y_i) = \text{secant } \theta_i$. The difference between seq_i and secant is not significant except for very large zenith angles. Even at $\theta = 58$ [deg], the difference for the case of ozone is only 0.9 percent which amounts to a difference in computed E_λ from eq. (A-10) of about 1 percent at 304.6 [nm] and 3 percent at 294.5 [nm]. For air, the difference between using $seq\theta$ and secant θ at $\theta = 58$ [deg] is about 0.2 percent which amounts to about 1/2 percent in E_λ in this same wavelength range.

The remaining quantity required to compute the terrestrial solar spectral irradiance E_λ is the extraterrestrial solar spectral irradiance E^e_λ. We needed high spectral resolution ($\Delta\lambda << 0.2$ [nm]) data for E^e_λ in order to determine the effect of instrumental spectral slit widths equal to or much larger than 0.2 [nm]. High resolution E^e_λ data could not be found for the spectral region of interest. However, high resolution ($\Delta\lambda = 0.003$ [nm]) L^e_λ data were available for the solar center and one portion of the solar limb [22]. These L^e_λ data were used to calculate E^e_λ in the following manner. We start with the relationship between spectral irradiance and radiance in eq. (A-6). As before [eq. (A-7)], for the case of terrestrial solar spectral irradiance, this becomes

$$E^e_\lambda = \int_\omega L^e_\lambda \cdot d\omega. \qquad \text{(A-7)}$$

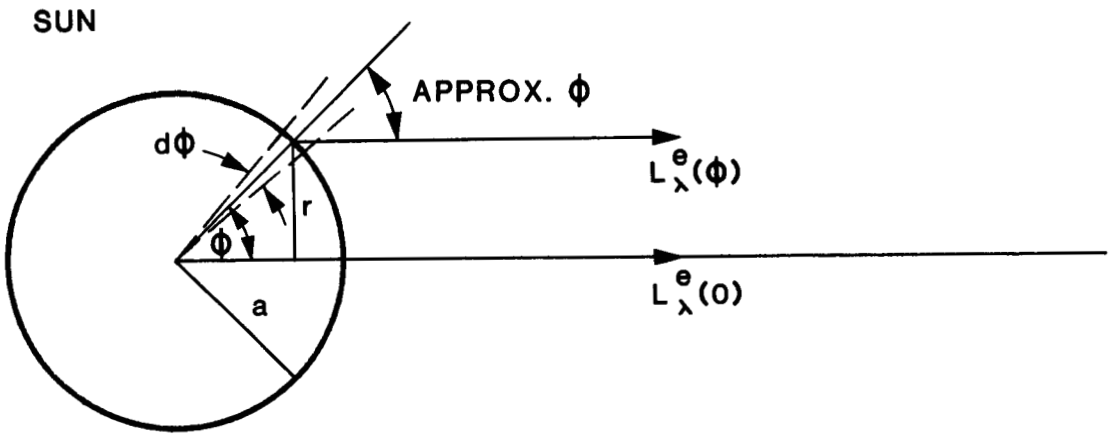

Figure A-3. Configuration for computing solar extraterrestrial spectral irradiance E^e_λ from solar extraterrestrial spectral radiance L^e_λ.

The solid angle $d\omega$ subtended at the earth's surface by the annular ring of area $2\pi \cdot r \cdot a \cdot d\phi$ [see figure (A-3)] on the sun's surface is

$$d\omega = \frac{2\pi \cdot r \cdot a \cdot d\phi \cdot \cos\phi}{R^2} = \frac{2\pi \cdot a^2 \cdot \sin\phi \cdot d\phi \cdot \cos\phi}{R^2} \qquad \text{(A-31)}$$

where R is the distance from the sun to the earth. Substituting this $d\omega$ in eq. (A-7) we obtain

$$E_\lambda^e = 2\pi \cdot \left(\frac{a}{R}\right)^2 \cdot \int_0^{\pi/2} L_\lambda^e \cdot \sin\phi \cdot \cos\phi \cdot d\phi. \tag{A-32}$$

If we let $\mu = \cos\phi$, $d\mu = -\sin\phi \cdot d\phi$ and

$$E_\lambda^e = 2\pi \cdot \left(\frac{a}{R}\right)^2 \cdot \int_1^0 L_\lambda^e \cdot \mu \cdot (-d\mu), \tag{A-33}$$

$$E_\lambda^e = 2\pi \cdot \left(\frac{a}{R}\right)^2 \cdot \int_0^1 L_\lambda^e \cdot \mu \cdot d\mu, \tag{A-34}$$

where $L_\lambda^e(\mu)$ for $\mu = 1$ and 0.23 are available from Kohl, et al [22]. Following Kohl et al [23], $L_\lambda^e(\mu)$ is assumed to be a straight line from $\mu = 1$ to $\mu = 0.23$ and from $\mu = 0.23$ to $\mu = 0$, and $L(0)$ is assumed to be zero. This simple functional dependence of $L^e(\mu)$ is estimated [23] to be accurate to a few percent. With these assumptions

$$L_\lambda^e(\mu) = \frac{L_\lambda^e(0.23)}{0.23} \cdot \mu \quad \text{for} \quad \mu = 0 \quad \text{to} \quad 0.23 \tag{A-35}$$

and

$$L_\lambda^e(\mu) = \frac{L_\lambda^e(0.23) - 0.23 L_\lambda^e(1)}{0.77} + \frac{\left(L_\lambda^e(1) - L_\lambda^e(0.23)\right)\mu}{0.77} \tag{A-36}$$

$$\text{for} \quad \mu = 0.23 \quad \text{to} \quad 1.$$

Substituting this into eq. (A-34) and performing the integrations, we obtain, using $a = 6.96 \cdot 10^8$ [m] and $R = 1.496 \cdot 10^{11}$ [m],

$$E_\lambda^e = 136 \cdot 10^{-6} \cdot \left[0.2050 \cdot L_\lambda^e(0.23) + 0.2861 \cdot L_\lambda^e(1)\right]. \tag{A-37}$$

Direct measurements of (spectrally averaged) extraterrestrial solar irradiance are available for a spectral slit width of 1.0 [nm] [24] and 0.34 [nm] [25]. These spectrally averaged quantities $\overline{E_\lambda^e}$ are related to E_λ^e by the expression

$$\overline{E_\lambda^e} = \frac{\int_{\Delta\lambda} E_\lambda^e \cdot z \cdot d\lambda}{\int_{\Delta\lambda} z \cdot d\lambda} \qquad \text{(A-38)}$$

where z is the slit-scattering function. Computations of $\overline{E_\lambda^e}$ using eqs. (A-37) and (A-38) and a triangular slit function (best estimate available) were compared to the direct measurements. Though the relative spectral values agreed within a few percent, the values themselves differed by factors of 0.852 (1.0 [nm] slit) and 0.813 (0.34 [nm] slit), the computed being larger than the observed in each case. We decided to use the more recent 1.0 [nm] data of Heath so we normalized eq. (A-37) by the factor of 0.852. That is,

$$E_\lambda^e = 0.852 \cdot 136 \cdot 10^{-6} \cdot [0.2050 \cdot L_\lambda^e(0.23) + 0.2861 \cdot L_\lambda^e(1)] \; . \qquad \text{(A-39)}$$

Tables A-1 and A-2 give values of E_λ^e convoluted (eq. A-38) with a triangular slit-scattering function having a spectral slit width $\Delta\lambda$ of 0.18 [nm] and 1.0 [nm], respectively.

Finally, we have all that is needed to compute the terrestrial solar spectral irradiance E_λ for $\lambda \leq 310$ [nm] which are the wavelengths of major interest to us. Figure 3 is the result of this calculation using $q_{20} = 0.5$ and $S_{20} = 0.003$ [nm^{-1}] and Bass' $k_3(t_o,\lambda)$. For a spectral slit width $\Delta\lambda >> 0.003$ [nm], such as in figures 2 or 4, one must convolute the computed E_λ with the slit-scattering function of the instrument; that is,

$$\overline{E(\lambda)^z} = \frac{\int_{\Delta\lambda} E_\lambda \cdot z \cdot d\lambda}{\int_{\Delta\lambda} z \cdot d\lambda} \qquad \text{(A-40)}$$

For figures 2 and 4, triangular slit-scattering functions were used with the spectral widths indicated in the figures.

Table A-1. Values of $\bar{E}^e_\lambda = (\int_{\Delta\lambda} E^e_\lambda \cdot z \cdot d\lambda)/(\int_{\Delta\lambda} z \cdot d\lambda)$ [$\mu W \cdot cm^{-2} \cdot nm^{-1}$], eq. (A-38), where E^e_λ is the extraterrestrial solar spectral irradiance used [eq. (A-39)] in this chapter and z is a triangular slit-scattering function with a width at half-height of 0.18 [nm]. (Solar distance = 1 AU.)

Wavelength [nm]	.0	.1	.2	.3	.4	.5	.6	.7	.8	.9
288	26.23	17.93	18.36	29.28	41.61	50.33	50.03	46.72	46.27	46.45
289	46.21	46.15	45.57	44.86	46.05	53.06	60.12	60.14	58.61	62.89
290	71.63	69.30	62.37	64.87	69.13	70.17	65.48	61.02	60.86	62.24
291	62.46	61.94	66.58	72.94	66.52	57.30	59.01	60.53	57.65	59.78
292	61.02	61.35	62.28	56.35	50.77	49.57	47.10	51.01	47.15	45.33
293	59.87	66.82	66.10	60.52	61.76	66.77	50.52	37.52	44.66	50.43
294	53.24	49.45	51.99	57.95	52.67	55.22	62.92	49.21	31.75	35.31
295	48.61	59.77	65.78	56.68	45.23	55.19	56.86	49.50	58.31	63.10
296	54.66	54.21	63.54	68.14	56.01	39.16	29.85	32.30	45.92	44.15
297	35.35	45.43	48.00	38.54	49.53	61.12	60.66	71.53	74.16	60.30
298	51.85	43.31	38.26	36.27	29.92	30.46	37.30	42.01	46.07	57.05
299	67.62	66.05	58.97	53.00	38.84	38.82	55.99	66.63	61.71	43.34
300	29.45	28.43	30.81	31.57	44.20	56.94	53.35	40.88	34.41	39.74
301	53.69	57.40	51.41	56.18	57.07	53.60	53.47	48.37	39.72	32.79
302	22.67	21.05	42.58	59.38	55.77	47.03	43.99	63.68	77.53	69.30
303	61.17	57.95	68.48	77.27	74.19	76.86	72.01	47.77	42.84	60.98
304	63.93	52.93	48.82	60.80	71.10	74.77	72.60	50.98	44.70	65.20
305	69.78	71.81	86.93	78.79	60.92	62.30	64.89	47.57	32.81	

Table A-2. Values of $\bar{E}^e_\lambda = (\int_{\Delta\lambda} E^e_\lambda \cdot z \cdot d\lambda)/(\int_{\Delta\lambda} z \cdot d\lambda)$ [$\mu W \cdot cm^{-2} \cdot nm^{-1}$], eq. (A-38), where E^e_λ is the extraterrestrial solar spectral irradiance used [eq. (A-39)] in this chapter and z is a triangular slit-scattering function with a width at half-height of 1.0 [nm]. (Solar distance = 1 AU.)

Wavelength [nm]	.0	.1	.2	.3	.4	.5	.6	.7	.8	.9
288	36.26	35.91	36.21	37.21	38.51	39.86	41.12	42.39	43.76	45.25
289	46.73	48.31	49.86	51.18	52.63	54.24	56.09	57.82	59.41	60.92
290	62.31	63.30	63.92	64.52	64.98	65.21	65.03	64.77	64.57	64.26
291	63.92	63.68	63.52	63.32	62.76	62.05	61.50	60.86	60.07	59.33
292	58.30	57.39	56.50	55.69	55.09	54.80	54.75	54.93	54.96	55.03
293	55.49	55.77	55.87	55.66	55.54	55.18	54.36	53.69	53.48	53.01
294	52.30	51.60	51.22	51.23	51.16	51.03	51.23	51.12	50.71	50.91
295	51.57	52.33	52.84	53.18	53.60	54.47	54.93	55.24	55.44	55.21
296	54.45	53.42	52.46	51.41	49.85	47.94	46.66	45.84	45.74	45.96
297	46.47	47.52	48.51	49.43	50.90	52.18	52.76	53.00	52.37	51.16
298	49.84	48.43	47.33	46.62	45.98	45.68	45.78	46.24	47.30	48.92
299	50.40	51.26	51.44	51.23	50.49	49.79	49.32	48.59	47.33	45.47
300	43.78	42.74	42.56	42.62	43.39	44.17	44.59	45.03	45.86	47.14
301	48.35	49.05	48.78	48.49	47.91	47.11	46.44	45.53	44.72	44.26
302	44.23	44.85	46.02	48.23	50.08	52.23	54.58	57.69	60.30	62.00
303	63.33	64.35	64.95	65.00	64.79	64.37	63.66	62.48	61.62	61.26
304	60.94	60.65	60.45	61.10	62.06	62.82	63.53	64.11	64.64	65.10

Appendix 1B (Part III)

Data and results from several experimental runs

(Tables B-1 to B-7, inclusive)

Table B-1. Run 68 - June 18, 1980, 11:51 AM to 12:09 PM EST

(p = 1012.6 millibars, θ = 10.8° to 7.9°)

λ [nm]	λ_o [nm]	S' [c]	C(S')	S'^S [c]	τ	P	E^S_λ [$\mu W \cdot cm^{-2} \cdot nm^{-1}$]	$\bar{E}^Z_\lambda$ [$\mu W \cdot cm^{-2} \cdot nm^{-1}$]
296.002	295.941	159913.6	1.0112603	6776.990	0.563099E+00	0.9651746	0.0017476544	7.673197E-02
295.000	294.938	46845.6	1.0032606	6383.133	0.557117E+00	0.9689441	0.0016790642	2.290186E-02
294.001	293.938	26152.6	1.0018165	6008.248	0.551448E+00	0.9686473	0.0016127002	1.316553E-02
293.002	292.937	8553.8	1.0005930	5650.614	0.546075E+00	0.9678902	0.0015483154	4.437116E-03
292.002	291.936	3968.0	1.0002750	5309.382	0.540991E+00	0.9666713	0.0014858102	2.123938E-03
291.000	290.932	874.3	1.0000606	4983.767	0.536193E+00	0.9649873	0.0014250929	4.832029E-04
289.998	289.928	287.3	1.0000199	4673.947	0.531692E+00	0.9628413	0.0013662527	1.640690E-04
288.998	288.926	51.1	1.0000036	4379.977	0.527496E+00	0.9608813	0.0013093641	3.012382E-05
287.999	287.925	10.3	1.0000007	4100.982	0.523598E+00	0.9586770	0.0012543250	6.245624E-06
287.000	286.924	4.6	1.0000003	3836.153	0.519996E+00	0.9562266	0.0012010413	2.926835E-06

P -- atmospheric pressure at spectroradiometer.

θ -- solar zenith angle.

λ -- indicated wavelength (instrument setting).

λ_o -- (=$\lambda+\delta\lambda$) -- corrected instrument wavelength setting where correction $\delta\lambda$ is determined by calibration (see figure 18).

S' -- instrument output produced by incident solar radiation.

C(S') -- correction factor for unresolved counts [eq. (1.15b)].

S'^S -- instrument output produced by incident radiation from calibration standard lamp.

τ -- spectral transmittance of filter or diffuser.

P -- polarization correction [eq. (1.23)].

E^S_λ -- spectral irradiance, from calibration standard lamp, at entrance slit or at diffuser when used.

$\bar{E}^Z_\lambda$ -- measured incident solar spectral irradiance given by eq. (1.22).

Corrections for spectral scattering below 290 [nm], or for not using a diffuser, have not yet been applied (see pp. 37 and 43).

Table B-2. Run 70 - June 18, 1980, 12:15 PM to 12:16 PM EST

(p = 1012.0 millibars, θ = 7.1° to 7.0°)

λ [nm]	λ_e [nm]	S' [c]	C(S')	S'^s [c]	τ	P	E^s_λ [$\mu W \cdot cm^{-2} \cdot nm^{-1}$]	E^z_λ [$\mu W \cdot cm^{-2} \cdot nm^{-1}$]
300.002	299.944	1651510.0	1.1339625	8537.541	0.100000E+01	0.9870363	0.0020424759	4.539112E-01
299.500	299.442	1182490.0	1.0919391	8299.409	0.100000E+01	0.9867143	0.0020035798	3.159104E-01
298.998	298.940	1570140.0	1.1264456	8066.333	0.100000E+01	0.9865151	0.0019652379	4.368012E-01
298.500	298.441	620166.0	1.0457163	7840.049	0.100000E+01	0.9864339	0.0019277442	1.616533E-01
298.000	297.941	928539.0	1.0705026	7617.739	0.100000E+01	0.9864688	0.0018906387	2.500846E-01
297.500	297.441	782060.0	1.0585589	7400.261	0.100000E+01	0.9866205	0.0018540680	2.102246E-01
297.002	296.942	298728.0	1.0213323	7188.393	0.100000E+01	0.9868877	0.0018181702	7.819482E-02
296.502	296.442	302722.0	1.0216261	6980.370	0.100000E+01	0.9872724	0.0017826523	7.999948E-02
296.001	295.940	272906.0	1.0194377	6776.588	0.100000E+01	0.9877751	0.0017475849	7.263450E-02

See Table B-1 for definitions of symbols used above.

Corrections for not using a diffuser have not yet been applied (see p. 43).

Table B-3. Run 72 - June 18, 1980, 12:25 PM to 12:28 PM EST

(p = 1012.0 millibars, θ = 6.4° to 6.3°)

λ [nm]	λ_e [nm]	S' [c]	C(S')	S'^{s} [c]	τ	P	E^s_λ [$\mu W \cdot cm^{-2} \cdot nm^{-1}$]	E^z_λ [$\mu W \cdot cm^{-2} \cdot nm^{-1}$]
349.999	349.854	1324170.0	1.1043007	58539.991	0.654000E-02	0.9995296	0.0096716592	3.695779E+01
347.998	347.859	1494680.0	1.1195596	56138.502	0.654000E-02	0.9990941	0.0091848616	4.190087E+01
346.002	345.868	1159020.0	1.0899192	53654.583	0.654000E-02	0.9988328	0.0087174651	3.141941E+01
344.001	343.873	1257490.0	1.0984470	51104.645	0.654000E-02	0.9987444	0.0082667514	3.420787E+01
342.001	341.879	1611730.0	1.1302758	48521.933	0.654000E-02	0.9988295	0.0078337330	4.502340E+01
340.001	339.884	1551990.0	1.1247819	45928.072	0.654000E-02	0.9990881	0.0074177748	4.314904E+01
337.999	337.888	991060.0	1.0756943	43340.670	0.654000E-02	0.9990902	0.0070180716	2.641974E+01
336.001	335.895	745675.0	1.0556398	40785.109	0.654000E-02	0.9990196	0.0066353759	1.960097E+01
334.000	333.899	1188310.0	1.0924412	38267.731	0.654000E-02	0.9989330	0.0062679098	3.254646E+01
332.001	331.905	1237480.0	1.0967028	35807.982	0.654000E-02	0.9988870	0.0059161775	3.432372E+01
330.002	329.911	1383300.0	1.1095450	33414.431	0.654000E-02	0.9988437	0.0055793782	3.923175E+01
327.999	327.913	958035.0	1.0729450	31091.782	0.654000E-02	0.9987939	0.0052564576	2.660436E+01
325.998	325.916	1155350.0	1.0896040	28854.698	0.654000E-02	0.9987417	0.0049479829	3.304936E+01
323.999	323.921	767494.0	1.0573880	26708.955	0.654000E-02	0.9985782	0.0046534948	2.165070E+01
322.000	321.926	767043.0	1.0573518	24656.879	0.654000E-02	0.9981950	0.0043722671	2.203001E+01
320.002	319.931	613140.0	1.0451675	22702.757	0.654000E-02	0.9976649	0.0041040260	1.775475E+01
318.000	317.932	387589.0	1.0279249	20844.105	0.654000E-02	0.9977037	0.0038477300	1.127132E+01
315.999	315.934	314310.0	1.0224801	19086.947	0.654000E-02	0.9980060	0.0036036548	9.296274E+00
314.000	313.937	463180.0	1.0336223	17432.177	0.654000E-02	0.9983471	0.0033715105	1.418160E+01
312.001	311.940	288219.0	1.0205601	15877.422	0.654000E-02	0.9985044	0.0031506706	8.938331E+00
309.999	309.940	132929.0	1.0093344	14419.298	0.654000E-02	0.9986269	0.0029404590	4.189332E+00
307.998	307.940	203016.0	1.0143580	13058.978	0.654000E-02	0.9988483	0.0027409493	6.616618E+00
306.001	305.944	108841.0	1.0076241	11795.730	0.654000E-02	0.9991108	0.0025520468	3.631311E+00
304.002	303.945	73686.0	1.0051430	10622.771	0.654000E-02	0.9991066	0.0023728217	2.531923E+00
302.001	301.944	13568.0	1.0009411	9537.155	0.654000E-02	0.9985251	0.0022029627	4.803701E-01
300.001	299.943	8533.0	1.0005916	8537.062	0.654000E-02	0.9975731	0.0020423979	3.130892E-01

See Table B-1 for definitions of symbols used above.

Corrections for not using a diffuser have not yet been applied (see p. 43).

Table B-4. Run 60 - June 17, 1980, 12:49 PM to 12:53 PM EST

(p = 1015.7 millibars, θ = 7.0° to 7.5°)

λ [nm]	λ_e [nm]	S' [c]	C(S')	S'^{s} [c]	τ	P	E^s_λ [$\mu W \cdot cm^{-2} \cdot nm^{-1}$]	$\bar{E}^z_\lambda$ [$\mu W \cdot cm^{-2} \cdot nm^{-1}$]
305.262	305.205	106512.0	1.0074592	11467.485	0.654000E-02	1.0010509	0.0024846581	3.551326E+00
304.841	304.784	43669.0	1.0030385	11217.585	0.654000E-02	1.0014413	0.0024468641	1.458808E+00
304.799	304.742	41178.0	1.0028645	11192.875	0.654000E-02	1.0014417	0.0024431172	1.376280E+00
304.780	304.723	43217.0	1.0030069	11181.710	0.654000E-02	1.0014416	0.0024414236	1.445074E+00
304.761	304.704	46693.0	1.0032499	11170.553	0.654000E-02	1.0014414	0.0024397309	1.562158E+00
304.741	304.684	50478.0	1.0035148	11158.818	0.654000E-02	1.0014410	0.0024379500	1.689777E+00
304.720	304.663	55258.0	1.0038495	11146.506	0.654000E-02	1.0014404	0.0024360812	1.851032E+00
304.679	304.622	64921.0	1.0045271	11122.497	0.654000E-02	1.0014388	0.0024324355	2.177628E+00
304.460	304.403	68896.0	1.0048063	10994.897	0.654000E-02	1.0014187	0.0024130308	2.319822E+00
303.362	303.305	57343.0	1.0039956	10371.354	0.654000E-02	1.0010296	0.0023174713	1.965018E+00
302.361	302.304	29887.0	1.0020766	9826.094	0.654000E-02	1.0002558	0.0022328326	1.040327E+00
302.142	302.085	13166.0	1.0009132	9709.705	0.654000E-02	1.0000332	0.0022146261	4.595709E-01
302.101	302.044	9308.0	1.0006454	9688.030	0.654000E-02	0.9999894	0.0022112299	3.250587E-01
302.081	302.024	8679.0	1.0006017	9677.470	0.654000E-02	0.9999678	0.0022095746	3.031894E-01
302.060	302.003	8339.0	1.0005781	9666.391	0.654000E-02	0.9999449	0.0022078376	2.914163E-01
302.041	301.984	8280.0	1.0005740	9656.376	0.654000E-02	0.9999241	0.0022062668	2.894534E-01
302.022	301.965	8846.0	1.0006133	9646.368	0.654000E-02	0.9999031	0.0022046969	3.093589E-01
301.980	301.923	10924.0	1.0007575	9624.274	0.654000E-02	0.9998562	0.0022012296	3.823778E-01
301.510	301.453	22063.0	1.0015317	9379.595	0.654000E-02	0.9992835	0.0021627041	7.796072E-01
300.561	300.503	14230.0	1.0009871	8899.792	0.654000E-02	0.9978585	0.0020864470	5.116985E-01
300.061	300.003	5572.0	1.0003862	8654.551	0.654000E-02	0.9969633	0.0020470840	2.022148E-01
299.760	299.702	13156.0	1.0009125	8509.394	0.654000E-02	0.9967206	0.0020236557	4.804042E-01
299.158	299.100	8223.0	1.0005701	8224.609	0.654000E-02	0.9964406	0.0019773986	3.035481E-01
298.539	298.480	417602.0	1.0301772	7939.373	0.100000E+01	0.9962089	0.0019306611	1.050132E-01
298.502	298.443	402772.0	1.0290627	7922.565	0.100000E+01	0.9961968	0.0019278937	1.012449E-01
298.481	298.422	404693.0	1.0292069	7913.037	0.100000E+01	0.9961901	0.0019263244	1.017823E-01
298.461	298.402	408222.0	1.0294719	7903.971	0.100000E+01	0.9961837	0.0019248306	1.027351E-01
298.441	298.382	413780.0	1.0298897	7894.913	0.100000E+01	0.9961774	0.0019233378	1.042154E-01
298.421	298.362	426575.0	1.0308531	7885.863	0.100000E+01	0.9961712	0.0019218457	1.075790E-01
298.379	298.320	463179.0	1.0336222	7866.883	0.100000E+01	0.9961583	0.0019187153	1.172169E-01
297.910	297.851	690464.0	1.0512467	7657.293	0.100000E+01	0.9960318	0.0018840166	1.793007E-01
297.761	297.702	783352.0	1.0586629	7591.606	0.100000E+01	0.9959985	0.0018730914	2.054382E-01
296.738	296.678	152296.0	1.0107155	7152.147	0.100000E+01	0.9958588	0.0017993517	3.888654E-02
296.698	296.638	135512.0	1.0095183	7135.369	0.100000E+01	0.9958565	0.0017965131	3.458670E-02
296.681	296.621	132725.0	1.0093199	7128.247	0.100000E+01	0.9958556	0.0017953077	3.387984E-02

Table B-4 (Continued)

λ [nm]	λ_0 [nm]	S' [c]	C(S')	S'^{s} [c]	τ	P	E^s_λ [$\mu W \cdot cm^{-2} \cdot nm^{-1}$]	E^z_λ [$\mu W \cdot cm^{-2} \cdot nm^{-1}$]
296.661	296.601	131405.0	1.0092259	7119.876	0.100000E+01	0.9958546	0.0017938904	3.355273E-02
296.638	296.578	135234.0	1.0094985	7110.258	0.100000E+01	0.9958535	0.0017922615	3.455510E-02
296.618	296.558	142469.0	1.0100140	7101.903	0.100000E+01	0.9958526	0.0017908459	3.643647E-02
296.580	296.520	154396.0	1.0108656	7086.048	0.100000E+01	0.9958511	0.0017881587	3.954914E-02
296.359	296.298	299292.0	1.0213737	6994.380	0.100000E+01	0.9958465	0.0017725900	7.779407E-02
295.961	295.900	186469.0	1.0131656	6831.590	0.100000E+01	0.9958567	0.0017448075	4.845248E-02
294.942	294.880	42525.0	1.0029586	6428.055	0.100000E+01	0.9959677	0.0016751565	1.115984E-02
294.898	294.836	36396.0	1.0025306	6411.054	0.100000E+01	0.9959596	0.0016721965	9.555808E-03
294.881	294.819	34546.0	1.0024015	6404.495	0.100000E+01	0.9959565	0.0016710539	9.072034E-03
294.858	294.796	32410.0	1.0022525	6395.629	0.100000E+01	0.9959523	0.0016695090	8.513795E-03
294.839	294.777	31917.0	1.0022181	6388.312	0.100000E+01	0.9959488	0.0016682336	8.387220E-03
294.819	294.757	33702.0	1.0023426	6380.616	0.100000E+01	0.9959452	0.0016668918	8.860969E-03
294.778	294.716	39848.0	1.0027716	6364.864	0.100000E+01	0.9959376	0.0016641437	1.049006E-02

See Table B-1 for definitions of symbols used above.

Corrections for not using a diffuser have not yet been applied (see p. 43).

Table B-5. Run 42 (without diffuser) - June 15, 1980, 12:11 PM to 12:16 PM EST

(p = 1015.9 millibars, θ = 7.6° to 7.0°)

λ [nm]	λ_ϕ [nm]	S' [c]	C(S')	S'^{s} [c]	τ	P	E^s_λ [$\mu W \cdot cm^{-2} \cdot nm^{-1}$]	E^z_λ [$\mu W \cdot cm^{-2} \cdot nm^{-1}$]
339.960	339.850	556296.0	1.0407532	47688.967	0.654000E-02	0.9950457	0.0074107493	1.382538E+01
339.918	339.808	554734.0	1.0406325	47629.382	0.654000E-02	0.9950711	0.0074022009	1.378594E+01
339.899	339.789	555829.0	1.0407171	47602.431	0.654000E-02	0.9950826	0.0073983361	1.381472E+01
339.879	339.769	561058.0	1.0411212	47574.065	0.654000E-02	0.9950946	0.0073942696	1.395057E+01
339.858	339.748	556497.0	1.0407687	47544.285	0.654000E-02	0.9951072	0.0073900016	1.383298E+01
339.838	339.728	544560.0	1.0398476	47515.926	0.654000E-02	0.9951191	0.0073859385	1.352475E+01
339.798	339.689	538818.0	1.0394052	47459.217	0.654000E-02	0.9951429	0.0073778172	1.337738E+01
332.572	332.482	488731.0	1.0355666	37552.416	0.654000E-02	1.0007868	0.0060163636	1.238867E+01
332.502	332.412	438138.0	1.0317258	37460.781	0.654000E-02	1.0009273	0.0060041693	1.106805E+01
332.482	332.392	416683.0	1.0301081	37434.618	0.654000E-02	1.0009678	0.0060006886	1.051038E+01
332.458	332.368	396069.0	1.0285600	37403.233	0.654000E-02	1.0010165	0.0059965138	9.976339E+00
332.439	332.350	380215.0	1.0273735	37378.395	0.654000E-02	1.0010552	0.0059932102	9.566668E+00
332.391	332.302	349654.0	1.0250966	37315.680	0.654000E-02	1.0011536	0.0059848704	8.779874E+00
329.252	329.170	424845.0	1.0307227	33323.107	0.654000E-02	1.0077924	0.0054580033	1.088208E+01
329.208	329.126	422605.0	1.0305539	33268.741	0.654000E-02	1.0078325	0.0054508733	1.082602E+01
329.188	329.107	425196.0	1.0307492	33244.044	0.654000E-02	1.0078506	0.0054476347	1.089588E+01
329.168	329.087	430954.0	1.0311834	33219.357	0.654000E-02	1.0078685	0.0054443976	1.104953E+01
329.149	329.068	434264.0	1.0314332	33195.913	0.654000E-02	1.0078853	0.0054413236	1.113848E+01
329.128	329.047	437095.0	1.0316470	33170.011	0.654000E-02	1.0079039	0.0054379276	1.121496E+01
329.088	329.007	445192.0	1.0322591	33120.704	0.654000E-02	1.0079387	0.0054314633	1.143251E+01
325.540	325.467	352304.0	1.0252935	28904.746	0.654000E-02	1.0088729	0.0048804930	9.243706E+00
325.500	325.427	322845.0	1.0231103	28859.048	0.654000E-02	1.0088591	0.0048745295	8.455883E+00
325.480	325.407	308579.0	1.0220575	28836.215	0.654000E-02	1.0088520	0.0048715498	8.075425E+00
325.460	325.387	132092.0	1.0092748	28813.393	0.654000E-02	1.0088448	0.0048685714	3.414216E+00
325.440	325.367	278403.0	1.0198402	28790.581	0.654000E-02	1.0088374	0.0048655944	7.272648E+00
325.420	325.347	273805.0	1.0195035	28767.780	0.654000E-02	1.0088299	0.0048626188	7.151519E+00
325.379	325.306	278650.0	1.0198583	28721.069	0.654000E-02	1.0088141	0.0048565229	7.283411E+00
317.730	317.671	136995.0	1.0096239	20803.885	0.654000E-02	1.0169098	0.0038151401	3.813908E+00
317.688	317.629	216437.0	1.0153281	20764.868	0.654000E-02	1.0169318	0.0038099275	6.062558E+00
317.670	317.611	216761.0	1.0153515	20748.161	0.654000E-02	1.0169411	0.0038076952	6.073046E+00
317.648	317.589	217433.0	1.0154001	20727.753	0.654000E-02	1.0169524	0.0038049681	6.093728E+00
317.628	317.569	211297.0	1.0149563	20709.213	0.654000E-02	1.0169626	0.0038024902	5.920555E+00
317.608	317.549	205897.0	1.0145660	20690.683	0.654000E-02	1.0169728	0.0038000135	5.768376E+00
317.569	317.510	195477.0	1.0138143	20654.583	0.654000E-02	1.0169924	0.0037951874	5.474890E+00
311.582	311.530	107111.0	1.0075016	15607.961	0.654000E-02	1.0158867	0.0031066851	3.233016E+00

Table B-5 (Continued)

λ [nm]	λ_e [nm]	S' [c]	C(S')	S'^{s} [c]	τ	P	E^s_λ [$\mu W \cdot cm^{-2} \cdot nm^{-1}$]	E^z_λ [$\mu W \cdot cm^{-2} \cdot nm^{-1}$]
311.542	311.490	108589.0	1.0076063	15577.504	0.654000E-02	1.0158484	0.0031024236	3.279996E+00
311.522	311.470	109192.0	1.0076490	15562.291	0.654000E-02	1.0158292	0.0031002945	3.299370E+00
311.502	311.450	105857.0	1.0074128	15547.089	0.654000E-02	1.0158098	0.0030981665	3.198840E+00
311.478	311.426	103296.0	1.0072316	15528.860	0.654000E-02	1.0157864	0.0030956143	3.122051E+00
311.458	311.406	99536.0	1.0069657	15513.681	0.654000E-02	1.0157668	0.0030934887	3.008547E+00
311.419	311.367	96482.0	1.0067498	15484.113	0.654000E-02	1.0157283	0.0030893468	2.917379E+00
308.930	308.880	8792.0	1.0006096	13679.411	0.654000E-02	1.0125287	0.0028334184	2.751760E-01
308.892	308.842	13575.0	1.0009416	13653.100	0.654000E-02	1.0124688	0.0028296375	4.252935E-01
308.869	308.819	52826.0	1.0036791	13637.193	0.654000E-02	1.0124323	0.0028273510	1.660174E+00
308.849	308.799	52826.0	1.0036791	13623.371	0.654000E-02	1.0124006	0.0028253637	1.660742E+00
308.831	308.781	47377.0	1.0032978	13610.941	0.654000E-02	1.0123719	0.0028235761	1.489330E+00
308.811	308.761	11488.0	1.0007967	13597.139	0.654000E-02	1.0123399	0.0028215909	3.603568E-01
308.769	308.719	39528.0	1.0027492	13568.189	0.654000E-02	1.0122725	0.0028174253	1.243233E+00
305.630	305.581	28088.0	1.0019512	11529.511	0.654000E-02	1.0060529	0.0025188005	9.344407E-01
305.590	305.541	31923.0	1.0022185	11505.094	0.654000E-02	1.0059586	0.0025151540	1.063121E+00
305.569	305.520	32770.0	1.0022776	11492.291	0.654000E-02	1.0059089	0.0025132411	1.091831E+00
305.550	305.501	32364.0	1.0022493	11480.716	0.654000E-02	1.0058639	0.0025115114	1.078666E+00
305.530	305.481	30988.0	1.0021533	11468.542	0.654000E-02	1.0058165	0.0025096916	1.033102E+00
305.510	305.461	29702.0	1.0020637	11456.377	0.654000E-02	1.0057689	0.0025078728	9.905201E-01
305.469	305.420	27987.0	1.0019442	11431.468	0.654000E-02	1.0056711	0.0025041472	9.339508E-01

See Table B-1 for definitions of symbols used above.

Corrections for not using a diffuser have not yet been applied (see p. 43).

Table B-6. Run 43 (with diffuser) - June 15, 1980, 12:17 PM to 12:22 PM EST

(p = 1015.9 millibars, θ = 6.9° to 6.6°)

λ [nm]	λ_o [nm]	S' [c]	C(S')	S'^{s} [c]	τ	P	E^s_λ [$\mu W \cdot cm^{-2} \cdot nm^{-1}$]	E^z_λ [$\mu W \cdot cm^{-2} \cdot nm^{-1}$]
339.960	339.850	49617.0	1.0034545	47688.967	0.643168E-03	0.9957766	0.0078628050	1.281744E+01
339.918	339.808	49193.0	1.0034248	47629.382	0.643011E-03	0.9958100	0.0078537351	1.271143E+01
339.899	339.789	49931.0	1.0034765	47602.431	0.642940E-03	0.9958251	0.0078496346	1.290459E+01
339.878	339.768	49179.0	1.0034238	47572.647	0.642862E-03	0.9958417	0.0078451044	1.271152E+01
339.858	339.748	49416.0	1.0034404	47544.285	0.642787E-03	0.9958575	0.0078407917	1.277487E+01
339.838	339.728	49046.0	1.0034145	47515.926	0.642713E-03	0.9958732	0.0078364807	1.268075E+01
339.798	339.689	48640.0	1.0033861	47459.217	0.642564E-03	0.9959047	0.0078278641	1.257913E+01
332.571	332.481	42870.0	1.0029827	37551.107	0.618789E-03	1.0043777	0.0063831768	1.176038E+01
332.499	332.409	38224.0	1.0026582	37456.856	0.618584E-03	1.0045851	0.0063698696	1.048825E+01
332.478	332.388	36143.0	1.0025129	37429.386	0.618524E-03	1.0046460	0.0063659922	9.917405E+00
332.458	332.368	34281.0	1.0023830	37403.233	0.618467E-03	1.0047043	0.0063623011	9.406704E+00
332.439	332.350	32409.0	1.0022524	37378.395	0.618413E-03	1.0047597	0.0063587960	8.893161E+00
332.391	332.302	29515.0	1.0020507	37315.680	0.618277E-03	1.0049006	0.0063499475	8.100376E+00
329.248	329.166	36927.0	1.0025676	33318.163	0.609961E-03	1.0144114	0.0057902534	1.039820E+01
329.209	329.127	36305.0	1.0025242	33269.976	0.609865E-03	1.0144641	0.0057835484	1.022664E+01
329.188	329.107	36301.0	1.0025239	33244.044	0.609813E-03	1.0144922	0.0057799405	1.022768E+01
329.169	329.088	36766.0	1.0025564	33220.591	0.609767E-03	1.0145174	0.0057766775	1.036102E+01
329.149	329.068	37212.0	1.0025875	33195.913	0.609718E-03	1.0145438	0.0057732444	1.048916E+01
329.128	329.047	37701.0	1.0026216	33170.011	0.609667E-03	1.0145712	0.0057696412	1.062963E+01
329.088	329.007	38549.0	1.0026808	33120.704	0.609569E-03	1.0146230	0.0057627826	1.087379E+01
325.540	325.467	30682.0	1.0021320	28904.746	0.601674E-03	1.0162091	0.0051782031	9.008952E+00
325.500	325.427	29384.0	1.0020415	28859.048	0.601593E-03	1.0161931	0.0051718758	8.631442E+00
325.480	325.407	28039.0	1.0019478	28836.215	0.601553E-03	1.0161848	0.0051687143	8.237682E+00
325.460	325.387	25785.0	1.0017908	28813.393	0.601513E-03	1.0161763	0.0051655543	7.576217E+00
325.439	325.366	24563.0	1.0017057	28789.441	0.601471E-03	1.0161672	0.0051622378	7.218489E+00
325.420	325.347	23749.0	1.0016491	28767.780	0.601433E-03	1.0161588	0.0051592385	6.980574E+00
325.379	325.306	23454.0	1.0016285	28721.069	0.601351E-03	1.0161401	0.0051527708	6.897344E+00
317.730	317.671	16352.0	1.0011346	20803.885	0.589617E-03	1.0305286	0.0040478636	5.242214E+00
317.688	317.629	17764.0	1.0012327	20764.868	0.589572E-03	1.0305460	0.0040423331	5.698684E+00
317.668	317.609	18440.0	1.0012797	20746.305	0.589551E-03	1.0305539	0.0040397015	5.917430E+00
317.648	317.589	18419.0	1.0012783	20727.753	0.589529E-03	1.0305618	0.0040370712	5.912289E+00
317.628	317.569	18573.0	1.0012890	20709.213	0.589508E-03	1.0305694	0.0040344421	5.963408E+00
317.608	317.549	18069.0	1.0012539	20690.683	0.589487E-03	1.0305769	0.0040318143	5.802961E+00
317.569	317.510	16901.0	1.0011727	20654.583	0.589445E-03	1.0305909	0.0040266938	5.430298E+00
311.582	311.530	8689.0	1.0006024	15607.961	0.585275E-03	1.0266348	0.0032961929	3.055780E+00

Table B-6 (Continued)

λ [nm]	λ_e [nm]	S' [c]	C(S')	S'^{s} [c]	τ	P	E^s_λ [$\mu W \cdot cm^{-2} \cdot nm^{-1}$]	$\bar{E}^z_\lambda$ [$\mu W \cdot cm^{-2} \cdot nm^{-1}$]
311.542	311.490	8948.0	1.0006204	15577.504	0.585261E-03	1.0265730	0.0032916714	3.149012E+00
311.522	311.470	9141.0	1.0006338	15562.291	0.585255E-03	1.0265420	0.0032894125	3.218045E+00
311.498	311.446	8721.0	1.0006046	15544.050	0.585247E-03	1.0265045	0.0032867032	3.071321E+00
311.478	311.426	8798.0	1.0006100	15528.860	0.585240E-03	1.0264732	0.0032844468	3.099486E+00
311.458	311.406	8573.0	1.0005944	15513.681	0.585234E-03	1.0264417	0.0032821915	3.021178E+00
311.419	311.367	8149.0	1.0005649	15484.113	0.585221E-03	1.0263800	0.0032777969	2.873539E+00
308.930	308.880	4678.0	1.0003242	13679.411	0.584802E-03	1.0212997	0.0030062569	1.721860E+00
308.891	308.841	4778.0	1.0003311	13652.408	0.584801E-03	1.0212004	0.0030021399	1.759918E+00
308.868	308.818	4758.0	1.0003297	13636.501	0.584801E-03	1.0211416	0.0029997139	1.753277E+00
308.849	308.799	4733.0	1.0003280	13623.371	0.584801E-03	1.0210929	0.0029977109	1.744661E+00
308.831	308.781	4569.0	1.0003166	13610.941	0.584800E-03	1.0210466	0.0029958143	1.684737E+00
308.811	308.761	4458.0	1.0003089	13597.139	0.584800E-03	1.0209950	0.0029937079	1.644390E+00
308.769	308.719	4172.0	1.0002891	13568.189	0.584800E-03	1.0208863	0.0029892882	1.540036E+00
305.630	305.581	2211.0	1.0001532	11529.511	0.585392E-03	1.0109540	0.0026724473	8.661149E-01
305.590	305.541	2506.0	1.0001736	11505.094	0.585407E-03	1.0108045	0.0026685784	9.824743E-01
305.569	305.520	2647.0	1.0001834	11492.291	0.585415E-03	1.0107258	0.0026665489	1.038196E+00
305.550	305.501	2777.0	1.0001924	11480.716	0.585422E-03	1.0106544	0.0026647136	1.089605E+00
305.530	305.481	2647.0	1.0001834	11468.542	0.585430E-03	1.0105791	0.0026627828	1.039001E+00
305.510	305.461	2592.0	1.0001796	11456.377	0.585438E-03	1.0105037	0.0026608530	1.017813E+00
305.469	305.420	2426.0	1.0001681	11431.468	0.585454E-03	1.0103486	0.0026569002	9.533952E-01

See Table B-1 for definitions of symbols used above.

Table B-7. Run 44 (without diffuser) - June 15, 1980, 12:23 PM to 12:28 PM EST

(p = 1015.8 millibars, θ = 6.5° to 6.3°)

λ [nm]	λ_o [nm]	S' [c]	C(S')	S'·S [c]	τ	P	E^s_λ [$\mu W \cdot cm^{-2} \cdot nm^{-1}$]	E^z_λ [$\mu W \cdot cm^{-2} \cdot nm^{-1}$]
339.960	339.850	541439.0	1.0396071	47688.967	0.654000E-02	0.9947134	0.0074107493	1.344582E+01
339.918	339.808	545075.0	1.0398873	47629.382	0.654000E-02	0.9947475	0.0074022009	1.354060E+01
339.899	339.789	550124.0	1.0402767	47602.431	0.654000E-02	0.9947628	0.0073983361	1.367153E+01
339.878	339.768	549822.0	1.0402534	47572.647	0.654000E-02	0.9947797	0.0073940663	1.366415E+01
339.858	339.748	538764.0	1.0394011	47544.285	0.654000E-02	0.9947958	0.0073900016	1.337877E+01
339.838	339.728	534395.0	1.0390648	47515.926	0.654000E-02	0.9948118	0.0073859385	1.326639E+01
339.798	339.689	527077.0	1.0385022	47459.217	0.654000E-02	0.9948437	0.0073778172	1.307845E+01
332.572	332.482	488711.0	1.0355651	37552.416	0.654000E-02	1.0030184	0.0060163636	1.236059E+01
332.502	332.412	452625.0	1.0328218	37460.781	0.654000E-02	1.0032165	0.0060041693	1.142004E+01
332.482	332.392	426578.0	1.0308533	37434.618	0.654000E-02	1.0032735	0.0060006886	1.074301E+01
332.458	332.368	304112.0	1.0217285	37403.233	0.654000E-02	1.0033422	0.0059965138	7.591576E+00
332.439	332.350	380746.0	1.0274132	37378.395	0.654000E-02	1.0033967	0.0059932102	9.558042E+00
332.391	332.302	348796.0	1.0250329	37315.680	0.654000E-02	1.0035352	0.0059848704	8.737000E+00
329.252	329.170	432003.0	1.0312625	33323.107	0.654000E-02	1.0128815	0.0054580033	1.101559E+01
329.208	329.126	429014.0	1.0310370	33268.741	0.654000E-02	1.0129392	0.0054508733	1.093992E+01
329.188	329.107	431902.0	1.0312549	33244.044	0.654000E-02	1.0129652	0.0054476347	1.101725E+01
329.168	329.087	434633.0	1.0314610	33219.357	0.654000E-02	1.0129909	0.0054443976	1.109049E+01
329.149	329.068	440446.0	1.0319002	33195.913	0.654000E-02	1.0130152	0.0054413236	1.124493E+01
329.128	329.047	450564.0	1.0326657	33170.011	0.654000E-02	1.0130418	0.0054379276	1.151328E+01
329.088	329.007	456465.0	1.0331128	33120.704	0.654000E-02	1.0130920	0.0054314633	1.167202E+01
325.540	325.467	364708.0	1.0262165	28904.746	0.654000E-02	1.0145534	0.0048804930	9.524149E+00
325.500	325.427	338425.0	1.0242634	28859.048	0.654000E-02	1.0145362	0.0048745295	8.824285E+00
325.480	325.407	325241.0	1.0232874	28836.215	0.654000E-02	1.0145273	0.0048715498	8.474036E+00
325.460	325.387	301795.0	1.0215579	28813.393	0.654000E-02	1.0145182	0.0048685714	7.851354E+00
325.439	325.366	290016.0	1.0206920	28789.441	0.654000E-02	1.0145085	0.0048654456	7.540022E+00
325.420	325.347	284018.0	1.0202518	28767.780	0.654000E-02	1.0144995	0.0048626188	7.382230E+00
325.379	325.306	286873.0	1.0204613	28721.069	0.654000E-02	1.0144795	0.0048565229	7.460879E+00
317.730	317.671	202989.0	1.0143561	20803.885	0.654000E-02	1.0275224	0.0038151401	5.619012E+00
317.688	317.629	219798.0	1.0155714	20764.868	0.654000E-02	1.0275450	0.0038099275	6.094571E+00
317.668	317.609	224715.0	1.0159277	20746.305	0.654000E-02	1.0275556	0.0038074472	6.234547E+00
317.648	317.589	221164.0	1.0156703	20727.753	0.654000E-02	1.0275660	0.0038049681	6.135904E+00
317.628	317.569	221146.0	1.0156690	20709.213	0.654000E-02	1.0275762	0.0038024902	6.136829E+00
317.608	317.549	213020.0	1.0150808	20690.683	0.654000E-02	1.0275864	0.0038000135	5.909289E+00
317.570	317.511	199995.0	1.0141400	20655.508	0.654000E-02	1.0276052	0.0037953110	5.545293E+00
311.582	311.530	108471.0	1.0075979	15607.961	0.654000E-02	1.0246532	0.0031066851	3.246365E+00

Table B-7 (Continued)

λ [nm]	λ_e [nm]	S' [c]	C(S')	S'^{s} [c]	τ	P	E^s_λ [$\mu W \cdot cm^{-2} \cdot nm^{-1}$]	$\bar{E}^z_\lambda$ [$\mu W \cdot cm^{-2} \cdot nm^{-1}$]
311.542	311.490	110481.0	1.0077403	15577.504	0.654000E-02	1.0245953	0.0031024236	3.309096E+00
311.522	311.470	111162.0	1.0077885	15562.291	0.654000E-02	1.0245661	0.0031002945	3.330715E+00
311.498	311.446	109091.0	1.0076418	15544.050	0.654000E-02	1.0245309	0.0030977410	3.269439E+00
311.478	311.426	105358.0	1.0073775	15528.860	0.654000E-02	1.0245014	0.0030956143	3.157742E+00
311.458	311.406	102734.0	1.0071918	15513.681	0.654000E-02	1.0244718	0.0030934887	3.079515E+00
311.419	311.367	99175.0	1.0069401	15484.113	0.654000E-02	1.0244138	0.0030893468	2.973946E+00
308.931	308.881	58076.0	1.0040470	13680.103	0.654000E-02	1.0196180	0.0028335179	1.811224E+00
308.891	308.841	59257.0	1.0041298	13652.408	0.654000E-02	1.0195224	0.0028295381	1.849529E+00
308.869	308.819	58317.0	1.0040639	13637.193	0.654000E-02	1.0194696	0.0028273510	1.820787E+00
308.850	308.800	57020.0	1.0039729	13624.062	0.654000E-02	1.0194239	0.0028254631	1.780737E+00
308.831	308.781	56078.0	1.0039069	13610.941	0.654000E-02	1.0193780	0.0028235761	1.751799E+00
308.811	308.761	55707.0	1.0038809	13597.139	0.654000E-02	1.0193296	0.0028215909	1.740789E+00
308.770	308.720	51999.0	1.0036212	13568.877	0.654000E-02	1.0192299	0.0028175244	1.625694E+00
305.630	305.581	28146.0	1.0019553	11529.511	0.654000E-02	1.0098671	0.0025188005	9.328373E-01
305.591	305.542	32483.0	1.0022576	11505.704	0.654000E-02	1.0097294	0.0025152451	1.077755E+00
305.569	305.520	34610.0	1.0024059	11492.291	0.654000E-02	1.0096514	0.0025132411	1.149009E+00
305.550	305.501	34263.0	1.0023817	11480.716	0.654000E-02	1.0095840	0.0025115114	1.137901E+00
305.530	305.481	32940.0	1.0022894	11468.542	0.654000E-02	1.0095128	0.0025096916	1.094307E+00
305.511	305.462	31958.0	1.0022210	11456.985	0.654000E-02	1.0094451	0.0025079637	1.062022E+00
305.469	305.420	29590.0	1.0020559	11431.468	0.654000E-02	1.0092950	0.0025041472	9.840085E-01

See Table B-1 for definitions of symbols used above.

Corrections for not using a diffuser have not yet been applied (see p. 43).

References

[1] G. M. B. Dobson, "Observer's Handbook for the Ozone Spectrophotometer", Annals of the International Geophysical Year, 5 (Pergamon Press, New York, 1957-1958) 46-81.

[2] L. M. Garrison, L. E. Murray, and A. E. S. Green, "Ultraviolet Limit of Solar Radiation at the Earth's Surface with a Photon Counting Monochromator", Appl. Opt., 17, No. 5 (March 1, 1978) 683-684.

[3] L. M. Garrison, D. D. Doda, and A. E. S. Green, "Total Ozone Determination by Spectroradiometry in the Middle Ultraviolet", Appl. Opt., 18, No. 6 (March 15, 1979) 850-855.

[4] Henry J. Kostkowski and Fred E. Nicodemus, "An Introduction to the Measurement Equation", Chapter 5 of "Self-Study Manual on Optical Radiation Measurements: Part I--Concepts", Nat. Bur. Stand. (U.S.), Tech. Note 910-2, 118 pages (Feb. 1978) pp. 58-92.

[5] Fred E. Nicodemus, "Physically Defining Measurement-Beam Geometry by Using Opaque Barriers", Chapter 9 of "Self-Study Manual on Optical Radiation Measurements: Part I--Concepts", Nat. Bur. Stand. (U.S.), Tech. Note 910-4, 134 pages (June 1979) pp. 91-119.

[6] Henry J. Kostkowski, "The Relative Spectral Responsivity and Slit-Scattering Function of a Spectroradiometer", Chapter 7 of "Self-Study Manual on Optical Radiation Measurements: Part I--Concepts", Nat. Bur. Stand. (U.S.), Tech. Note 910-4, 134 pages (June 1979) pp. 2-34.

[7] Paul Bener, "Approximate Values of Intensity of Natural Ultraviolet Radiation for Different Amounts of Atmospheric Ozone", Physikalisch-Meteorologisches Observatorium Davos, Davos-Platz, Switzerland, ARDG(E) Contract No. DAJA37-68-C-107, Final Tech. Rept., Feb. 71-Feb. 72, (June 1972) [NTIS, AD 752-115].

[8] Henry J. Kostkowski, "Precise Instruments and Accurate Standards Do Not Insure Accurate Measurements", Optical Radiation News, Radiometric Physics Division, Nat. Bur. Stand. (U.S.), No. 28 (April 1979).

[9] John B. Shumaker, "Distribution of Optical Radiation with Respect to Polarization", Chapter 6 of "Self-Study Manual on Optical Radiation Measurements: Part I--Concepts", Nat. Bur. Stand. (U.S.), Tech. Note 910-3, 62 pages (June 1977) pp. 1-53.

[10] L. M. Garrison, Z. Blaszczak, and A. E. S. Green, "Polarization Characteristics of an Altazimuth Sky Scanner", Appl. Optics, 19, No. 9, (May 1, 1980) 1419-1424.

[11] John B. Shumaker, "Deconvolution", Chapter 8 of "Self-Study Manual on Optical Radiation Measurements: Part I--Concepts", Nat. Bur. Stand. (U.S.). Tech. Note 910-4, 134 pages (June 1979) pp. 35-90.

[12] Robley D. Evans, "The Atomic Nucleus", Chapter 28 (McGraw-Hill Book Company, New York, 1955).

[13] R. D. Saunders and J. B. Shumaker, "Optical Radiation Measurements: The 1973 NBS Scale of Spectral Irradiance", Nat. Bur. Stand. (U.S.), Tech. Note 594-13, 36 pages (April 1977).

[14] L. M. Garrison, L. E. Murray, D. D. Doda, and A. E. S. Green, "Diffuse-Direct Ultraviolet Ratios with a Compact Double Monochromator", Appl. Optics, 17, No. 6, (March 1, 1978) 827-836; also A. T. Chai and A. E. S. Green, "Ratio Measurement of Diffuse to Direct Solar Irradiances in the Middle Ultraviolet", Appl. Optics, 15, No. 5 (May 1976) 1182-1187.

[15] F. E. Nicodemus and H. J. Kostkowski, "Distribution of Optical Radiation with Respect to Position and Direction--Radiance", Chapter 2 of "Self-Study Manual on Optical Radiation Measurements: Part I--Concepts", Nat. Bur. Stand. (U.S.), Tech. Note 910-1, 93 pages (Mar. 1976) pp. 10-44.

[16] Fred E. Nicodemus, "More on the Distribution of Optical Radiation with respect to Position and Direction", Chapter 4 of "Self-Study Manual on Optical Radiation Measurements: Part I--Concepts", Nat. Bur. Stand. (U.S.), Tech. Note 910-2, 118 pages (Feb. 1978) pp. 1-57.

[17] Alex E. S. Green and P. F. Schippnick, "UV-B Reaching the Surface", in "The Role of Solar Ultraviolet Radiation in Marine Ecosystems", John Calkins, ed. (Plenum Press, in publication).

[18] Arnold M. Bass and Richard J. Paur, National Bureau of Standards, Washington, D.C., 20234, personal communication.

[19] A. E. S. Green, K. R. Cross and L. A. Smith, "Improved Analytic Characterization of Ultraviolet Skylight", Photochem. and Photobiol., 31, No. 1 (Jan. 1980) pp. 59-65.

[20] United States Committee on Extension to the Standard Atmosphere. U.S. Standard Atmosphere, 1962. Supplements, 1966. Prepared under sponsorship of Environmental Science Services Administration, National Aeronautics and Space Administration, and the United States Air Force. (Superintendent of Documents, U.S. Government Printing Office, Washington, D.C. 20402; 1966) p. 17.

[21] A. E. S. Green, T. Sawada and E. P. Shettle, "The Middle Ultraviolet Reaching the Ground", Photochem. and Photobiol., 19, (1974) pp. 251-259.

[22] John L. Kohl, William H. Parkinson and Robert L. Jurucz, "Center and Limb Solar Spectrum in High Spectral Resolution 225.2 nm to 319.6 nm", Smithsonian Center for Astrophysics (Harvard University Printing Office, Cambridge, 1978).

[23] John L. Kohl, William H. Parkinson, and Carlos A. Zapata, "Solar Spectral Radiance and Irradiance, 225.2 nm to 319.6 nm", The Astrophysical Journal Supplement Series, Vol. 44 (Nov. 1980) pp. 295-317.

[24] D. F. Heath, Goddard Space Flight Center, Greenbelt, Maryland 20771, personal communication.

[25] A. Lyle Broadfoot, "The Solar Spectrum 2100-3200 Å", The Astrophysical Journal, 173 (May 1972) pp. 681-689.

[26] John B. Shumaker, "Introduction to Coherence in Radiometry", Chapter 10 of "Self-Study Manual on Optical Radiation Measurements; Part I--Concepts", Nat. Bur. Stand. (U.S.) Tech. Note 910-6 (in preparation).

ADDENDUM to Chapter 4 in NBS Tech Note 910-2:

p. 28; 1st line below eq. (4.35):
Insert a superscript one - - - inverse-square law[1] - - - referring to the following footnote at the bottom of the page:

---

[1]See Explanatory Note following end of Appendix 4 on p. 102.

---

p. 102, following end of Appendix 4, add:

Explanatory Note concerning unit-dimensions in eq. (4.36) on p. 28 as an expression of the inverse-square law.

In this Manual we have insisted on the need for recognizing and treating solid angles as having a unit-dimension of [sr], as in Tables 4-1, 4-2, and 4-3, on pp. 3 to 6, inclusive. However, in eq. (4.36) there appears to be an exception to this where we take the quotient of I $[W \cdot sr^{-1}]$ and the square of D [m] and equate that quotient to $dE_n = dF_t$ $[W \cdot m^{-2}]$, seemingly ignoring the unit-dimension [sr]. Actually, there is no inconsistency and the [sr] is not ignored. To demonstrate this, we need to distinguish between the always orthogonal radial lengths, with dimension $[L_r]$ or unit-dimension $[m_r]$, and transverse lengths, with dimension $[L_t]$ or unit-dimension $[m_t]$, as discussed in examining the concepts of plane angle and solid angle and their dimensionality in Appendix 2 of NBS Tech Note 910-1, particularly on p. 69. In those terms, the unit-dimension of a plane angle is $[\theta] = [m_t \cdot m_r^{-1}]$ and that of a solid angle is $[\omega] = [m_t^2 \cdot m_r^{-2}]$ (the quotient of the dimensions of an intercepted or enclosed area subtended by the solid angle on the surface of a sphere about its vertex divided by the dimensions of the square of the radius of that sphere). In eq. (4.36), the unit dimension of D, the distance along the direction of propagation, is clearly $[D] = [m_r]$ not $[m_t]$. But that of the normal irradiance dE_n or fluence rate dF_t, the flux per unit area perpendicular to the direction of propagation, is $[dE_n] = [dF_t] = [W \cdot m_t^{-2}]$ not $[W \cdot m_r^{-2}]$. The unit dimensions of radiant intensity I are then $[I] = [W \cdot sr^{-1}] = [W \cdot m_t^{-2} \cdot m_r^{2}]$. Accordingly, the unit dimensions of the quotient I/D^2 are $[I \cdot D^{-2}] = [W \cdot m_t^{-2} \cdot m_r^{2} \cdot m_r^{-2}] = [W \cdot m_t^{-2}] = [dF_T] = [dE_n]$, so we are consistent after all.